

**“The role of DNA damage in the  
pathogenesis of nitrate tolerance -  
nitrosative versus oxidative DNA  
damage”**

**DISSERTATION**

zur Erlangung des Grades

**„DOKTOR DER  
NATURWISSENSCHAFTEN“**

Am Fachbereich Biologie  
der Johannes Gutenberg-Universität Mainz

Yuliya Mikhed

Geboren am 02.11.1988 in Lviv, Ukraine

Mainz, 2015

Tag der mündlichen Prüfung: 10.12.15

To my mother

## Index of contents

Index of contents .....	1
Index of figures.....	4
Index of abbreviations.....	7
1. Introduction.....	10
1.1 Organic nitrates and their bioactivation pathways.....	10
1.2 Nitric oxide and/or nitric oxide related species signaling mechanisms via soluble guanylyl cyclase pathway.....	11
1.3 Nitrate tolerance phenomena.....	13
1.3.a Pseudotolerance.....	14
1.3.b True vascular tolerance.....	15
1.4 Suggested mechanisms of true vascular tolerance development.....	16
1.5. Oxidative stress as a hall-mark of nitrate tolerance.....	19
1.6 Endothelial dysfunction as a consequence of organic nitrate treatment.....	22
1.7. Genotoxicity associated with organic nitrates.....	23
1.8 DNA repair, as a cellular response to genotoxicity induced by organic nitrates. .....	27
1.9 First clinical evidence of DNA damage association with prolonged organic nitrate therapy.....	32
2. Aims of the study.....	34
3. Materials and Methods .....	35
3.1 Materials.....	35
3.2 Animals and treatment protocol.....	35

3.3 Tissue excision from the experimental animals and preparation of isolated tissues. ....	36
3.5 Isometric tension studies. ....	38
3.6 Detection of oxidative and nitro-oxidative stress in whole blood and aorta. ....	41
3.7 Detection of oxidative and nitro-oxidative stress in heart. ....	42
3.8 Protein concentration determination by Lowry method. ....	43
3.9 Detection of nitrosyl-iron hemoglobin in whole blood by electron paramagnetic resonance (EPR) spectroscopy. ....	44
3.10 Protein extraction from the cardiac tissue. ....	47
3.11 Protein concentration determination by Bradford method. ....	48
3.12 Western Blot analysis in cardiac tissue. ....	49
3.13 Cell culture. ....	51
3.14 Comet assay. ....	52
3.15 DNA extraction from the EA.hy 926 cells, aortic and cardiac tissue. ....	53
3.16 Immuno-dot blot analysis for DNA damage in EA.hy 926 cells, aortic and cardiac tissue. ....	54
3.17 Immuno-histological analysis of aortic and cardiac tissue for DNA damage. .	55
3.18 Cell death detection assay. ....	55
3.19 Statistical analysis. ....	56
4. Results .....	57
4.1. DNA damage parameters in cell culture upon GTN treatment. ....	57
4.2 Vascular reactivity in rat aortas. ....	60
4.3 Nitro-oxidative stress parameters. ....	62
4.4 Chronic GTN treatment causes DNA damage in the aortic and cardiac tissue of Wistar rats. ....	65
4.5 Chronic GTN treatment causes apoptosis. ....	68

4.6 Nitrate tolerance parameters in MGMT <sup>-/-</sup> mice.....	71
5. Discussion .....	77
6. Summary .....	84
References .....	87
Acknowledgments .....	107
Curriculum Vitae .....	108
List of publications .....	109
Original research articles:.....	110
Reviews:.....	112
Oral presentations and posters: .....	112
Oral presentation: .....	112
Poster presentations: .....	113

## Index of figures

Figure 1. Summary of organic nitrates bioactivation process. ....	11
Figure 2. Summary of organic nitrates down-stream signaling cascades.....	13
Figure 3. Molecular mechanisms of GTN-induced nitrate tolerance.....	18
Figure 4. Proposed mechanisms underlying GTN-induced eNOS uncoupling and endothelial dysfunction. ....	21
Figure 5. Mechanism of $\cdot\text{NO}$ genotoxicity.....	24
Figure 6. Products of DNA base deamination .....	27
Figure 7. Crystallographic X-ray structure of the OGG-1 enzyme bound to the double- stranded DNA with the 8-hydroxyguanine modification. ....	29
Figure 8. Crystallographic X-ray structure of the human MGMT enzyme and schematic representation of MGMT mechanism of action. ....	31
Figure 9. Schematic representation of the formation of micronuclei.....	33
Figure 10. Schematic representation of the implantation of an osmotic mini-pump into a Wistar rat. ....	36
Figure 11. DNA damage induced by GTN administration to EA.hy 926 cells. ....	59
Figure 12. Nitric oxide levels in whole blood and the degree of endothelial dysfunction and nitrate tolerance in rats upon treatment with different GTN doses...	61
Figure 13. Nitro-oxidative stress parameters in GTN-treated Wistar rats.....	65
Figure 14. Oxidative and alkylating DNA modifications in GTN-treated Wistar rats...	68
Figure 15. Increased apoptosis in cardiac and aortic tissue from nitrate tolerant animals.....	70
Figure 16. Comparison of GTN (30 mg/kg/d) effects in MGMT <sup>-/-</sup> and C57BL/6 mice. .....	75

Figure 17. MNU chemical structure .....	78
Figure 18 Summary of the study protocol and outcome. ....	85



## **Index of Tables**

Table 1. Hypothesis proposed to explain the development of nitrate tolerance. .... 15

## Index of abbreviations

ACE – angiotensin converting enzyme;

Ach - acetylcholine;

ALDH-2 – aldehyde dehydrogenase 2;

AP-site – apurinic/apyrimidinic site;

APE – apurinic/apyrimidinic endonuclease;

BER – base excision repair;

BH<sub>4</sub> – tetrahydrobiopterin;

BKca - Ca<sup>2+</sup>-activated (Maxi) K<sup>+</sup> - channel;

t-BOOH - tert-butyl hydroperoxide;

BSA – bovine serum albumin;

CDD assay – Cell death detection assay;

cGK-I, -II – cGMP-dependent protein kinase I, II;

cGMP – cyclic guanosine monophosphate;

DHE - dihydroethidium;

DMEM - Dulbecco's modified Eagle's medium;

ECL - enhanced chemiluminescence;

EDTA - ethylenediaminetetraacetic acid;

EGTA - ethylene glycol tetraacetic acid;

eNOS - endothelial <sup>•</sup>NO synthase (type 3);

EPC – endothelial progenitor cells;

EPR - electron paramagnetic resonance;

EtOH - ethanol;

Fpg - formamidopyrimidine-DNA glycosylase;

Fapy - 2,6-diamino-4-hydroxy-5-N-methylformamidopyrimidine;

GDN – glyceryl dinitrate;

GTN - glyceryl trinitrate (nitroglycerin);

GTPCH-I – GTP-cyclohydrolase-I;

IHC - immuno-histochemistry;

ISDN – isosorbide dinitrate;

ISMN – isosorbide-5-mononitrate;

ISNT – *in situ* end labeling;

L-012 - 8-amino-5-chloro-7-phenylpyrido[3,4-d]pyridazine-1,4-(2H,3H)dione sodium salt;

Lig1 – ligase 1

MGMT - O<sup>6</sup>-methylguanine-DNA methyltransferase;

MMR – mismatch repair;

MN assay – micronucleus assay;

MNU – N-Nitroso-N-methylurea;

NEIL1, 2, 3 - nei endonuclease VIII-like 1, 2 or 3;

·NO - nitric oxide;

Hb-NO - nitrosyl-iron hemoglobin;

NOS – nitric oxide synthase;

3NT - 3-nitrotyrosine;

NTHL1 - nth endonucleaselll-like 1;

OGG-1 - 8-oxo-guanine DNA glycosylase;

O<sup>6</sup>-me-G - O<sup>6</sup>-methyl-guanine;

8-oxo-G - 8-oxo-guanine;

PBS – phosphate buffered saline;

PBS-T – phosphate buffered saline with Tween-20;

PDE – phosphodiesterase;

PGF2 $\alpha$  - 8-epi-prostaglandin F2 $\alpha$ ;

ONOO $^-$  - peroxyne nitrite;

PETN - pentaerythritol tetranitrate;

PGI2 – prostacyclin (prostaglandin I2);

PGIS – prostacyclin synthase

PKC – protein kinase C;

Pol $\beta$  – polymerase  $\beta$ ;

RAAS – renin-angiotensin-aldosterone system;

ROS – reactive oxygen species;

RONs - reactive oxygen and nitrogen species;

RSNO – S-nitrosothiols;

SDS-Page - sodium dodecyl sulfate – polyacrylamide electrophoresis;

SEM – standard error of means;

sGC – soluble guanylate cyclase;

SIN-1 - 3-Morpholino-sydnorimine;

SOD – superoxide dismutase;

SSC buffer – saline sodium citrate buffer;

O $_2^{\cdot-}$  - superoxide anion radical.

TE buffer – Tris-EDTA buffer;

TUNEL - Terminal deoxynucleotidyl transferase dUTP nick end labeling.

## 1. Introduction

### 1.1 Organic nitrates and their bioactivation pathways.

Up to now, organic nitrates are still among the most commonly prescribed medications for the treatment of angina pectoris and myocardial infarction [1, 2]. Their beneficial anti-ischemic effects are mainly based on endothelium independent vasodilation of coronary arteries, venous capacity vessels, and collaterals [3]. The mechanism of action of these compounds generally relies on the bioactivation processes conducted by various classes of enzymes [4, 5]. The proteins that are responsible for the bioactivation of the organic nitrate moiety are highly compound-specific. For example, it has been shown that aldehyde dehydrogenase 2 (ALDH-2) preferentially bioactivates nitroglycerin (GTN) [6] and cytochrome p450 enzymes perform similar activities on less potent organic nitrates, such as isosorbide-5-mononitrate (ISMN) and isosorbide dinitrate (ISDN) [7]. In the case of GTN, the bioactivation yields 1,2- and 1,3-GDN, nitrite, nitrate, and  $\cdot\text{NO}$ . On top of that, bioactivation pathways can also produce NO-like species, such as S-nitrosothiols [8].

Classical high potency nitrates, such as GTN or pentaerythrityl tetranitrate (PETN) can be activated through at least 2 different molecular mechanisms. The first one is initialized at therapeutic concentrations of the compound, eliciting clinically relevant vasodilator potency, while the second one accounts for higher, supra-pharmacological doses of the organic nitrates [9]. A summary of the organic nitrates bioactivation process is shown in Figure 1.

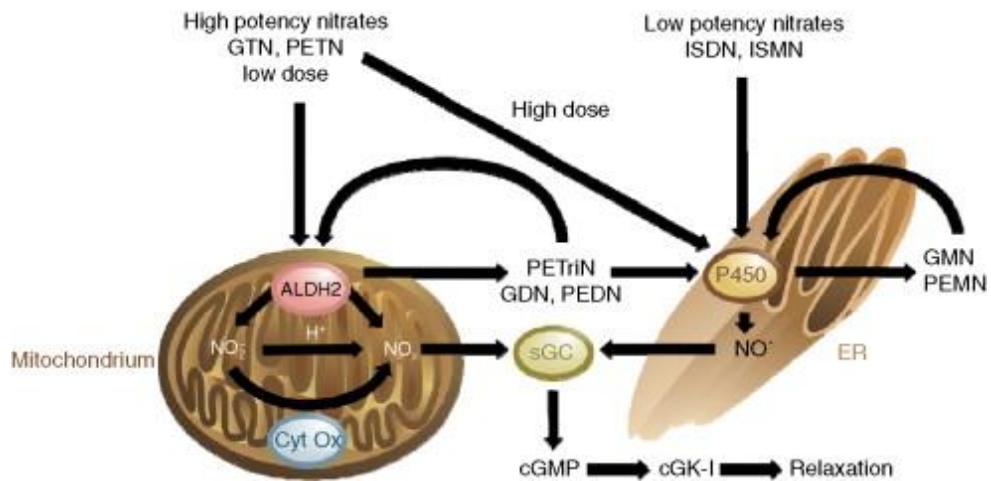


**Figure 1. Summary of organic nitrates bioactivation process.**

High potency nitrates such as nitroglycerin (GTN) and pentaerithrityl tetranitrate (PETN) are activated by ALDH-2, yielding an ·NO containing compound. This molecule then activates the soluble guanylyl cyclase, which subsequently causes blood vessels relaxation. The right part of the figure describes the bioactivation of low potency nitrates such as isosorbide dinitrate (ISDN) and isosorbide-5-mononitrate (ISMN). These molecules are most probably metabolized by P450 enzyme(s) in the endoplasmic reticulum (ER) directly yielding nitric oxide. Adapted from [10].

## **1.2 Nitric oxide and/or nitric oxide related species signaling mechanisms via soluble guanylyl cyclase pathway.**

Consensus is achieved regarding the bioactivation products of organic nitrates. Most scientists believe that once a certain organic nitrate passed a designated activation pathway, either nitric oxide itself, or ·NO related species (RSNO or NO-metal-complex) are released, causing activation of the soluble guanylyl cyclase (sGC) and up-regulation of the secondary messenger – cyclic

guanosine monophosphate (cGMP) [11]. This process is followed by activation of cGMP-dependent protein kinases (cGK-I, cGK-II), and/or cyclic nucleotide-gated ion channels [12]. The major function of cGK-I, which is expressed in vascular smooth muscle cells, is to lower agonist-induced contractile tone. The vasodilating mechanism is based on the principle of agonist-induced decrease of intracellular free  $\text{Ca}^{2+}$  levels in smooth muscle cells and a desensitization of contractile elements to  $\text{Ca}^{2+}$  [9]. Additionally, cGK-I reduces extracellular  $\text{Ca}^{2+}$  entry through voltage-gated calcium channels by phosphorylation of the  $\text{Ca}^{2+}$ -activated (Maxi)  $\text{K}^+$  - channel ( $\text{BK}_{\text{Ca}}$ ), consecutively increasing the open probability of this channel and hyperpolarizing the smooth muscle cell membrane [13]. cGMP-dependent protein kinases differ in their cellular and tissue distribution. cGK-II is typically anchored to the plasma membrane by N-terminal myristoylation [14]. This isoform was found mainly in kidney, cerebellum and mucosa [15]. cGK-II is involved in bone ossification [16], controls renin release in the kidney [17] and regulates the intestinal chloride- and water-secretion [18].

In endothelium-intact coronary arteries it has been shown that GTN relaxation was partially inhibited by iberiotoxin (specific inhibitor of  $\text{BK}_{\text{Ca}}$ -channels), thus supporting the notion that GTN might relax endothelium-intact vessels also by activating  $\text{BK}_{\text{Ca}}$ -channels [19]. Finally, organic nitrates can also affect vascular eicosanoid production, which leads to the speculation that they might affect vascular tone by this mechanism as well [20]. A summary of the down-stream signaling cascades of organic nitrates is presented in Figure 2.

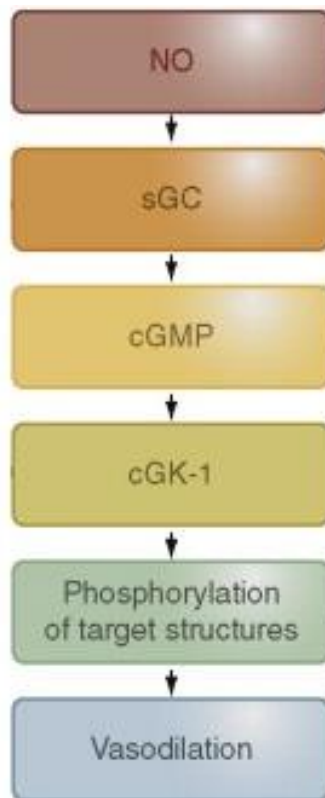


**Figure 2. Summary of organic nitrates down-stream signaling cascades.**

Figure has been modified and adapted from [10].

### **1.3 Nitrate tolerance phenomena.**

Under chronic therapy with organic nitrates, such as GTN [21, 22] or ISDN [23] and/or ISMN [24], hemodynamic and clinical effects of these compounds are gradually lost or less pronounced. Depending on the clinical setting, the manifestation of this pathological condition is observed in diverse manner. For coronary artery disease patients, nitrate tolerance has been described as a loss of effects on treadmill walking time and time of onset of angina [25]. For congestive heart failure patients, it was reported as the loss of hemodynamic effects of the prescribed organic nitrates [26] and in hypertension setting it is characterized as a loss of antihypertensive effects of these compounds. Similar loss of organic nitrate



hemodynamic effects was also described for healthy subjects [24]. Mechanisms of nitrate tolerance development are quite complex and still not fully understood.

### **1.3.a Pseudotolerance.**

After 24 h of continuous nitrate administration, a phenomenon of pseudotolerance has been described in patients. It is associated with neurohormonal counter-regulation and expansion of plasma volume [3, 27, 28]. This process is associated with the release of catecholamines, increases in plasma vasopressin and aldosterone levels, as well as plasma renin activity [29, 30]. Upregulation of these neurohormonal vasoconstrictors has been demonstrated in patients with heart failure, patients with coronary artery disease and healthy individuals that received nitroglycerin treatment [30, 31]. Additionally, long-term therapy with GTN was associated with increased sensitivity to other vasoconstrictors such as angiotensin II, serotonin, thromboxane A and phenylephrine. Increased production of endothelin 1 was proposed as an explanation for this phenomenon and it is thought to function through a protein kinase C-mediated mechanism [32]. A significant increase in intravascular volume, secondary to the aldosterone-mediated salt and water retention [29, 30] has also been observed in patients treated with GTN. Although these changes could diminish the preload effect of GTN, evidence suggests that these mechanisms are not fully sufficient to explain the loss of previously observed properties of organic nitrates. For example, there is a time difference between neurohormonal activation, plasma expansion, and development of tolerance [29]. Although the potential prognostic significance of these changes needs to be acknowledged, other mechanisms of tolerance and a hypothesis that explains all these changes have to be found in the future.

### 1.3.b True vascular tolerance.

Already after 48 h of continuous organic nitrate therapy, true vascular tolerance has been reported in patients suffering from cardio-vascular diseases [33] but also in healthy volunteers [3, 24]. The definition of true vascular tolerance is the loss of the vasodilatory potency of a given organic nitrate due to the desensitization of the  $\cdot\text{NO}/\text{cGMP}$  signaling pathway (e.g. by altered protein expression/function, oxidative impairment of  $\cdot\text{NO}$  signaling effects) but not due to pseudotolerance-dependent (hormonal) counter-regulatory mechanisms [34]. This was also nicely shown in *in vivo* nitrate tolerance animal models with the help of isometric tension recordings where isolated aortic ring segments showed a blunted reaction to the endothelium independent vasodilator GTN [35]. There have been several hypothesis proposed to explain the phenomena of pseudotolerance and true vascular tolerance and they are summarized in the Table 1.

**Table 1. Hypothesis proposed to explain the development of nitrate tolerance.**

Adapted from [3].

<i>Pseudotolerance</i>	<ul style="list-style-type: none"><li>• Activation of the renin-angiotensin-aldosterone system</li><li>• Increase in circulating catecholamine levels and catecholamine release rates</li><li>• Increase in vasopressin levels</li><li>• Volume expansion</li></ul>
<i>True vascular tolerance</i>	<ul style="list-style-type: none"><li>• Impaired GTN biotransformation</li><li>• Increased vascular superoxide production</li><li>• Desensitization of the soluble guanylate cyclase</li></ul>

- 
- |  |  |
|--|--|
|  | <ul style="list-style-type: none"><li>• Increase in phosphodiesterase activity</li><li>• Increased sensitivity to vasoconstrictors</li><li>• Increased endothelin-1 expression</li></ul> |
|--|--|
- 

#### **1.4 Suggested mechanisms of true vascular tolerance development.**

Previous investigations in the field of organic nitrate tolerance development lead to several possible mechanisms for the induction of this serious side effect. Among these traditional concepts are: impaired nitrate biotransformation, increase in phosphodiesterases (PDE) activity; desensitization of sGC; depletion of intracellular SH-groups [34].

Initial data on the involvement of thiol depletion in the pathogenesis of nitrate tolerance came from the observation that thiol-dependent proteins are inhibited in the mitochondria of rats treated with GTN [36]. Additionally, organic nitrates have been shown to cause swelling of rat liver mitochondria [37]. Needleman and coworkers also emphasized the importance of sulfhydryl groups for the correct mitochondrial enzymatic functioning during organic nitrate therapy. They determined a direct correlation between loss of vasodilation and the depletion of thiol groups [38]. Consecutively, this theory has been expanded and the formation of S-nitrosothiols was proposed as an explanation for the massive depletion of the cellular thiol groups after nitroglycerin treatment [39]. Later on these hypotheses have been confirmed by the prevention of nitrate tolerance by sulfhydryl-donors such as N-acetylcysteine [40].

Desensitization of the sGC was one of the initial hypotheses that has been proposed in order to explain the phenomenon of nitrate tolerance [41]. This paradigm was in line with the observation that patients treated with one type of organic nitrate exhibited reduced sensitivity to other ·NO-dependent vasodilators (cross-tolerance).

Additionally, it has been reported that S-nitros(yl)ation of sGC results in its decreased reactivity to  $\cdot\text{NO}$  and down-stream of this, by diminished cGK-I activity [42]. Desensitization of sGC was concentration- and time-dependent on exposure to S-nitrosocysteine. Later it was proposed that S-nitros(yl)ation of sGC is a way by which  $\cdot\text{NO}$  exposure is kept in the memory of smooth muscle cells and could be a mechanism of  $\cdot\text{NO}$  tolerance. These results were later confirmed in the *in vivo* setting of a 3-day continuous treatment with GTN, leading to desensitized and S-nitros(yl)ated sGC in the tolerant tissue [43]. These effects were reversed by the co-treatment with the sulfhydryl donor N-acetylcysteine [43]. Furthermore, our group has recently shown that oxidative inhibition of the sGC is a critical point in the desensitization of this enzyme, leading to GTN tolerance and being corrected by sGC activators, a novel class of  $\cdot\text{NO}$ -independent sGC activity enhancing drugs [35].

First indications that phosphodiesterases can be involved in the pathogenesis of nitrate tolerance came from the detection of altered cGMP turn-over rates in the blood vessels that were *in vitro* treated with organic nitrates [44]. Furthermore, vasodilatory and hemodynamic properties of the nitrate compounds were improved with the unspecific PDE inhibitor – dipyridamole [45]. Nitroglycerin-mediated activation of the PDE 1A1 isoform was also shown in calcium-pre-constricted vessels that led to impaired  $\cdot\text{NO}$ /cGMP-dependent vasodilation as well as aggravated vascular nitrate tolerance and cross-tolerance to acetylcholine-mediated relaxation [46]. Such negative effects were mitigated by the PDE-1 specific inhibitor – vinpocetine.

The identification of a role for mitochondrial enzymes in the biotransformation of GTN and PETN opened a new direction for the research on nitrate tolerance development. The oxidation of thiol groups in the structure of ALDH-2, as well as in sGC, reduces the rates of GTN biotransformation and impairs the down-stream  $\cdot\text{NO}$

signaling. Though, should be mentioned that this perspective is only applicable to GTN tolerance but not to ISMN or ISDN tolerance, since these compounds do not (or only marginally for ISDN) undergo mitochondrial metabolism [47].

A summary of the currently known molecular processes contributing to the development of GTN-induced nitrate tolerance are shown in Figure 3.

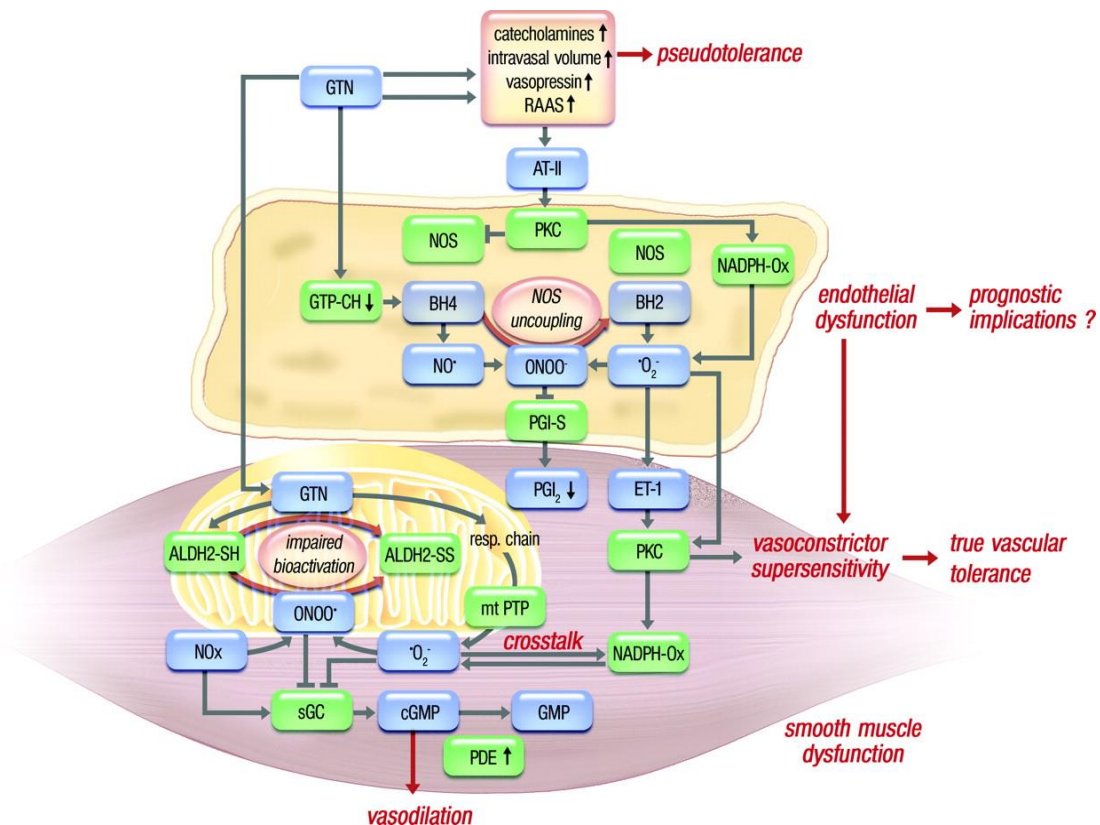


**Figure 3. Molecular mechanisms of GTN-induced nitrate tolerance.**

Approximately within first 24 h of continuous GTN administration a phenomenon of pseudotolerance takes place. It is described by increased catecholamine and vasopressin plasma levels, increased intravascular volume, and activation of the renin-angiotensin-aldosterone system (RAAS). Within 48-72 h of continuous GTN treatment, true vascular tolerance has been detected. This pathological condition is associated with endothelial and smooth muscle dysfunction and vasoconstrictor supersensitivity. Additionally,

several sources of RONS have been shown to be up-regulated, among them: NADPH oxidase activation by protein kinase C (PKC), inhibition of nitric oxide synthase (NOS) activation by PKC, uncoupling of endothelial NOS. Furthermore, bioactivation of GTN by ALDH-2 in mitochondria is impaired due to elevated RONS levels, in particular - ONOO<sup>-</sup>. Figure has been adapted from [3].

### **1.5. Oxidative stress as a hall-mark of nitrate tolerance.**

As early as in 1995, it has been shown that tolerant vessels produced approximately twice the amount of reactive oxygen species (ROS) compared to the controls and this increase was corrected by the addition of superoxide dismutase (by O<sub>2</sub><sup>-</sup> decomposition to hydrogen peroxide and oxygen) [48]. Additionally, nitroglycerin triggered the release of peroxynitrite from the vasculature and particularly from the endothelium of the tolerant animals [49]. These data have been confirmed in human arterial segments from patients receiving chronic GTN therapy [33, 50]. Other parameters supporting the oxidative stress hypothesis of nitrate tolerance development were: elevated free-radical induced lipid peroxidation products, such as esterified 8-epi-prostaglandin F<sub>2</sub>α (PGF<sub>2</sub>α), cytotoxic aldehydes and isoprostanes [51]. Several sources of nitrate-induced reactive oxygen and nitrogen species were identified: the mitochondrial respiratory chain complexes [52, 53], activation of the phagocytic NADPH oxidase [48, 54] and uncoupling of the endothelial nitric oxide synthase (eNOS) [28, 55].

The identification of oxidative stress as one of the driving forces in the pathogenesis of nitrate tolerance provides a direct link to the previously discussed

impaired biotransformation of organic nitrates in the setting of tolerance. In addition, this provides a unified explanation for the observed vascular phenotype.

Several mechanisms have been postulated for the GTN stimulated mitochondrial ROS production. To name just a few: mitochondrial swelling, premature release of partially reduced oxygen from mitochondrial complex I or III, depolarization of mitochondrial membrane potential and initiation of lipid peroxidation [56]. By increasing mitochondrial ROS production, GTN can either oxidatively inhibit ALDH-2 or deplete its essential repair cofactors, such as dihydrolipoic acid [57]. Additionally, recent data obtained with purified ALDH-2 provide evidence that ALDH-2 itself could be a source of GTN-triggered ROS formation [58].

Negative effects of ROS are not only limited to mitochondria and there is clear evidence that leakage of mitochondrial ROS into the cytoplasm, where it has been demonstrated to activate a cross-talk with the vascular NADPH oxidase, leads to further ROS production and the formation of highly reactive peroxynitrite [54]. Due to a very short half-life and high diversity of reactive oxygen and nitrogen species it is hard to determine a specific role for every species. Though, several activities have been specifically ascribed to ONOO<sup>-</sup>. It may cause tyrosine nitration of the prostacyclin synthase, reducing endothelial prostacyclin formation [49]; oxidize the endothelial ·NO synthase (eNOS) cofactor BH<sub>4</sub>; and directly inhibit the activity of the sGC and/or other enzymes involved in ·NO signaling (for review see [34]). The impact of ROS on BH<sub>4</sub> is particularly important. GTN may cause a phenomenon called eNOS uncoupling by oxidative BH<sub>4</sub> depletion, and this will switch the enzyme from ·NO to superoxide production [28], which may further increase oxidative stress in vascular tissue in a positive feedback fashion [59] (for mechanisms of uncoupling see figure 4). These observations are consistent with the hypothesis that nitrate-

induced oxidative stress impairs endogenous  $\cdot\text{NO}$  production, accounting for ISMN-induced endothelial dysfunction (cross-tolerance) [60].

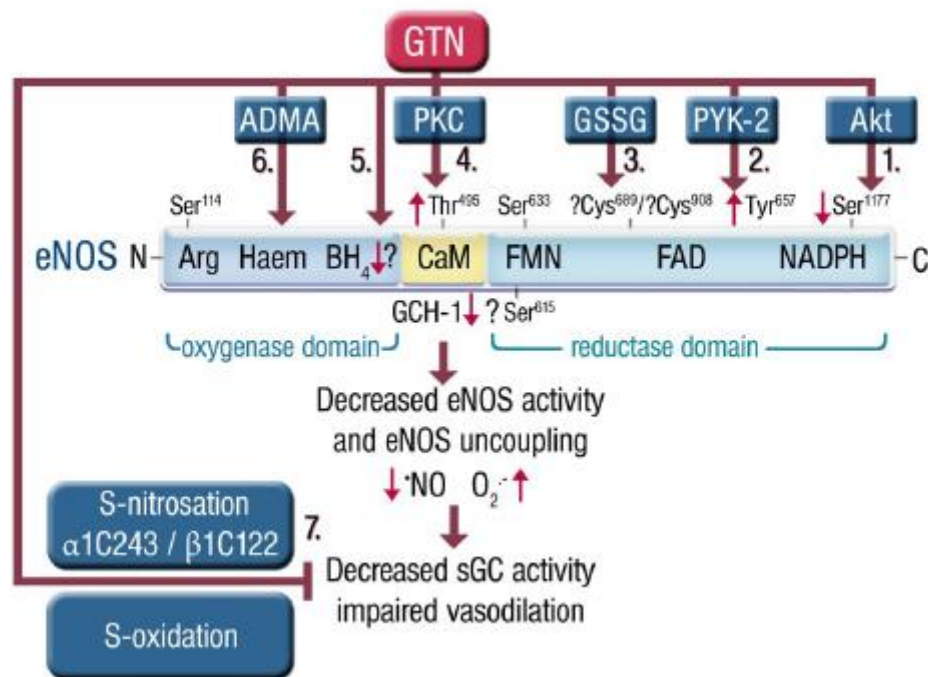


**Figure 4. Proposed mechanisms underlying GTN-induced eNOS uncoupling and endothelial dysfunction.**

GTN treatment causes a decrease in Ser1177 and an increase in Tyr657 and Thr495 phosphorylation of the endothelial nitric oxide synthase, leading to a decreased activity (eventually also uncoupling) of the enzyme. In addition, the key enzyme of the *de novo* synthetic pathway of the endothelial nitric oxide synthase (eNOS) cofactor tetrahydrobiopterin (BH<sub>4</sub>), GTP-cyclohydrolase-1 (GCH-1), is downregulated by chronic GTN treatment [61], also leading to a dysfunctional, superoxide (O<sub>2</sub><sup>-</sup>)-producing nitric oxide synthase. S-glutathionylation, a novel regulatory pathway of eNOS coupling state [62], is increased in the setting of tolerance [28]. The endogenous inhibitor of eNOS, ADMA, is upregulated in response to oxidative stress conditions. In addition,



down-stream of eNOS, the  $\cdot\text{NO}$  receptor sGC, is desensitized by GTN mediated S-nitrosation and potentially S-oxidation and/or oxidative depletion of heme. ADMA, asymmetric dimethylarginine; PKC, protein kinase C; PYK-2, protein tyrosine kinase-2; eNOS, endothelial nitric oxide synthase; Haem, heme moiety (iron porphyrin); CaM, calmodulin; FMN, flavin mononucleotide; FAD, flavin adenine dinucleotide; GSSG, glutathione disulfide (oxidized glutathione); Akt, protein kinase B. Adapted from [63].

### **1.6 Endothelial dysfunction as a consequence of organic nitrate treatment.**

During prolonged treatment with organic nitrates such as GTN, ISMN, and ISDN, impairment of the release of endothelium-derived  $\cdot\text{NO}$  in response to endogenous stimuli (e.g. acetylcholine) has been detected in patients. This phenomenon, also known as nitrate-triggered endothelial dysfunction (cross-tolerance), has been observed in animal studies and in humans during continuous therapy (for review see [3]). In large coronary arteries, 5 days treatment with transdermal GTN leads to an enhanced acetylcholine-induced paradoxical constriction instead of endothelium-dependent vasodilation [64]. Endothelial dysfunction in response to organic nitrates may be caused by different mechanisms, including decreased expression and/or activity of the endothelial NOS or even uncoupling of this enzyme [65]. Additionally, minimal concentration of an eNOS inhibitor caused blood vessels dilation, which was compatible with the inhibition of eNOS-dependent vasoconstrictory superoxide formation and interpreted as human *in vivo* evidence of GTN-induced eNOS uncoupling. Further supporting these data, GTN-induced endothelial dysfunction was prevented by folic acid, a compound that facilitates recoupling of eNOS [66]. Importantly, endothelial dysfunction is not only a

unique feature of the GTN induced nitrate tolerance; it has been also detected during the treatment with intermittent doses of ISMN [60]. Of note, eNOS expression is rather up- than down-regulated in the setting of nitrate tolerance, implying a feedback compensatory mechanism for the dysfunctional uncoupled eNOS [55]. The rebound phenomenon, which is often observed during withdrawal of nitrate therapy, is also associated with endothelial dysfunction [64].

### **1.7. Genotoxicity associated with organic nitrates.**

As it has been previously discussed, organic nitrates after passing their respective biotransformation pathways elicit diverse reaction products. It is assumed that nitric oxide is the major vasodilator generated during the bioactivation process but also other  $\cdot\text{NO}$ -related species (Fe-NO, RSNO) might be formed.  $\cdot\text{NO}$  and its products demonstrate genotoxic effects. Considerably high genotoxicity originates from the reaction of  $\cdot\text{NO}$  with oxygen and/or superoxide [67]. The interaction of nitric oxide and its related species with DNA can be classified into two groups: direct and indirect DNA damage. Figure 5 illustrates the possible reactions suggested for both groups.

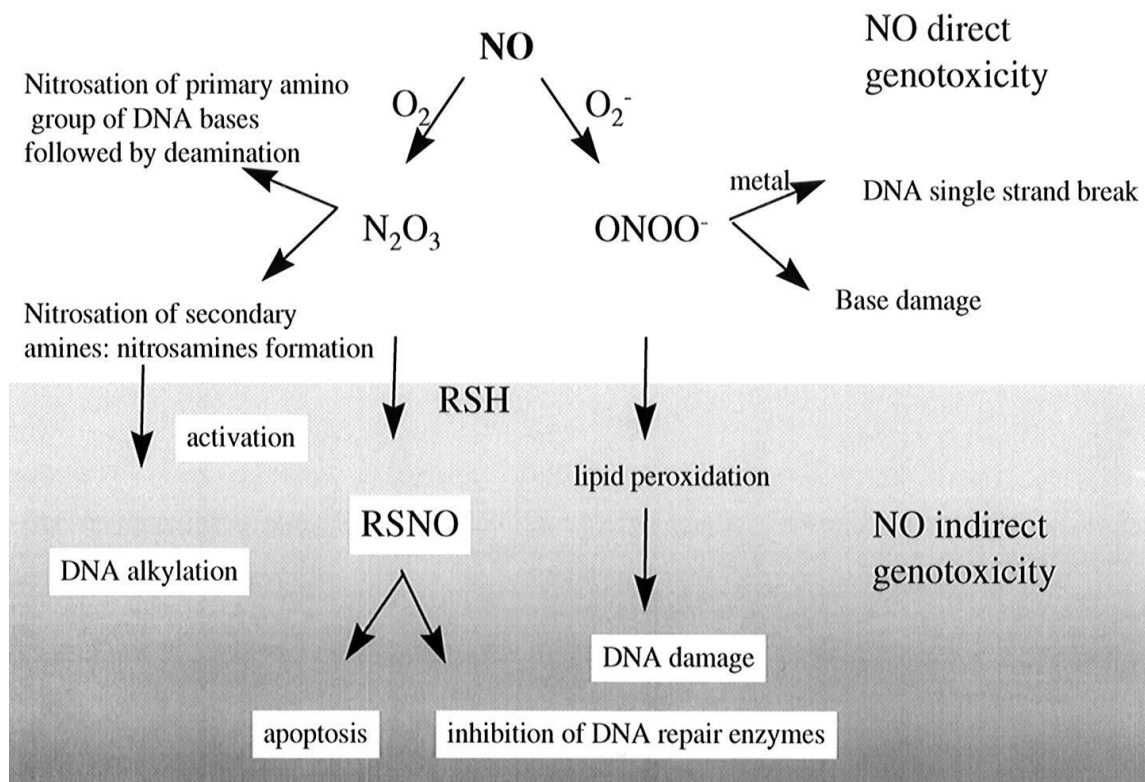


**Figure 5. Mechanism of ·NO genotoxicity.**

The DNA damaging effects of ·NO are based on its reaction with oxygen and/or superoxide. The genotoxicity is mediated either by  $N_2O_3$  and/or peroxynitrite, or via indirect effect on DNA due to the activation of the intermediary formed nitrosamines and inhibition of DNA repair pathways. Adapted from [67].

·NO reacts with molecular oxygen to produce  $NO_2\cdot$  along with other nitrosating agents like  $N_2O_3$ . Both nitrogen oxides react with water to yield  $NO_2^-$  and  $NO_3^-$  [68]. As a result, the abundance of reactive species that might have DNA damaging properties increases exponentially, especially in favorable *in vivo* environment.

In general, there are three mechanisms of action by which nitric oxide or ·NO related species could exert DNA damaging effects upon reaction with  $O_2$  and/or

superoxide. These are: formation of N-nitroso compounds, direct DNA attack by peroxynitrite and/or hydroxyl radicals and deamination of nucleobases [69].

Nitrosation of amines and amides to form N-nitroso compounds occurs at various pHs in the presence of  $\cdot\text{NO}$  and  $\text{O}_2$ . It is important to note that without oxygen this reaction is not possible [69]. In the *in vivo* setting N-nitroso amines are metabolized to strong alkylating electrophiles that react with DNA at multiple nucleophilic sites: N-7 and O-6 positions on guanine and N-3 positions on adenine. Alkylation on the O-6 position of guanine is considered as the most mutagenic one, leading to G  $\rightarrow$  A transitions during the DNA replication process [70].

The reaction of  $\cdot\text{NO}$  with superoxide anion is approximately 5 times faster than the decomposition of superoxide by SOD [71]. Therefore the generation of the reaction product peroxynitrite under *in vivo* conditions is a fact and its formation rate only depends on the relative amounts of  $\cdot\text{NO}$ , superoxide and SOD [72]. It is a potent oxidizing agent that might have  $\text{OH}^\bullet$  like reactivity [73]. As a result of its reaction with the nucleic acids, DNA strand breaks and oxidative modifications have been detected [74]. The exact mutagenic profile of peroxynitrite has been determined *in vitro* using bacterial and mammalian cell cultures. Exposure of the cells to peroxynitrite induced transversion mutation in DNA, mostly G  $\rightarrow$  T at GC pairs [75]. Additionally, peroxynitrite causes formation of the 8-nitroguanine adduct, which is rapidly depurinated to form an apurinic site, increasing the possibility of G  $\rightarrow$  T transversions [76]. Furthermore, hydroxyl radicals are potent DNA damaging agents that are able to induce strand breaks, cross links, abasic sites and modified bases. One of the classical markers of its base oxidizing activity is 8-hydroxyguanine (8-oxo-G) [77].

Spontaneous DNA deamination is an extremely rare event, so when this process is detected with higher frequency, this points to the deleterious effects of a specific group of reactive species. Starting from 1991 there were several reports

published demonstrating that  $\cdot\text{NO}$  and its derivatives can deaminate DNA at physiological pH [68]. Nguyen et. al. reported that 22  $\mu\text{mol/ml}$   $\cdot\text{NO}$  can lead to deamination of adenine and guanine [78]. The results obtained with the individual nucleobases were partially at odds with the data received with nucleic acids. When single nucleobases were incubated with  $\cdot\text{NO}$ , adenine showed higher deamination yields than guanine and the pattern was changed to the opposite with the complete DNA or RNA molecules. Similar yields were also observed for xanthine and hypoxanthine. The deamination of cytosine leads to the formation of uracil, which triggers the activation of uracil glycosylase which is responsible for its removal from the DNA strands. Once being excised it leaves an abasic site that is quite often mismatched by the insertion of adenine after the replication process. This will lead to G:C  $\rightarrow$  A:T transitions. If aberrant uracil is not detected by a glycosylase it could be paired with an adenine in the following replication cycle. The deamination of guanine, on the other hand, could explain the G:C  $\rightarrow$  T:A and G:C  $\rightarrow$  C:G transversions. Another pattern is observed when methylated cytosine is deaminated, resulting in the formation of thymine. This defect is especially significant from the epigenetic perspective, since DNA methylation patterns are critically important for gene regulation, differentiation and genomic imprinting [69]. A summary of the DNA deamination processes is shown in Figure 6.

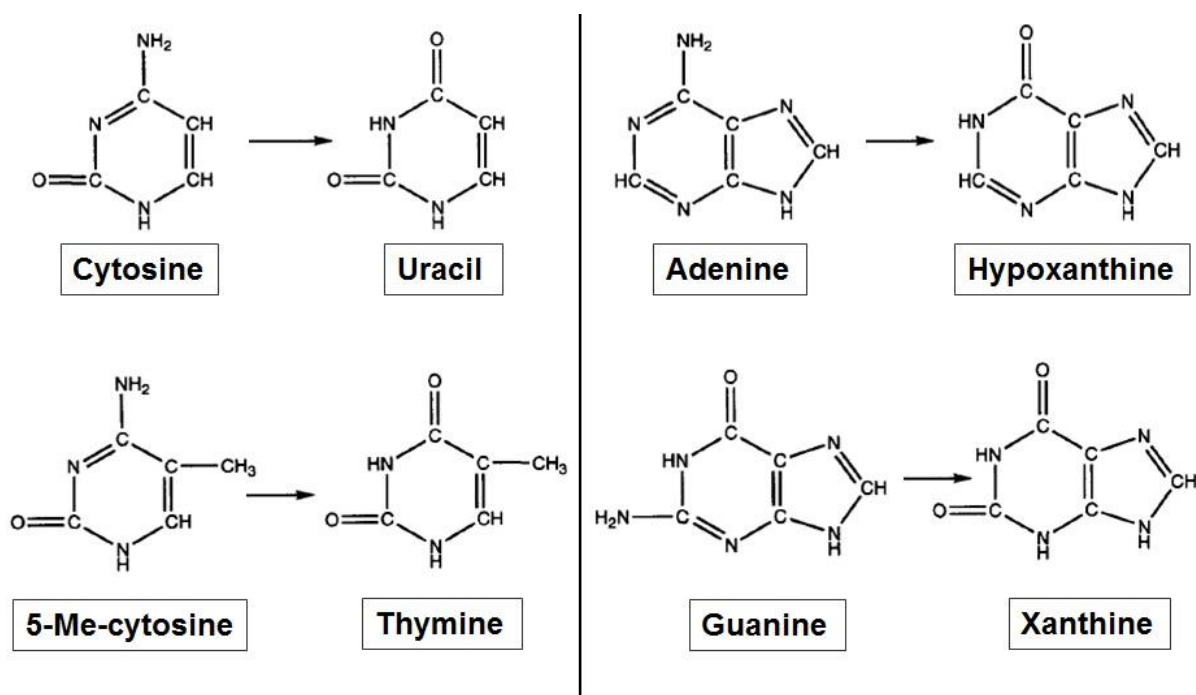


**Figure 6. Products of DNA base deamination**

Adapted from [69].

### 1.8 DNA repair, as a cellular response to genotoxicity induced by organic nitrates.

Depending on the type of DNA modification, different repair mechanisms will be activated in order to remove the resulting damage. Whenever a toxic modification on a specific nucleobase appears or leads to formation of abasic sites, base excision repair (BER) is activated to resolve this problem [79]. Key players of the BER are DNA glycosylases (uracil-DNAglycosylase(UNG) [80], 8-oxo-guanine DNA glycosylase (OGG1) [81], nth endonuclease III-like 1 (NTHL1) [82] and nei endonuclease VIII-like 1, 2 or 3 (NEIL1/NEIL2/ NEIL3) [83]), all of which recognize different base modifications; DNA endonucleases such as apurinic/apyrimidinic endonuclease 1 (APE1) [84]; DNA polymerases (Pol $\beta$ ) and DNA ligases (Lig1) [85].

The specificity of this repair pathway is achieved by the activity of the glycosylases that “scan” DNA molecules by slightly pulling the nucleotide strain. If there is a distortion of the helix, caused by a lack of hydrogen bonding between damaged Watson–Crick base pairs, these enzymes will flip this nucleobase out, insert it into the catalytic pocket, consequently cleave the N-glycosidic bond between the damaged base and the 2'-deoxyribose, and generate an apurinic- or apyrimidinic- (AP) site. All, AP sites are then processed by apurinic/apyrimidinic endonuclease 1 (APE-1), leaving clean 3' and 5' ends that allow DNA polymerase  $\beta$  (Pol $\beta$ ) and DNA ligase I (Lig1) to insert and ligate the appropriate base [86].

OGG-1 is a glycosylase evolved to specifically remove 8-hydroxyguanine. By definition it is a bi-functional enzyme with the associated AP-lyase activity [87]. It contains two DNA binding motifs, a HhH and Cys<sub>2</sub>-His<sub>2</sub> zinc finger like motif. A general view of the OGG-1-dependent recognition of the damaged nucleobase is shown by the crystallographic X-ray structure (see Figure 7).

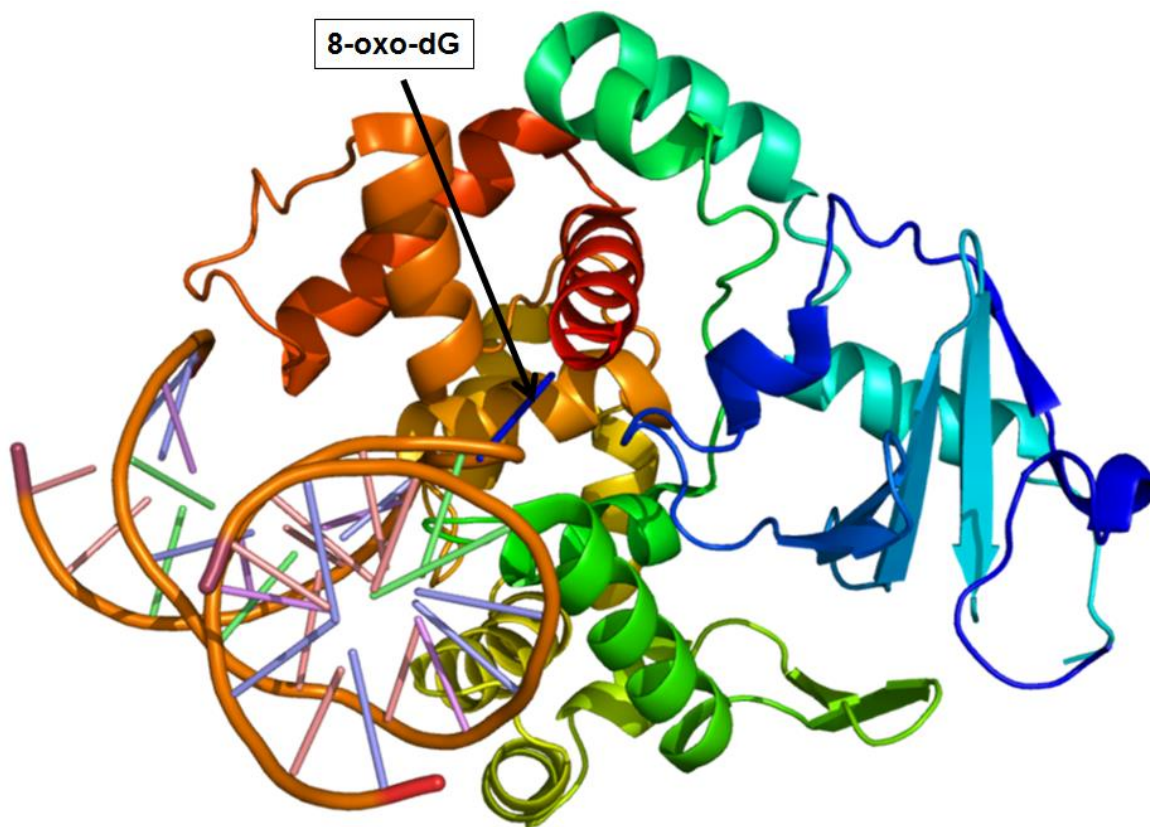


**Figure 7. Crystallographic X-ray structure of the OGG-1 enzyme bound to the double-stranded DNA with the 8-hydroxyguanine modification.**

OGG-1 structure is represented in the form of  $\beta$ -sheets and  $\alpha$ -helices designated with various colors. 8-hydroxyguanine is designated in blue color and marked with an arrow. It flips out of the DNA helix into the catalytic pocket of the enzyme. The protein database file (1YQR) was used for rendering the structure with PyMOL (Schrödinger, USA).

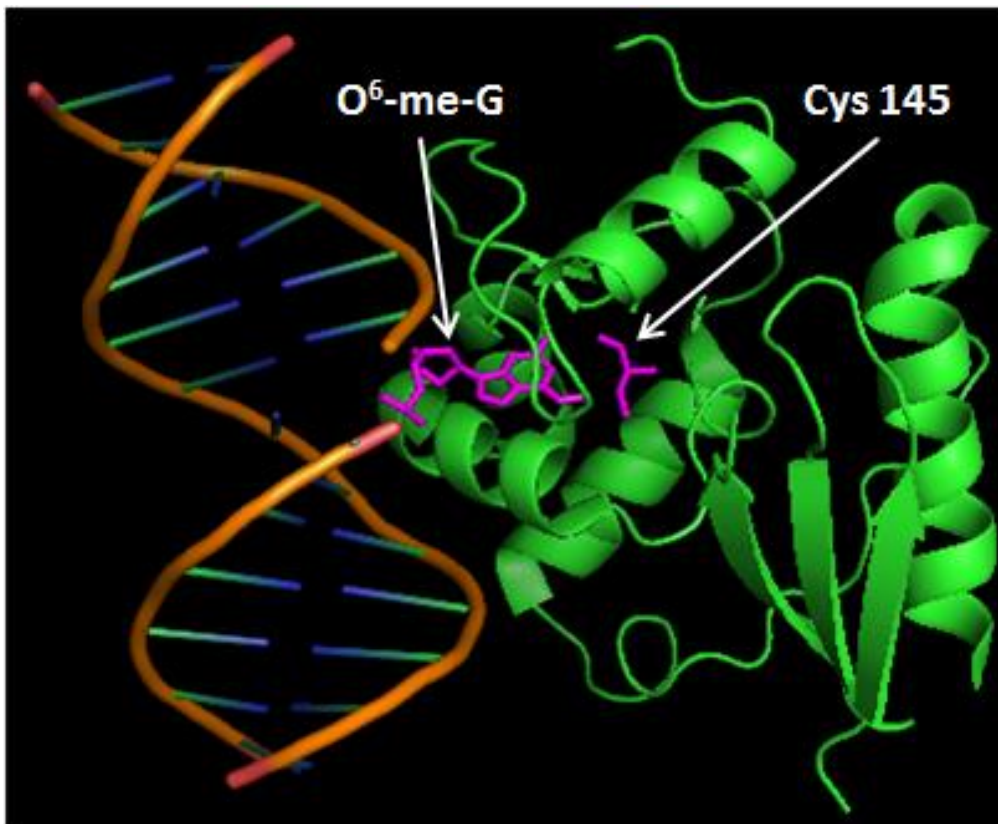
After recognition of the C:8-oxo-G base pair, OGG-1 disrupts the hydrogen bonds between the nucleobases and inserts the 8-oxo-G part into the catalytic pocket. At the same time the glycosylase activity takes place, supported by a local conformational change induced by the presence of cytosine on the opposite strand.



After excision of the damage, OGG-1 retains the modified nucleobase and uses it as a cofactor for the subsequent  $\beta$ -lyase cascade [88].

O<sup>6</sup>-methyl-guanine (O<sup>6</sup>-me-G) is one of the major mutagenic lesions in DNA induced by alkylating compounds, such as nitrosating amines. During the DNA replication process it has a higher preference for thymine instead of cytosine due to more efficient Watson-Crick base pairing [89, 90]. O<sup>6</sup>-methyl-guanine-DNA methyltransferase (MGMT) is a ubiquitously expressed nuclear enzyme which removes alkyl groups from the O<sup>6</sup>-position of guanine [91]. The alkyl group extracted from the O<sup>6</sup> position of guanine is transferred to a cysteine residue within the active site of MGMT in a stoichiometric second-order reaction. This process leads to the inactivation of MGMT enzyme and this process is termed "suicide inhibition" [92]. Therefore, the efficiency of O<sup>6</sup>-me-G repair is limited by the number of MGMT enzyme molecules available, considering that the removal of this modification is the sole function of MGMT and this mechanism does not have alternatives. If such nucleobase damage is not repaired, O<sup>6</sup>-me-G forms a base pair with thymine. The mismatched O<sup>6</sup>-me-G:T base pair is recognized by the mismatch repair pathway (MMR) involving proteins such as MLH1, MSH2 and MSH6 [91]. In certain cases, the DNA repair process can be initiated, followed by the recognition component in the chain of events, but afterwards, due to the mistakes in the consecutive steps or other reasons, it can be stopped and not completed, eventually leading to cell cycle arrest and apoptosis [91]. The crystallographic structure of human MGMT enzyme is shown in Figure 8.

A



B

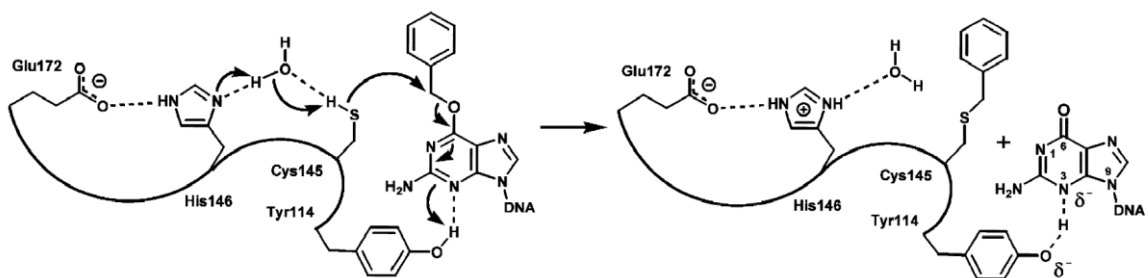


**Figure 8. Crystallographic X-ray structure of the human MGMT enzyme and schematic representation of MGMT mechanism of action.**

(A) Crystallographic structure of the human MGMT enzyme covalently cross-linked with the DNA molecule. The O<sup>6</sup>-me-G molecule and the cysteine residue responsible for the alkyl transfer are highlighted in magenta color. The

protein database file (1T38) was used for rendering the structure with PyMOL (Schrödinger, USA).

**(B)** Schematic representation of the alkyl transfer reaction initiated by MGMT in order to repair the modified O<sup>6</sup>-me-G base on the DNA molecule. The figure was adapted from [93].

### **1.9 First clinical evidence of DNA damage association with prolonged organic nitrate therapy.**

Considering that cardiovascular diseases are the leading cause of morbidity and mortality in the developed countries there is a growing interest in the search of new prognostic biomarkers, that might serve as an early determinant of the disease development [94]. Recently, special interest has been paid to investigations of the DNA damage involvement in the pathogenesis of organic nitrate-associated side effects (drug-induced complications). Andreassi and coworkers suggested the measurement of micronuclei formation in peripheral blood lymphocytes of patients undergoing long term organic nitrate therapy as a read-out of the somatic DNA damage [95]. The micronuclei formation (MN) assay is based on the microscopic evaluation of the fixed lymphocytes, where the formation of chromosomal fragments is present. Such chromosomal fractionation might originate from the extrinsic factors such as reactive species and/or impaired DNA repair that cause chromosome breakage. Also intrinsic factors might come into play, when chromosomes are not correctly distributed during the mitosis process leading to the formation of micronuclei, visible in the interphase part of the replication process [95]. The schematic representation of this process is shown in Figure 9.

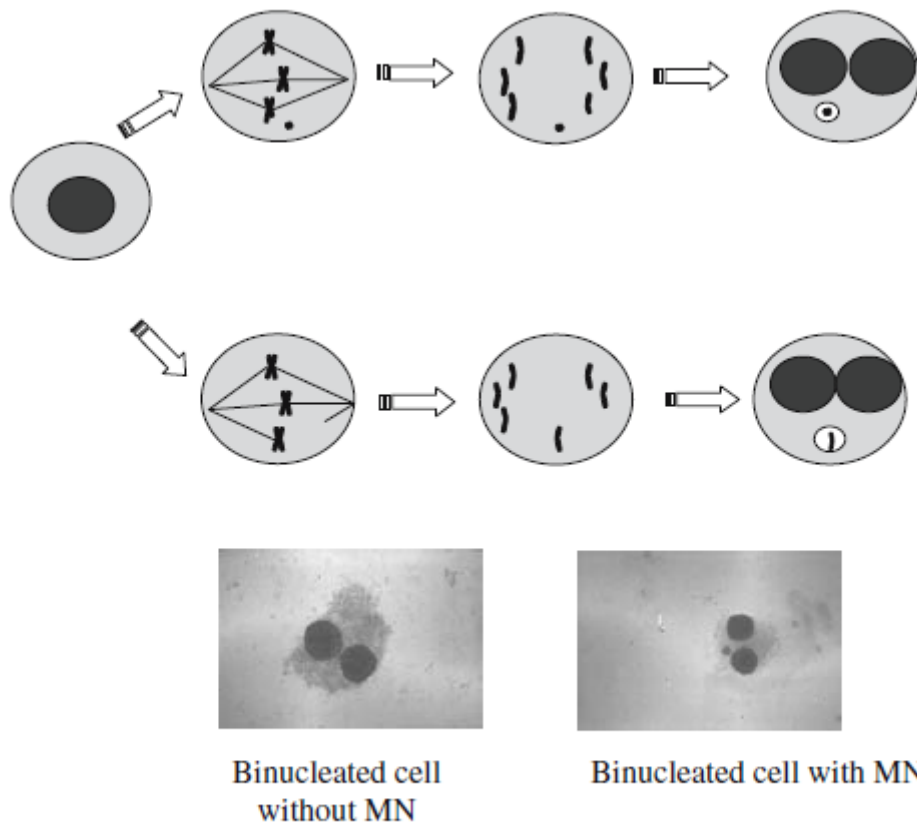


**Figure 9. Schematic representation of the formation of micronuclei.**

There are two major pathways leading to the formation of micronuclei. The upper part of the figure represents the formation of this modification during the metaphase/ anaphase during the mitosis process. The lower part of the image describes the formation of micronuclei after breakage of the chromosome or unsuccessful integration of a chromosome in the daughter nuclei. Figure adapted from [96].

With the help of the MN assay, Andreassi and coworkers have shown a significant increase in DNA damage in patients under chronic organic nitrate therapy [96], however, without providing mechanistic insights and also without a specification of the used organic nitrates. This observation does not only raise the question whether organic nitrate-induced DNA damage contributes to the pathogenesis of

nitrate tolerance but also warrants caution for their long-term use since mutagenic DNA lesions may contribute to the development of cancer, as observed with other NO donors [67], or increased rates of apoptosis [97]. In this respect, previous meta-analyses of clinical trials with more than 4,000 patients revealed that chronic organic nitrate therapy was associated with decreased life expectancy [98, 99].

## **2. Aims of the study.**

With the present study I aimed to investigate the interaction between DNA damage, oxidative stress and vascular dysfunction in experimental nitrate tolerance. For this purpose I employed an *in vitro* model of cultured human endothelial cells (EA.hy 926) treated with nitroglycerin (GTN) and *in vivo* GTN administration in Wistar rats. Another question that I sought to answer with this study was the direct implication of DNA damage in the severity of nitrate tolerance and associated side effects. In order to pursue this line of research I used GTN-treated O<sup>6</sup>-methylguanine-DNA methyltransferase (MGMT) knockout mice with impaired DNA damage repair capacity.

### **3. Materials and Methods**

#### **3.1 Materials.**

GTN was used either as a nitrolingual infusion solution (1 mg/ml) from G. Pohl-Boskamp (Hohenlockstedt, Germany) for isometric tension studies, or as an ethanolic solution (100 g/l) from Novasep (Leverkusen, Germany) for induction of nitrate tolerance *in vivo*. L-012 (8-amino-5-chloro-7-phenylpyrido[3,4-d]pyridazine-1,4-(2H,3H)dione sodium salt) was from Wako Pure Chemical Industries (Osaka, Japan). The Bradford reagent was obtained from BioRad, Munich, Germany. Osmotic mini-pumps (product #:2001, release rate 1 µl/h; product #:1007, release rate 0.5 µl/h) for the subcutaneous delivery of GTN were obtained from Alzet (Cupertino, CA, USA). All other chemicals were of analytical grade and were obtained from AppliChem, Merck, Fluka or Sigma-Aldrich.

#### **3.2 Animals and treatment protocol.**

All animal treatment was in accordance with the Guide for the Care and Use of Laboratory Animals as adopted and promulgated by the U.S. National Institutes of Health and approved by the Ethics Commission according to the German Law on the Protection of Animals (Landesuntersuchungsamt Rheinland-Pfalz, Koblenz, Germany: #23 177-07/G12-1-084). In total, 68 male Wistar rats (6 weeks old, 300 g, Charles River Laboratories, Sulzfeld, Germany) were studied. Nitrate tolerance in Wistar rats was induced by twice daily subcutaneous injection of ethanolic GTN solution (50 mg/kg/d – high dose) or by subcutaneously implanted osmotic pumps (Alzet model 2001, CA, USA) and infusion of GTN with doses of 10 mg/kg/d (low dose) and 20 mg/kg/d (medium dose) for 3.5 days [28]. Ethanol injections (similar

volume as for the ethanolic GTN solution) served as a solvent control. MGMT<sup>-/-</sup> knockout mice on a C57BL/6 background [100] and C57BL/6 mice as corresponding wild type controls were also used in this study. A total number of 50 MGMT<sup>-/-</sup> knockout and age matching C57BL/6 mice (12-14 weeks old, ~30 g) were treated with subcutaneous injection of ethanolic nitroglycerin solution (30 mg/kg/d) or ethanol injections for 3.5 days. The schematic representation of the implantation of osmotic mini-pumps is shown in Figure 10.

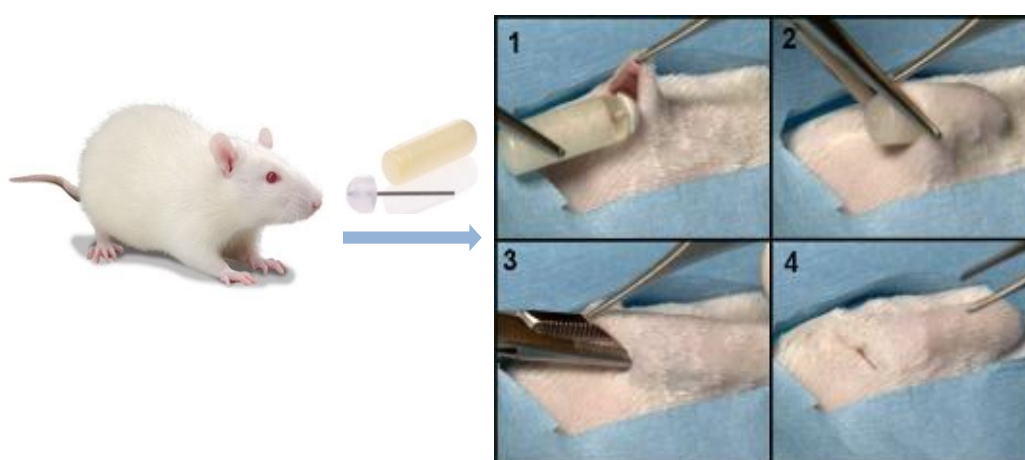


**Figure 10. Schematic representation of the implantation of an osmotic mini-pump into a Wistar rat.**

Image courtesy: Harlan laboratories, [www.alzet.com](http://www.alzet.com).

### **3.3 Tissue excision from the experimental animals and preparation of isolated tissues.**

Under a stable isofluran anesthesia, animals were cut open longitudinally from the *symphysis* to the *jugulum*. As a next step, ribs and *sternum* were cut and the pericardium was opened. 200  $\mu$ l (for mice) and 1 ml (for rats) of the anticoagulant – heparin, were injected directly into the heart to prevent the animal's blood from clotting. Subsequently, approximately 700  $\mu$ l (for mice) and 8 ml (for rats) of blood

were withdrawn from the animal's circulation using a syringe, thereby causing death by exsanguination. The obtained blood was stored for later ROS and RNS measurements. Afterwards, the heart was excised by carefully dissecting the ascending aorta as well as the pulmonary trunk and *venae cavae* and immersed in pre-chilled Krebs-Hepes buffer (NaCl 99.01 mM, KCl 4.69 mM, CaCl<sub>2</sub> 2.5 mM, MgSO<sub>4</sub> 1.2 mM, NaHCO<sub>3</sub> 25 mM, K<sub>2</sub>HPO<sub>4</sub> 1.03 mM, Na-Hepes 20 mM, D-Glucose 11.1 mM). Aortae were gently separated from the animal's body, with an emphasis on preventing any damage (stretching, bending etc.) to the vessels from ensuing. They were later on placed in ice-cold Krebs-Hepes buffer for further preparation.

In a petri dish adhesive adipose and connective tissue were removed from the aortae, immersed in pre-chilled Krebs-Hepes buffer on ice. The remaining clotted blood in the vessel was rinsed out with the syringe filled with Krebs-Hepes buffer. Following the preparation, aortae were cut with scalpel into rings and kept in modified Krebs-Hepes buffer (aprotinin 10 µg/ml, leupeptin 5 µg/ml, pepstatin 7 µg/ml in 10 ml of Krebs-Hepes buffer) at +4 °C for protein extraction and cryo-conservation at -80 °C.

### **3.4 Cryo-conservation of the aortic ring segments.**

Extracted and cleaned from the adhesive tissues, aortae were cut into 4 mm segments and incubated in the Krebs-Hepes buffer for 15 min at 37 °C. After the incubation, aortic ring segments were placed into small reservoirs made out of aluminum foil and filled with 1 ml of polymeric resin (Tissue Tek, Sakura, Staufen, Germany). The afore mentioned containers with aortae fixed in polymeric resin were placed in liquid nitrogen avoiding it's spilling over the reservoirs edges. Such low temperature enhanced gradual freezing of the resin and lead to tissue preservation for a prolonged period of time at -80 °C. The prepared cryo-samples were then cut



with the cryostat (Cryostat Leica CM3050S, Leica Biosystems Nussloch GmbH, Nussloch, Germany) at -25 °C, into cryo-sections with 6 µm in width and transferred onto SuperFrost® microscope slides (Thermo Fisher Scientific, Langenselbold, Germany). The slides were either used directly, or stored at -80 °C for a maximum of 2 weeks.

### **3.5 Isometric tension studies.**

The endothelial function can be assessed with the help of isometric tension studies. The concept of this assay is based on the recording of different relaxation patterns of aortic ring segments upon subjection to different vasoconstrictors and vasodilators in organ chambers. If endothelial function of the blood vessel is fully operational an appropriate endothelium-dependent relaxation in response to the endogenous neurotransmitter and vasodilator acetylcholine will be observed. A less pronounced acetylcholine-dependent relaxation will be detected upon development of the endothelial dysfunction. On the other hand, vasorelaxation can be assessed using substances that directly yield the formation of nitric oxide as for instance GTN, spermine NONOate, or sodium nitroprusside (SNP), initiating direct activation of the sGC/cGMP/cGK-1 pathway in the vessel's media and lead to vasorelaxation, bypassing the endothelium. Relaxation by cumulative concentrations of GTN will also allow the identification of the development of true vascular nitrate tolerance in GTN treated animals. This state is characterized by an impaired relaxation of the smooth muscle in response to the endothelium-independent relaxant. Vasodilator responses to the endothelium-dependent vasodilator acetylcholine (ACh) and the endothelium independent vasodilator GTN were assessed with endothelium-intact isolated rat and mouse aortic rings (thoracic aorta, 4 mm in length) mounted for isometric tension

recordings in organ chambers filled with Krebs-Hepes buffer [47, 101]. A constant temperature of 37 °C and bubbling of the buffer solution with carbogen gas (95% oxygen, 5% carbon dioxide v/v) was maintained in the organ chambers throughout the experimental measurements.

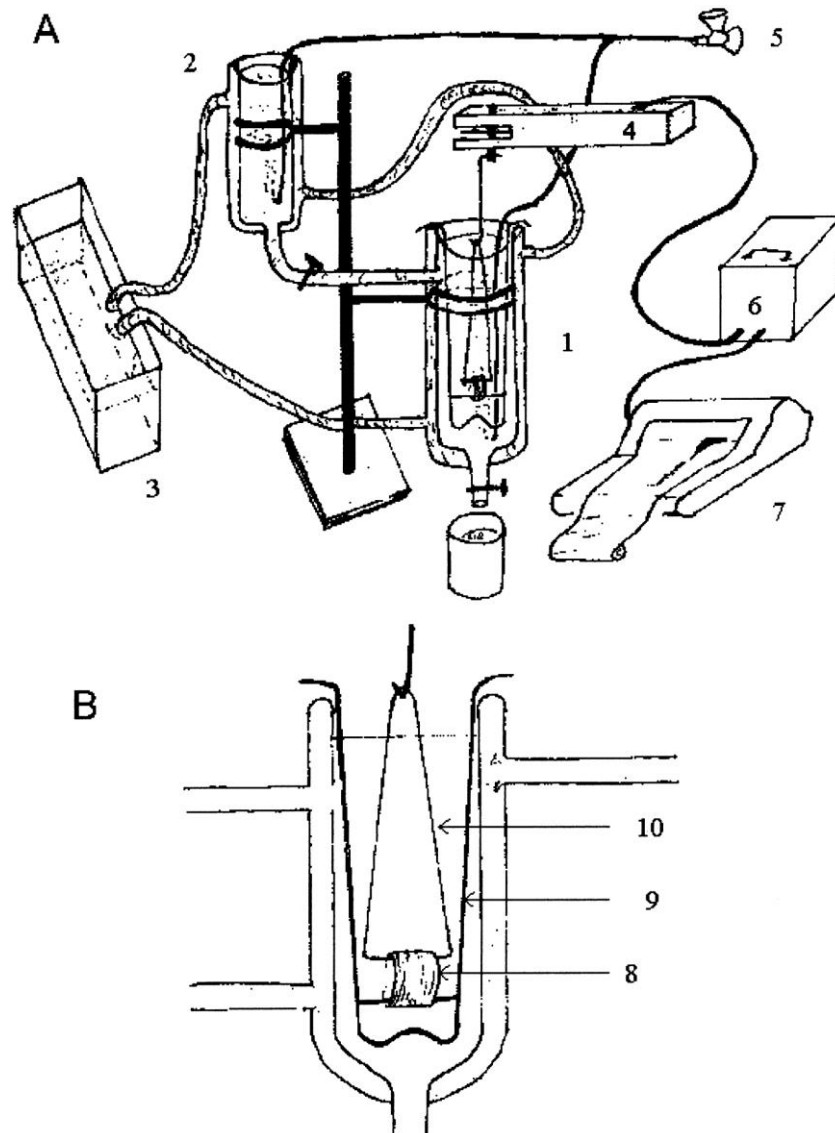


**Figure 11. Schematic representation of the measurement of isometric tension in isolated vessels in an organ bath chamber.**

(A) The picture shows the general set-up of this method, where an aortic ring is placed in a 30 mL tissue bath (1) filled with Krebs-Hepes buffer, and

maintained at 37 °C with the help of a water bath circulating system (2) and constantly bubbled with carbogen gas mixture (CO<sub>2</sub> (5%) and O<sub>2</sub> (95%)) (5). The change of the force (=tension) in the aortic ring segment is detected with a force transducer (4), connected to an amplifier (6) and in our case to the computer (7).

**(B)** The picture shows a magnification of the organ bath chamber in section A. The aortic ring segment (8) is mounted on a fixed, stainless steel hook (9), connected to the tissue bath and to another mobile stainless steel hook (10) that is connected to the force transducer. Figure adapted from [102].

As it is seen in Figure 11, the isometric tension recording apparatus consist of organ bath chambers, a force transducer on top and a fixed support at the bottom. Inside the chambers substances can be added to the surrounding buffer and instantaneously washed out after a defined period of time. The force transducer is used to register slight changes in vascular tone response of the vessels (constriction and relaxation, measured in g). The obtained values are then electronically processed and graphically visualized. The cyclooxygenase inhibitor indomethacin (10 µM) is added to the chambers to prevent the production of prostaglandins and other vasoactive eicosanoids that might mitigate the results of the measurement to ensure more specific measurement of ·NO/cGMP-dependent relaxation.

Several preparatory steps should be made before the experimental procedure, among them - aortic pre-stretching. The force applied to the tissue is gradually increased, up to 1.1 g, as has been previously predetermined. Constant isometric constriction is induced by increasing concentrations of potassium chloride (5, 10, 20, 40 and 80 mM) in order to create a dose-response curve. After a washing step, the basal tone of 1.1 g was reestablished and the aortic segments were again pre-

constricted either with phenylephrine (rat tissue) or with to prostaglandin F<sub>2α</sub> (mouse tissue) at a concentration of approximately 3 μM leading to a constriction of 50-60 % of the maximal constriction caused by 80 mM KCl. Afterwards, contracted aortic segments were subjected to cumulative concentrations of acetylcholine (10<sup>-9</sup> to 10<sup>-5.5</sup> M), and after 3 subsequent wash-out procedures and de novo pre-constriction with the species-specific vasoconstrictor, subjected to cumulative concentrations of GTN (10<sup>-9</sup> to 10<sup>-4.5</sup> M). This method has been conducted in collaboration with and help of Joerg Schreiner.

### **3.6 Detection of oxidative and nitro-oxidative stress in whole blood and aorta.**

Leukocyte-dependent RONS formation was measured in fresh citrate blood, which was diluted 1:50 in PBS buffer containing Ca/Mg (1 mM) upon stimulation with zymosan A (50 μg/ml) by L-012 (100 μM) enhanced chemiluminescence (ECL) at 37 °C [103, 104]. The chemiluminescence signal was measured in a Lumat LB 9507 luminometer (Berthold, Bad Wildbad, Germany) and accumulated over 1 s, detected in intervals of 10 min over a time period of 60 min and the value at 30 min was used for the evaluation of data.

Vascular RONS formation was determined using dihydroethidium (DHE, 1 μM)-dependent fluorescence microtopography in aortic cryo-sections as described [55, 105]. DHE was incubated for 30 min at 37 °C. RONS-derived red fluorescence was detected using a Zeiss Axiovert 40 CFL microscope, Zeiss lenses and AxioCam MRm camera. Intensity of the DHE fluorescence products was evaluated by densitometry using the Gel-Pro Analyzer software (Media Cybernetics, Bethesda, MD).

For the immuno-histochemical (IHC) analysis of 3-nitrotyrosine (3-NT) as a direct product of peroxynitrite induced nitro-oxidative stress, aortic segments were fixed in paraformaldehyde (4 %) and then paraffin-embedded. In order to unmask the antigen, the obtained samples were treated with target retrieval solution (pH 6 or 9, depending on the antibody) in a steamer. Consecutively, tissues were stained with mouse monoclonal 3-nitrotyrosine antibody (Upstate Biotechnology, MA, USA) at a dilution of 1:100; anti-mouse biotinylated secondary antibody (1:1,000) was used following the manufacturer's instructions. For immuno-chemical detection, ABC reagent (Vector) and then DAB (peroxidase substrate Kit, Vector) reagent were used as substrates. The procedure was previously described [106]. Evaluation of the immuno-histochemical results was done with the ImageJ software (NIH, USA).

### **3.7 Detection of oxidative and nitro-oxidative stress in heart.**

The excised animal hearts were placed in an ice-cold petri dish and thoroughly cut with a scalpel. For assessment of mitochondrial RONS formation, further tissue homogenization was conducted in an ice-cold HEPES-mito buffer (Hepes 45 mM, sucrose 70 mM, mannitol 220 mM, EGTA 1 mM, BSA 30  $\mu$ M), pH 7.4. After centrifugation at 1,500xg for 6 min at 4 °C the supernatant was transferred to a new Eppendorf tube and once again centrifuged at 2,000xg for 6 min at 4 °C. The supernatant was again collected and centrifuged for a third time at 20,000xg for 20 min at 4 °C. Following these centrifugation steps the supernatant was discarded and the remaining pellet was washed and later on re-suspended in Tris-mito buffer (sucrose 340 mM, KCl 100 mM, Tris-HCl 20 mM, EDTA 1 mM), pH 7.5. The protein concentration was determined by Lowry method using SDS to break the mitochondrial membrane and equal amounts of proteins (0.1 mg/ml) were used for

further ROS detection. In the presence of L-012 (100  $\mu$ M) and the mitochondrial complex II substrate succinate (5 mM) at a final volume of 500  $\mu$ l, achieved by the addition of an appropriate volume of PBS to each sample, the chemiluminescence signal was measured in a Lumat LB 9507 luminometer (Berthold, Bad Wildbad, Germany) [47]. The signal was detected in intervals of 30 s over a time period of 5 min and the value of the last interval was used for the evaluation of data. According to previous reports, L-012 has the highest specificity for peroxynitrite [104, 107].

### **3.8 Protein concentration determination by Lowry method.**

The principle of the Lowry protein concentration determination method is based on the Biuret reaction: under alkaline conditions, peptide bonds form a violet complex with copper (II) ions, thus giving protein concentrations detection range of 1 - 10  $\mu$ g/ml. In order to optimize measuring conditions of this reaction, a second step has been added. Using the Folin-Ciocalteu reagent, detection threshold can be lowered to 0.1-1  $\mu$ g/ml.

For the detection of cardiac mitochondria protein concentration all samples were incubated for 10 minutes at 37 °C with 0.1% (w/v) SDS-solution in 1:20 dilution. The incubation with SDS results in the destruction of cellular membranes and a more complete protein release from the tissue samples. Subsequently, 25  $\mu$ l of this mixture were transferred to a cuvette. Next, 125  $\mu$ l of a reagent A+S mixture (pre-warmed in a 50:1 proportion) were added to the cuvette followed by 1 ml of reagent B, thoroughly stirred and incubated for another 10 minutes at room temperature (Bio-Rad D<sub>c</sub> Protein Assay, Bio-Rad Laboratories, Hercules, CA, USA). The protein concentration was determined photometrically at 700 nm (Thermo Fisher Scientific, Langenselbold, Germany). Samples of various BSA concentrations (0 (solvent only),

2.5, 5 and 10 mg/ml) were used to establish a standard curve, used for the calculation of the protein concentration of the experimental samples. Following the concentration determination step all samples were diluted with a Tris buffer to a given protein concentration (preferably > 5 mg/ml) in the stock solution that was used for further measurements at a final protein concentration of 0.1 mg/ml in PBS buffer.

### **3.9 Detection of nitrosyl-iron hemoglobin in whole blood by electron paramagnetic resonance (EPR) spectroscopy.**

Electron paramagnetic resonance (EPR) spectroscopy is a technique used to study chemical species with unpaired electrons. EPR spectroscopy plays an important role in the understanding of organic and inorganic radicals, transition metal complexes, and some biomolecules [108].

Each electron ( $e^-$ ) has a magnetic moment (electron spin) and a spin quantum number  $s = \frac{1}{2}$  with associated magnetic components  $m_s = -\frac{1}{2}$  and  $m_s = +\frac{1}{2}$ . In an external magnetic field with the strength  $B_0$ , the magnetic moment of the electron is directed either parallel  $m_s = -\frac{1}{2}$  or antiparallel  $m_s = +\frac{1}{2}$  to the magnetic field.

Each of these orientations has a specific energy level, where parallel orientation corresponds to the lower energy state and the antiparallel alignment corresponds to the higher energy state. The energy difference between the low and the high energy states can be described with the following equation (1) and is called the Zeeman effect:

$$(1) \Delta E = g_e * \mu_B * B_0,$$

$g_e$  - electron g-Factor  
 $\mu_B$  - Bohr's magneton.

As it can be derived from the equation, splitting of the energy level is directly proportional to the magnetic field strength. A free electron can move between the two

energy levels by absorption or emission of electromagnetic resonance energy (e.g. from a microwave source). This absorption or emission energy can be detected by an EPR spectrometer with a resonator cavity such as the X-band spectrometer MiniScope MS400 (Magnettech GmbH, Berlin, Germany).

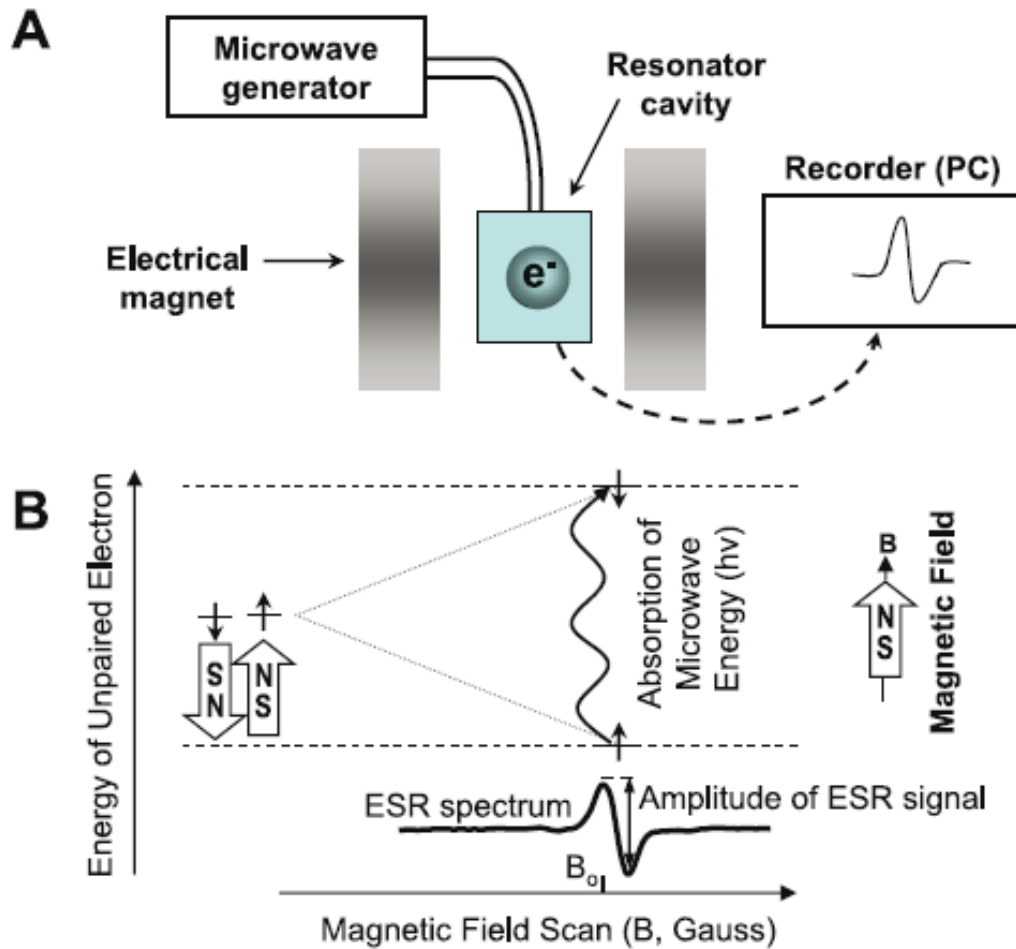


**Figure 12 Schematic representation of the EPR concept.**

A standard EPR device - spectrometer (A) consists of a microwave generator, a resonator, and magnets. The spectrometer measures the energy difference between the two different spin states of an unpaired electron that are present in a magnetic field (B). Because of the magnetic moment, electrons will have the lowest energy when their spin is aligned with the magnetic field ( $\uparrow$ , parallel)



and the highest energy when it is directed in the opposite direction to the magnetic field ( $\downarrow$ , antiparallel). Absorption of microwave energy at a certain wavelength will remove this difference between the different spin states, which is termed the resonance case. Figure adapted from [109].

•NO bioavailability in whole blood was measured using EPR spectroscopy by assessment of nitrosyl-iron hemoglobin (Hb-NO) levels. Iron (III) in Hb is diamagnetic (EPR silent) but upon binding of NO the resulting nitrosyl-iron Hb complex becomes paramagnetic (EPR active). Samples of venous blood were obtained by cardiac puncture of anesthetized rats and were later on transferred to a specially pre-cut 1 mL syringe (top part of the syringe and plunger were cut to allow an even surface formation for the EPR blood sample), snap frozen and stored in liquid nitrogen [105]. Samples were pushed out of the syringes right before the measurement at 77 K to prevent thawing of the blood, followed by transfer of the sample into a special dewar vessel as it is shown in Figure 13. The EPR measurements were carried out at 77 K using an X-band table-top spectroscope MS400. The instrument settings were as follows: 10 mW microwave power, 7000 mG amplitude modulation, 100 kHz modulation frequency, 3300 G center field, 300 G sweep width, 30 s sweep time and 10 scans. The intensity of the resulting triplet signal of NO-Hb was used for the quantification of NO-Hb levels in whole blood.

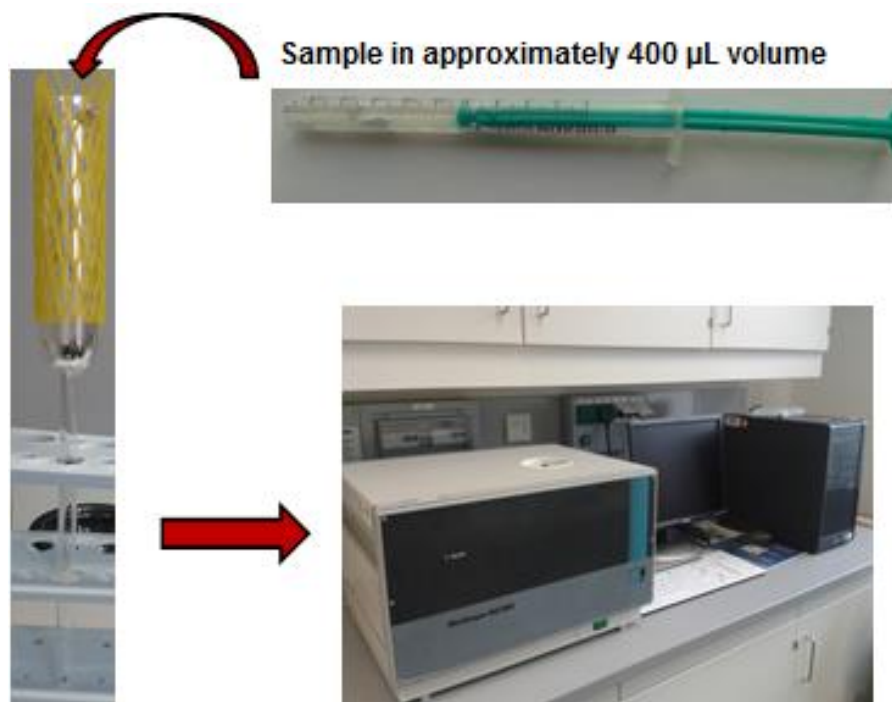


**Figure 13. Visual representation of the EPR experimental set-up.**

1 mL syringes were specially pre-cut - top part of the syringe and plunger were removed to allow an even surface formation for the EPR blood samples that were obtained via a cardiac puncture of the experimental animals. Further, blood samples were snap frozen and transferred into a dewar at 77K right before the measurement. Afterwards, the dewar with the sample was placed into a spectrometer and evaluated for Hb-NO levels.

### **3.10 Protein extraction from the cardiac tissue.**

As previously described, tissue extracted from the experimental animals was snap frozen in liquid nitrogen and stored at  $-80^{\circ}\text{C}$ . For the purpose of protein extraction, frozen cardiac tissue pieces were homogenized, or more precisely pulverized using a liquid nitrogen-cooled ceramic mortar and pestle and kept in

Eppendorf tubes under conditions of liquid nitrogen. After all samples were pulverized, an equal volume of the homogenization buffer (Tris HCl 20 mM, Sucrose 250 mM, EGTA 3 mM, EDTA 20 mM, protease inhibitor cocktail 100  $\mu$ l, phosphatase inhibitor cocktail 100  $\mu$ l, PMSF 2.5  $\mu$ M, Triton X-100 100  $\mu$ l) was added to the amount of powder present in each Eppendorf tube. The resulting mixture was kept on ice for 1 h and vigorously vortexed every 5-10 min. Following the 1 h incubation all samples were centrifuged at 10,000xg for 10 min at +4 °C. The resulting supernatant was transferred to a new Eppendorf tube and kept at -20 °C until the concentration of protein was determined and the pellet was discarded as it contained only cell debris.

### **3.11 Protein concentration determination by Bradford method.**

The spectroscopic procedure of the protein concentration determination was first described by M. Bradford in 1976 [110]. The concept of this analysis relies on a specific colored dye - Coomassie Brilliant Blue-G250. The cationic form or protein unbound form of this triphenylmethane dye is green, but the protein-bound form is blue and has an absorption spectrum maximum at 595 nm. The increase in absorbance at this wavelength is proportional to the concentration of protein. This proportion is linear for the protein range of 10 - 100  $\mu$ g/ml. All protein concentration measurements were compared to a standard curve generated from dilutions of a bovine serum albumin (BSA) stock (1, 5, 10, 20 and 30  $\mu$ g/ml). Distilled water was used as a blank solution. All previously prepared samples were at first diluted 1:2,000 with distilled water that was the most suitable dilution for the detection range of BSA standard curve. Every measurement was conducted in transparent Nunclon™ 96-well plates acquired from Thermo Fisher Scientific. After dilution, 80  $\mu$ l of the protein solution were transferred into the respective well of the plate. Subsequently 200  $\mu$ l of the

reagent Roti® Quant (Carl Roth GmbH, Karlsruhe, Germany) were added and thoroughly mixed, before the plate was measured at MRX II plate reader (Dynex Technologies, Berlin, Germany) at 595 nm. The results were assessed using the program Revelation (ilf bioserve, Germany).

### **3.12 Western Blot analysis in cardiac tissue.**

After receiving a crude protein mixture, as it was previously discussed in section 3.9 and determination of the protein concentration, as it was highlighted in section 3.10, samples were subjected to SDS-PAGE gel electrophoresis. Polyacrylamide gels have pores of uniformed size, thus allowing proteins to migrate and separate in the stream of an electrical current predominantly based on their molecular weight and charge. Since different protein molecules might have different charges, sodium dodecyl sulfate (SDS) was added as a neutralizer to gel mixture leading to the homogenization of the proteins charge to the negative value.

Before loading to the gel, all protein samples were mixed in 1:2 ratio with 3x Lämmli buffer (Tris-HCl 125 mM, glycerol 17 % v/v, SDS 10 % w/v, 2-mercaptoethanol 5 % v/v, bromphenol blue 0.01 % w/v), and subsequently boiled at 95 °C for 5 min. As a consequence, all proteins were denatured and disulfide bonds were broken by 2-mercaptoethanol.

The electrophoresis procedure with SDS-PAGE gels was conducted using a Mini Protean™-system (Bio-Rad laboratories, Hercules, California). Polyacrylamide gels were prepared as follows: the resolving gel containing 12 % of polyacrylamide (H<sub>2</sub>O - 4.3 ml, Tris HCl 1.5 mM, pH 8.8 - 2.5 ml, acrylamide 40 % - 3 ml, SDS 10 % w/v - 100 µl, APS 10 % w/v - 100 µl, TEMED - 10 µl) was poured into the assembled electrophoresis-system. In order to get an even surface line on the

resolving gel, 1 ml of isopropanol was pipetted onto it. The gel was allowed to polymerize for 20 min. Afterwards, the 4 % stacking gel (H<sub>2</sub>O - 3.2 ml, Tris HCl 0.5 mM, pH 6.8 - 1.2 ml, acrylamide 40 % - 0.5 ml, SDS 10 % w/v – 50 µl, APS 10 % w/v – 50 µl, TEMED – 5 µl) was applied on top of the resolving gel and the combs were placed, resulting in the formation of pockets into which the denatured protein samples as well as a pre-stained- protein ladder were loaded after complete polymerization of the gel.

The electrophoresis was conducted at +4 °C in SDS-PAGE running buffer (Tris Base 25 mM, glycine 192 mM, SDS 3.5 mM) starting with 60 V for approximately 10 min until the proteins reached the resolving gel and then the voltage was set at constant 120 V. As the Laemmli buffer contained bromophenol blue, the advance of the samples could be clearly observed. This process lasted for approximately 2 h until the pre-stained protein ladder reached the end of the resolving gel.

After the electrophoresis process was over proteins from the resolving gel were transferred onto a nitrocellulose membrane, using the Mini-Trans Blot® system from Biorad. The transfer system consists of a gel holder cassette with attached electrodes, a gel transfer cell, foam pads, a tank and a cooling unit. All pads, filter papers and membranes were first soaked in a pre-chilled transfer buffer (Tris Base 25 mM, glycin 192 mM, distilled water ad. 800 ml and methanol 200 ml). For the assembly of the gel transfer sandwich at first a foam pad was placed onto a gel transfer cell, followed by a filter paper, the nitrocellulose membrane and the gel. The transfer sandwich making process was continued in a reverse manner, keeping all components completely immersed in ice cold transfer buffer to prevent drying out of any of its components. Finally, the gel transfer cell was closed and inserted into the gel holder cassette with the membrane facing the anode. The transfer tank was filled

with transfer buffer and blotting was performed for 2.5 h at +4 °C, at constant electric force of 230 mA. Upon completion, the system was dismantled, and the nitrocellulose membrane, now containing the transferred proteins, was stained with the dye Ponceau S, which allows reversible visualizing of the proteins on a nitrocellulose membrane. Next, Ponceau S was washed away with distilled water. Finally, the membrane was cut into stripes according to the molecular weight markers and we proceeded with the immuno-staining procedure.

Immuno-staining was performed with the following primary antibodies: polyclonal rabbit  $\beta$ -actin (42 kDa, 1:2,500, Sigma, USA) as a control for loading and transfer, polyclonal rabbit fractin (1:1,000, Millipore, Germany), polyclonal rabbit caspase 3 (1:1,000, Cell Signalling, USA). Detection and quantification were performed by chemiluminescent dye Luminol (Pierce ECL Western Blotting Substrate, Perbio Science, Belgium) with peroxidase conjugated anti-rabbit (1:10,000, Vector Lab., Burlingame, CA) secondary antibody. Densitometric quantification of antibody-specific bands was performed with a ChemiLux Imager (CsX-1400 M, Intas, Göttingen, Germany) and Gel-Pro Analyzer software (Media Cybernetics, Bethesda, MD).

### **3.13 Cell culture.**

The human endothelial cell line EA.hy 926 was a kind gift from C.-J. S. Edgell (University of North Carolina at Chapel Hill, USA) [111]. EA.hy 926 cells were grown at 10% CO<sub>2</sub> in Dulbecco's modified Eagle's medium (DMEM, Sigma) with 10% fetal calf serum, 2 mM L-glutamine, 100 IU/ml penicillin, 100  $\mu$ g/ml streptomycin and 1 mM sodium pyruvate. For experiments, the cells were seeded in 6-well plates at a density of  $1.5 \times 10^5$  cells/well and grown to 60–70% confluence.

### **3.14 Comet assay.**

As a positive control, the DNA strand breaks generator tert-butyl hydroperoxide (t-BOOH) was used. Experimental DNA strand breaks were induced by treatment with various GTN concentrations (10 – 1000  $\mu$ M) for 48 h. After 2 thorough washes with PBS buffer the cells were trypsinized and then embedded in 0.5 % low melting point-agarose followed by relocation onto an agarose-pre-coated slide. As a next step, slides were incubated in a lysis buffer containing 1 % sodium lauryl sarcosinate, 10 mM Tris, pH 10, 2.5 M NaCl, 100 mM EDTA for 45 min followed by an unwinding step in electrophoresis buffer consisting of 1 mM EDTA pH 13 and 300 mM NaOH for 20 min at +4 °C. Electrophoresis was conducted at 25 V and 300 mA for 15 min. Afterwards samples were neutralized three times with 0.4 M Tris pH 7.5 and fixed in 100 % ethanol, air-dried and stained with 50  $\mu$ g/ml propidium iodide. Results were microscopically analyzed by Olympus BX50 equipped with a ColorView camera (Olympus, Münster, Germany) [112]. As an output, 50 cells were scored using Comet IV software (Perceptive Instruments Ltd., Bury St Edmunds, UK) for each sample. The Fpg modified alkaline comet assay was executed as previously described for the alkaline comet assay with several modifications. When the cell lysis was finished, slides were incubated in a buffer containing Fpg (1  $\mu$ g/ml), 0.5 mM EDTA pH 8.0, 0.1 M KCl, 40 mM HEPES and 0.2 mg/ml BSA for 37 min at 37 °C. Next the DNA unwinding step was performed as described above [113]. This method has been conducted in collaboration with and help of Anna Frumkina and Dr. Joerg Fahrer.

### **3.15 DNA extraction from the EA.hy 926 cells, aortic and cardiac tissue.**

Depending on the source, either cell culture or animal tissues, two different protocols for DNA extraction were used. EA.hy 926 cells were washed at room-temperature with PBS buffer, followed by trypsin digest. After centrifugation at 4,000xg for 5 min, the cell pellet was re-suspended in the lysis buffer (100 mM NaCl, 10 mM Tris pH 8.0, 10 mM EDTA pH 8.0, 0.5 % SDS, 20 mg/ml proteinase K) and incubated overnight at +56 °C. Next morning, samples were subjected to two rounds of phenol:chloroform:isoamyl alcohol (25:24:1) extraction followed by a chloroform washing step. Each extraction step was finished with centrifugation at 12,000xg for 5 min at room temperature. The extraction procedure was finalized by DNA precipitation with one volume of sodium acetate (3 M) and three volumes of ice-cold isopropanol, and then RNA digest was applied. For this purpose, the precipitate was dissolved in TE buffer (10 mM Tris, pH 8.0, 1 mM EDTA, pH 8.0) and digested with RNase A/T1 mix (80 µg/ml RNase A, 200 U/ml RNase T1) for 2 h at 37 °C. Next, the solution was subjected to the 2<sup>nd</sup> procedure of phenol:chloroform:isoamyl alcohol extraction and DNA precipitation. Finally, DNA was again re-suspended in TE buffer and its concentration was checked with NanoDrop 2000 UV-Vis spectrophotometer (ThermoFisher Scientific, Wilmington, USA). In the case of tissue samples, the aortae and hearts were snap frozen in liquid nitrogen immediately after the dissection and then homogenized with a pestle in a mortar in the presence of liquid nitrogen. In order to achieve a complete tissue digest, extraction buffer (0.1 M NaCl, 20 mM Tris pH 8.0, 25 mM EDTA pH 8.0, 0.5 % SDS, 20 mg/ml proteinase K) was added to the pulverized samples. Subsequently, DNA extraction protocol was performed as for EA.hy 926 experimental set-up.



### **3.16 Immuno-dot blot analysis for DNA damage in EA.hy 926 cells, aortic and cardiac tissue.**

In order to detect and quantify levels of the oxidative and alkylated DNA damage, I developed a new immuno-dot blot method based on the previous work of Nehls and colleagues [114]. Initially, genomic DNA was denatured at 95 °C for 5 min and mixed with an equal volume of 2 M ammonium acetate solution. Afterwards, samples were transferred to the nitrocellulose membrane, previously equilibrated with 1 M ammonium acetate. In order to enhance DNA binding, the membrane was incubated in 5x SSC buffer (0.75 M NaCl, 0.075 M tri-sodium citrate). For final fixation, the membrane was kept on the heat block for 2 h at 80 °C. 0.5 % casein in PBS-T solution (0.1 % Tween 20) was used as a blocking buffer for 2 h at room temperature. Subsequently, appropriate primary antibodies were applied: monoclonal mouse anti-O<sup>6</sup>-methyl-2-deoxyguanosine (1:500, Squarix, Marl, Germany) and monoclonal mouse anti-8-hydroxyguanosine, clone 15A3 (1:4,000, Abcam, UK). PBS-T/NaCl solution (0.1 % Tween 20, 0.16 M NaCl) was used as a washing buffer. Next, incubation with the peroxidase conjugated anti-mouse (1:10,000, Vector Lab., Burlingame, CA) secondary antibody was performed. Detection of the modification-specific dots was done by ECL reagent (ThermoFischer scientific, Wilmington, USA). Densitometric quantification was performed with a ChemiLux Imager (CsX-1400 M, Intas, Göttingen, Germany) and Gel-Pro Analyzer software (Media Cybernetics, Bethesda, MD). Positive controls for O<sup>6</sup>-me-dG were generated by treatment of cells with N-nitroso-N-methylurea (MNU), 500 µM for 30 min at 37 °C and for 8-oxo-dG with Fenton reaction conditions (1 mM H<sub>2</sub>O<sub>2</sub>, 100 µM FeSO<sub>4</sub>) for 10 min at 37 °C.

### **3.17 Immuno-histological analysis of aortic and cardiac tissue for DNA damage.**

Immuno-histochemical analysis of the aortic and cardiac tissue for the presence of the oxidative and alkylated DNA damage modifications was done as has been already described above for 3NT modification. The same primary antibodies as in the section **3.15** were used with a modification in the dilution range only for the O<sup>6</sup>-methyl-2-deoxyguanosine antibody (1:250), anti-8-hydroxyguanosine antibody was used in the dilution previously mentioned (1:4000). All other details were previously reported [115].

### **3.18 Cell death detection assay.**

Programmed cell death or apoptosis is a physiological cellular suicide mechanism that preserves homeostasis, and it is naturally occurring during normal tissue turnover. In general, cells undergoing apoptosis display a characteristic pattern of structural changes in the nucleus and cytoplasm, including rapid blebbing of plasma membrane and nuclear disintegration. The nuclear collapse is associated with the extensive damage to chromatin and DNA cleavage after activation of calcium-dependent endogenous endonucleases. Endonucleolysis is considered a key biochemical event of apoptosis.

Cleavage of the genomic DNA during apoptosis may yield double-stranded low molecular weight DNA fragments (mono- and oligo-nucleosomes) as well as single strand breaks in high molecular weight DNA. Those DNA strand breaks can be identified by labeling free 3'-OH termini with modified nucleotides in an enzymatic reaction with terminal deoxynucleotidyl transferase, which catalyzes polymerization of labeled nucleotides in a template-independent manner.

Previously described paraffin embedded aortic sections were de-paraffinated, rehydrated and treated with proteinase K (20 µg/ml in 10 mM Tris, pH 8.0) for 30 min at 37 °C. In the subsequent steps, the tissue was permeabilized with 0.1 M citrate buffer, pH 6.0 for 20 min at 80 °C in humidified chambers. TUNEL reaction mixture was applied to the tissue according to the manufacturer's instructions (*In Situ* Cell Death Detection Kit, Roche, Switzerland) for 60 min at 37 °C in the humidified chamber. After several washing steps, slides were covered with the mounting medium and cover slipped for the microscopic evaluation. Fluorescence was detected using a Zeiss Axiovert 40 CFL microscope, Zeiss lenses and Axiocam MRm camera. Intensity of the fluorescence products was evaluated by densitometry with the help of Gel-Pro Analyzer software (Media Cybernetics, Bethesda, MD).

### **3.19 Statistical analysis.**

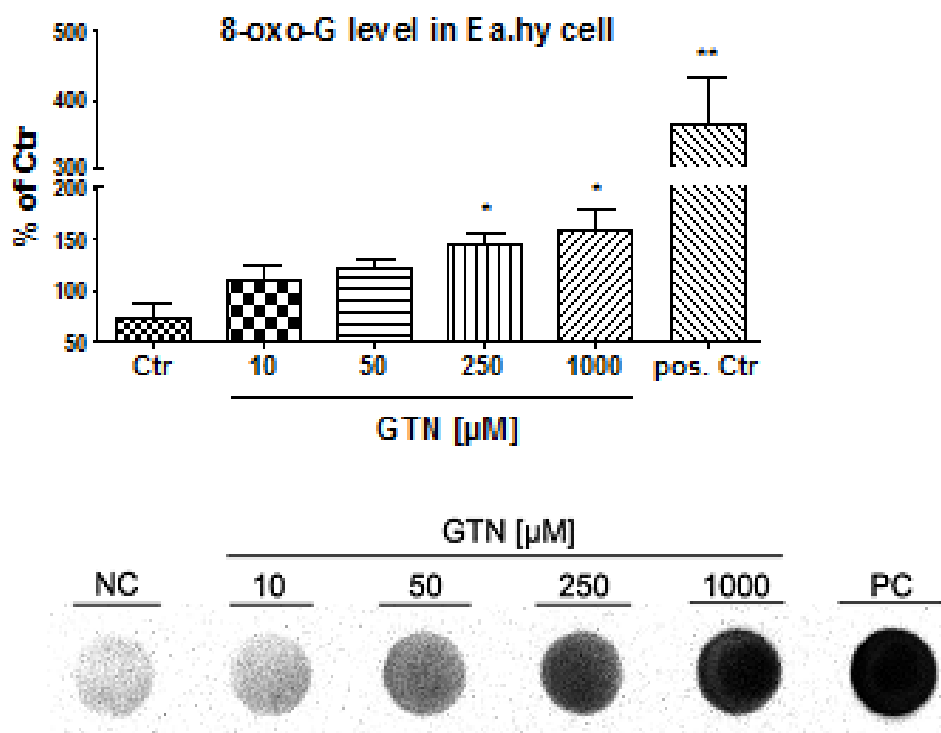
Data is presented as the mean value  $\pm$  SEM. Two-way ANOVA (with Bonferroni's correction for comparison of multiple means) was used for comparisons of vasodilator potency and efficacy results of the isometric tension studies. 1-way ANOVA, Kruskal-Wallis 1-way ANOVA on Ranks (with Bonferroni's or Dunn's correction, or Tukey's test for comparison of multiple means) was used for the evaluation of mitochondrial RONS data, comet assay without Fpg, immunohistochemical measurement of the O<sup>6</sup>-me-G, 8-oxo-G and 3NT levels, protein expression analysis and DHE staining in the tissues of rats and mice. Mann Whitney Rank Sum test was used for the evaluation of the comet assay results with the Fpg enzyme, oxidative burst measurement in whole blood from rats or mice. t test was applied for the evaluation of the Hb-NO EPR data of rat whole blood.

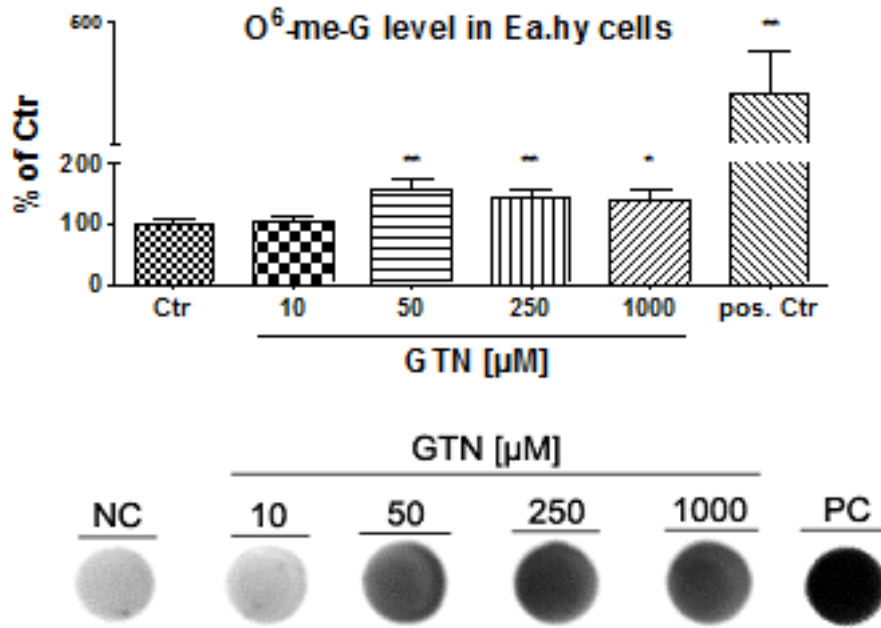
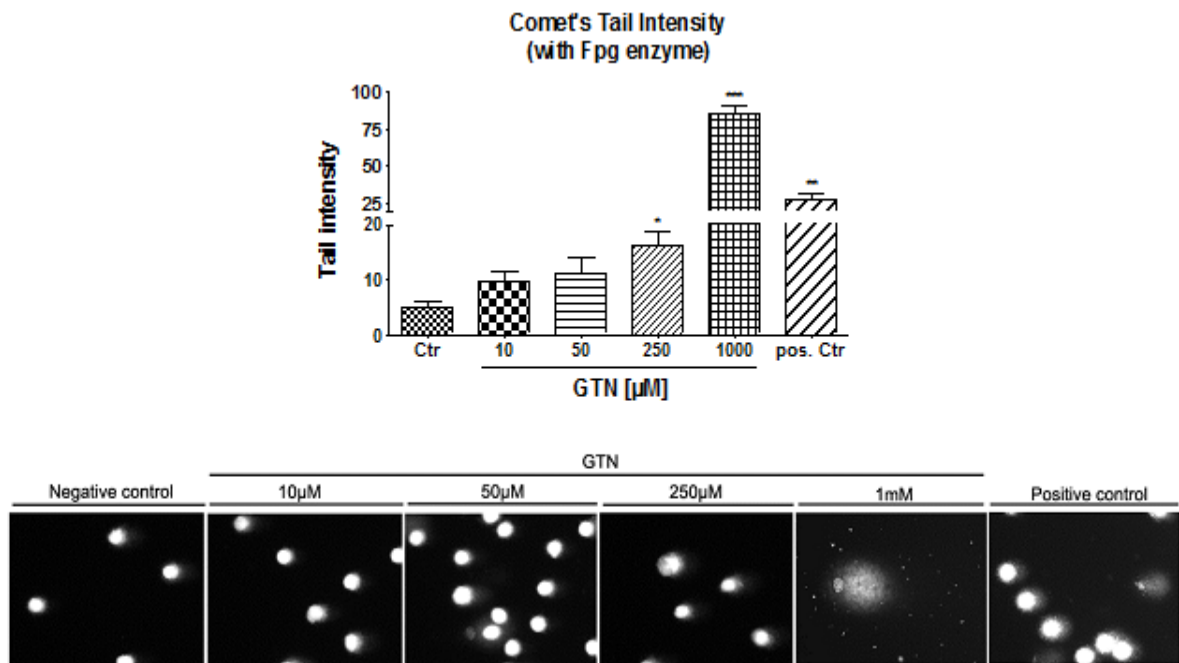
## 4. Results

### 4.1. DNA damage parameters in cell culture upon GTN treatment.

First, I determined classical oxidative and alkylation stress DNA damage parameters, in particular 8-oxo-G and O<sup>6</sup>-me-G. There was a concentration-dependent increase in both DNA modifications that became significant with a GTN concentration of 50 or 250  $\mu$ M (Figures 11A and 11B). The induction of DNA strand breaks by GTN was confirmed by the comet assay performed with or without Fpg enzyme (Figures 11C and 11D). The pronounced increase in comet assay detectable DNA strand breaks in the presence of Fpg also confirmed the induction of the 8-oxo-G DNA lesion by GTN treatment since enzymatic excision of 8-oxo-G lesions by the Fpg enzyme will induce “artificial” DNA strand breaks (Figures 11C).

A



**B****C**

D

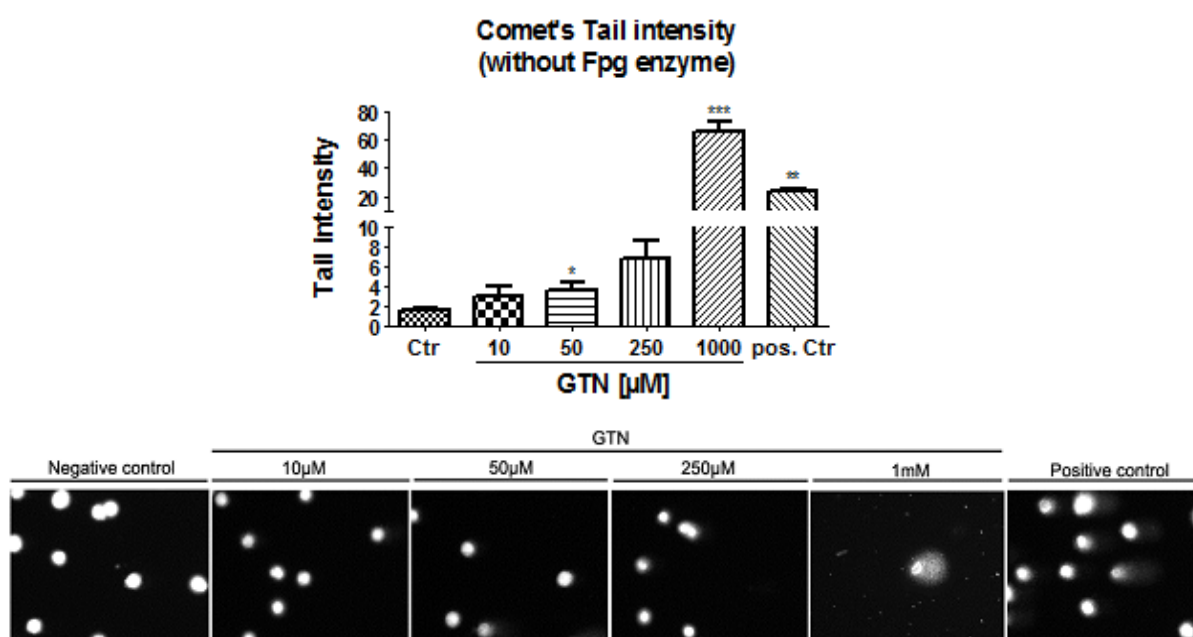


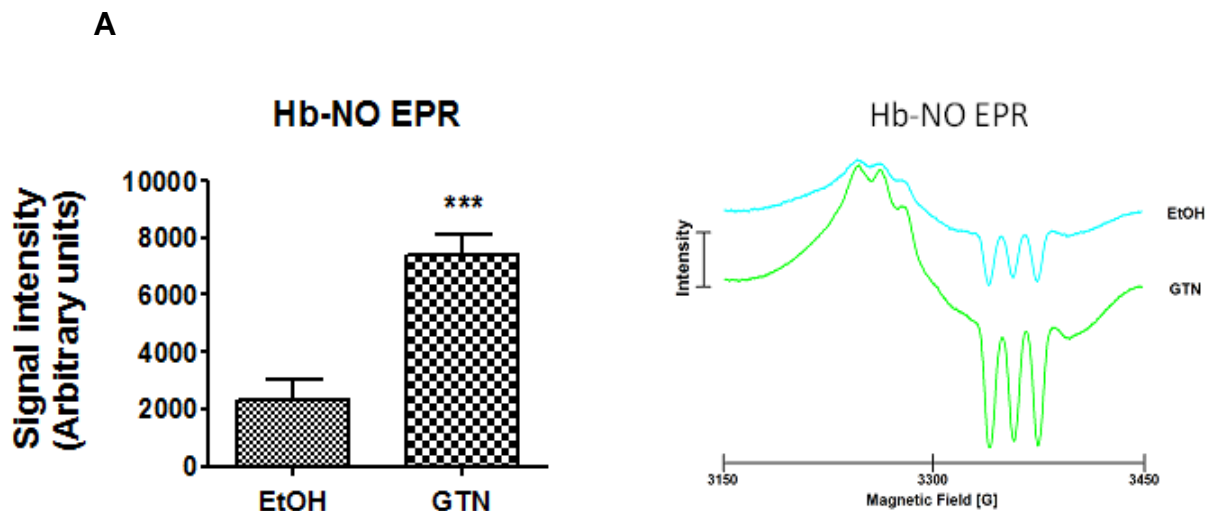
**Figure 11. DNA damage induced by GTN administration to EA.hy 926 cells.**

**A** Immuno-dot blot analysis for 8-oxo-G in EA.hy 926 cells that were treated for 48 h with increasing concentrations of GTN (10 µM – 1000 µM). Representative blots are shown below the densitometric quantification. **B** Immuno-dot blot analysis for O<sup>6</sup>-me-G in EA.hy 926 cells that were treated for 48 h with increasing concentrations of GTN (10 µM – 1000 µM). Representative blots are shown below the densitometric quantification. **C** Read-out of alkaline comet assay with Fpg enzyme for the measurement of 8-oxo-G dependent DNA strand breaks. **D** Results of the alkaline comet assay without Fpg for the detection of natural DNA strand breaks. Representative images are shown below the densitometric quantification. The data are presented as mean value ± SEM of **(A)** 4; **(B)** 4; **(C)** 3-4; **(D)** 3-4 experiments.

\* p<0.05 vs. control, \*\* p<0.01 vs control, \*\*\* p<0.001 vs control.

## 4.2 Vascular reactivity in rat aortas.

·NO consists of seven electrons from the nitrogen atom and eight electrons from the oxygen atom. Therefore, ·NO is a paramagnetic molecule with one unpaired electron and can be detected with the help of EPR spectroscopy. In order to assess the nitrosative stress induced by GTN therapy I measured the nitrosyl-iron hemoglobin (Hb-NO) levels in whole blood, which is a marker of ·NO bioavailability and inducible ·NO synthase activity in the circulation as previously shown for sepsis [116]. With the help of EPR spectroscopy a significant increase in Hb-NO in the GTN (high dose) treated animals was determined (Figure 12A) suggesting nitrosative stress conditions that provide the basis for (alkylation) DNA damage. GTN treatment at all doses resulted in an impaired aortic response to either acetylcholine (Ach) or GTN, confirming the development of endothelial dysfunction (cross-tolerance) and nitrate tolerance in the animals (Figures 12B and 12C).



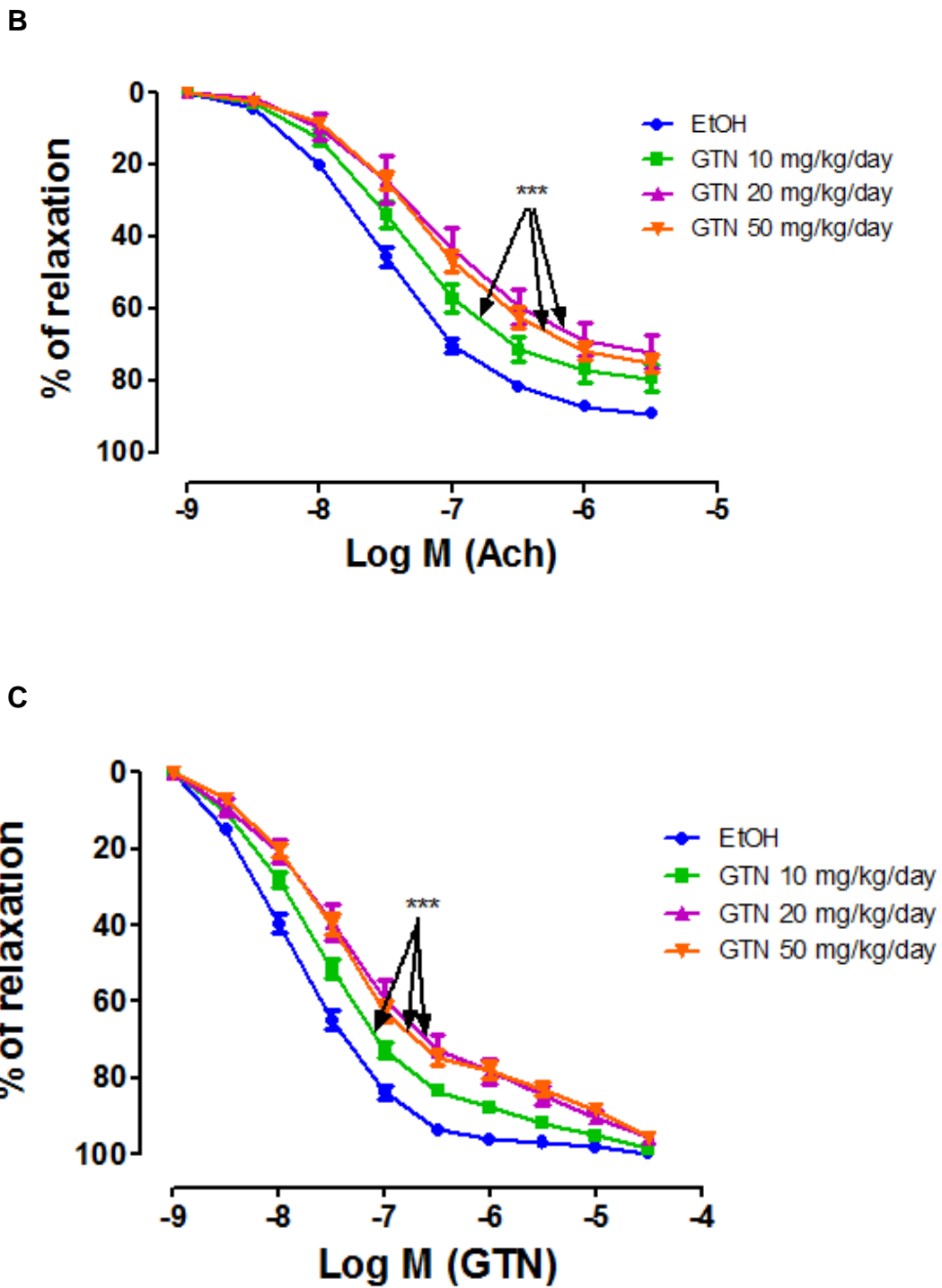


Figure 12. Nitric oxide levels in whole blood and the degree of endothelial dysfunction and nitrate tolerance in rats upon treatment with different GTN doses.

A Determination of whole blood nitrosyl-iron hemoglobin (Hb-NO) levels by EPR as a read-out of GTN (50 mg/kg/d)-induced nitrosative stress. The

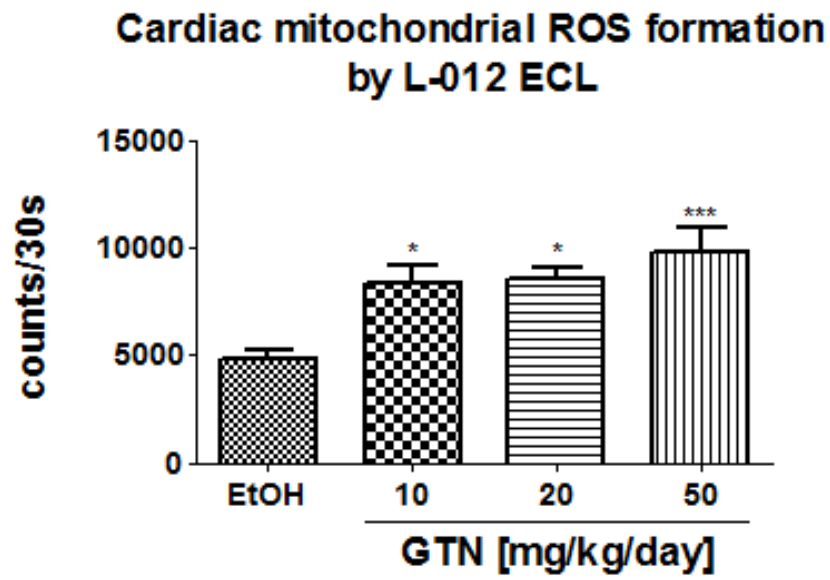


original spectra show the presence of the Hb-NO triplet signal in whole blood. **B** Results of the isometric tension recordings for the endothelium-dependent aortic relaxation (ACh), as a read-out for the development of endothelial dysfunction. **C** Results of the isometric tension recordings for the endothelium-independent aortic relaxation (GTN), as a read-out for the development of nitrate tolerance. The data are presented as mean value  $\pm$  SEM of (**A**) 8; (**B**) 5-18; (**C**) 5-18 experimental animals per group. \*\*\*  $p < 0.001$  vs EtOH treated solvent control.

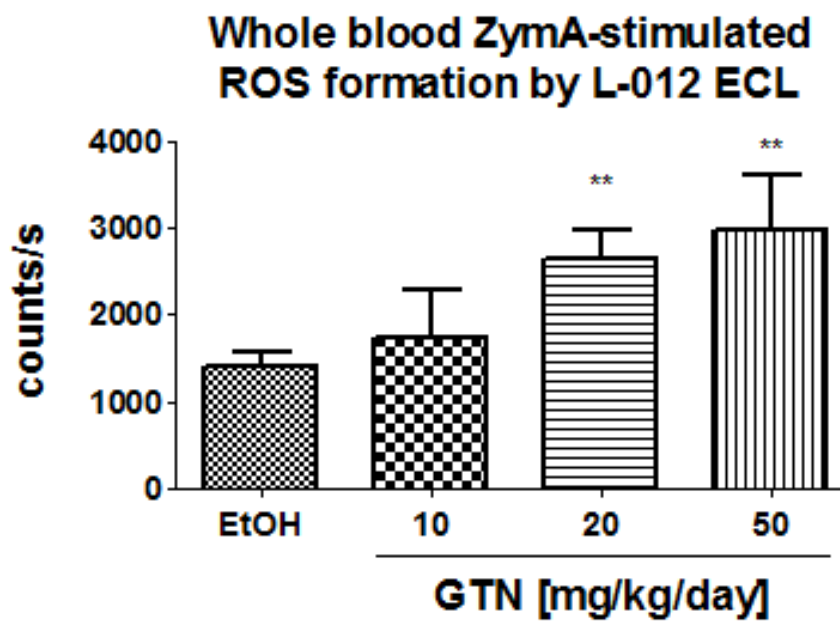
### **4.3 Nitro-oxidative stress parameters**

Levels of cardiac mitochondrial RONS were elevated in a GTN dose-dependent fashion (Figure 13A). Also RONS formation in zymosan A-stimulated whole blood, as a read-out for leukocyte-dependent oxidative burst, was increased in a GTN dose-dependent manner (Figure 13B). Likewise, vascular RONS formation as measured by DHE staining showed a GTN dose-dependent increase (Figure 13C). The nitration of protein tyrosine residues by GTN therapy was confirmed by immunohistochemical detection of 3NT-positive proteins in the rat aorta (Figure 13D).

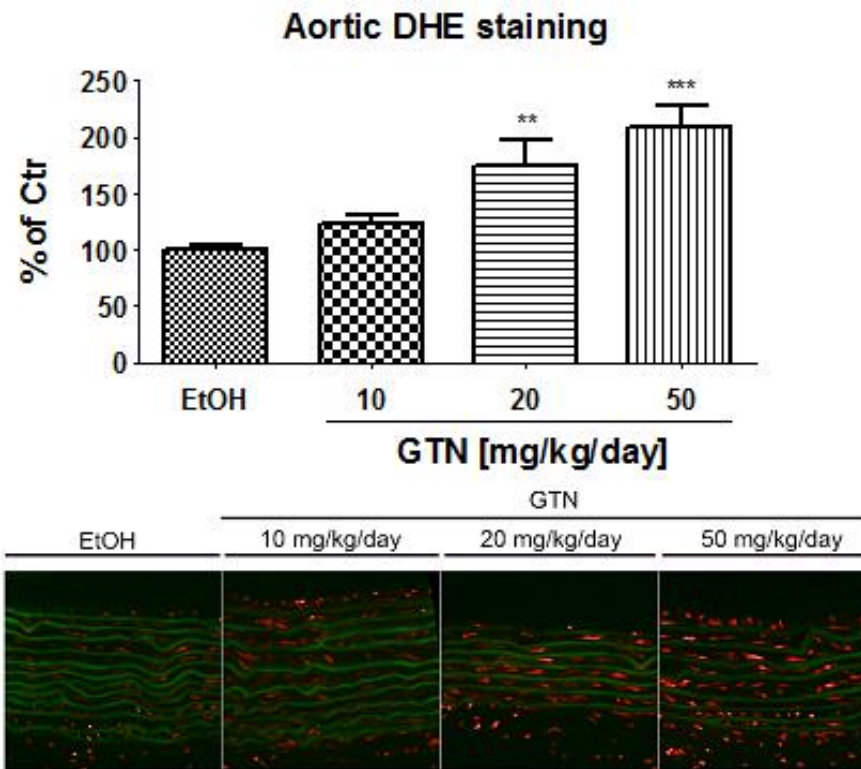
A



B



C



D

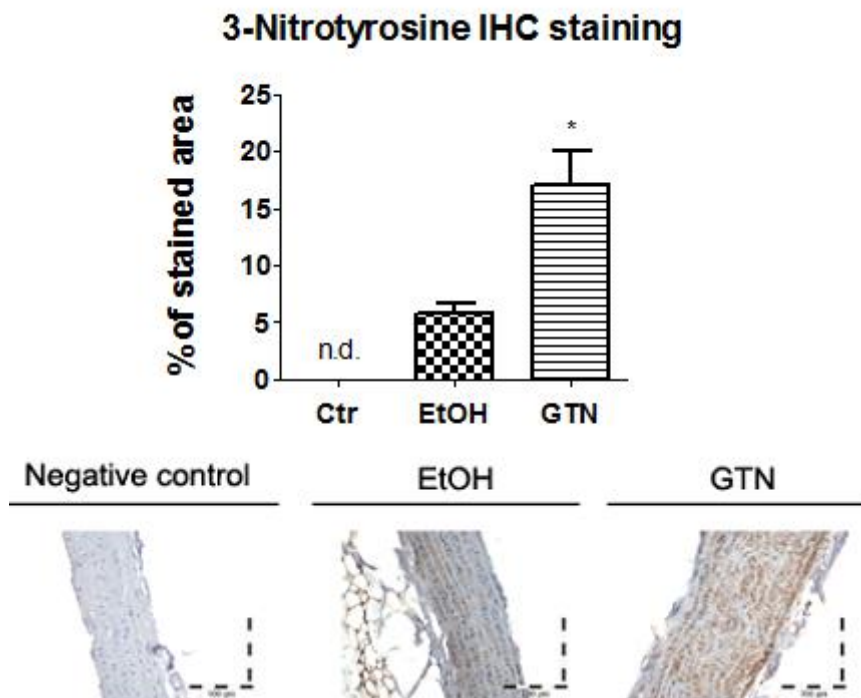


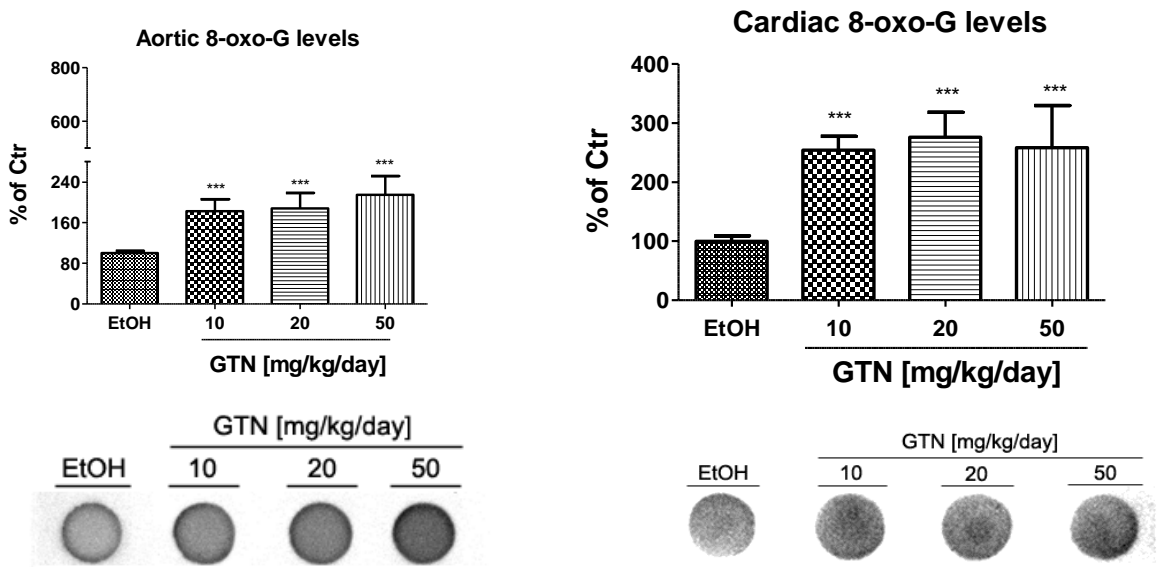
### **Figure 13. Nitro-oxidative stress parameters in GTN-treated Wistar rats.**

**A** Measurement of RONS formation in cardiac mitochondria by L-012-enhanced chemiluminescence. **B** Evaluation of whole blood nitro-oxidative stress, by quantification of the white blood cell-dependent oxidative burst in response to zymosan A stimulation. **C** DHE-dependent oxidative fluorescence microtopography in cryo-preserved aortic segments as a read-out for vascular ROS formation. Representative images are shown below the densitometric quantification. Red fluorescence indicates ROS formation, green fluorescence indicates autofluorescence of the basal laminae. **D** Immuno-histochemical quantification of 3NT-positive proteins, as a read-out of peroxynitrite presence. Representative images are shown below the densitometric quantification. The data are presented as mean value  $\pm$  SEM of **(A)** 5-25; **(B)** 5-25; **(C)** 5-25; **(D)** 6 experimental animals per group. \*  $p < 0.05$  vs. EtOH treated solvent control, \*\*  $p < 0.01$  vs EtOH treated solvent control, \*\*\*  $p < 0.001$  vs EtOH treated solvent control.

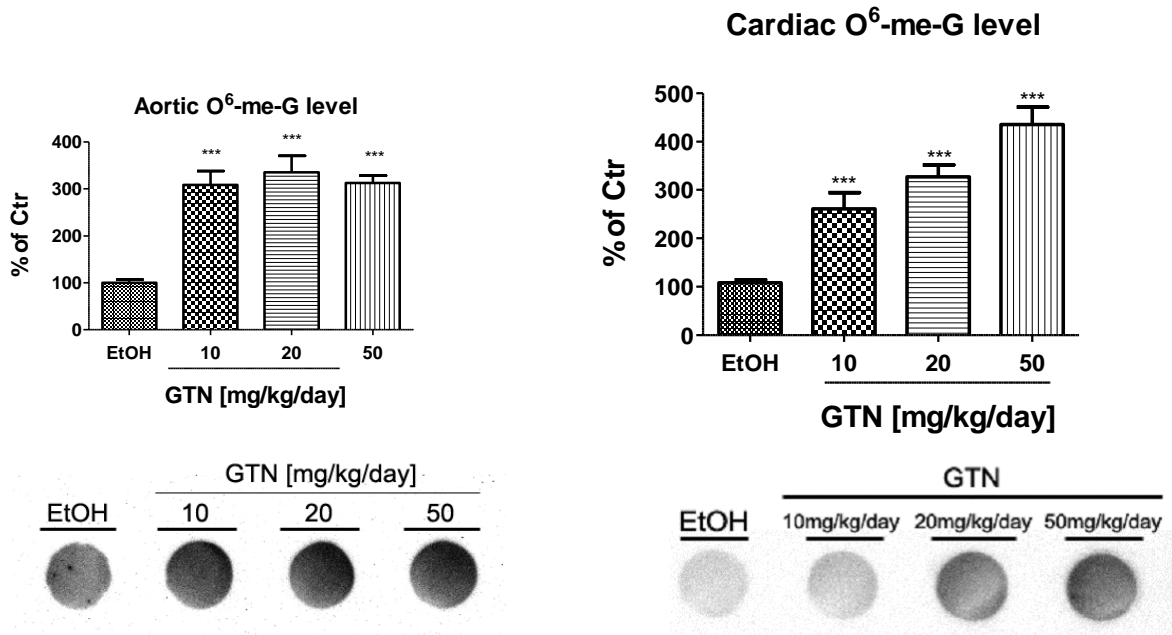
#### **4.4 Chronic GTN treatment causes DNA damage in the aortic and cardiac tissue of Wistar rats.**

Induction of nitrate tolerance by prolonged GTN treatment was associated with a significant increase in 8-oxo-G and O<sup>6</sup>-me-G levels in aorta and heart as measured by dot blot analysis, although not all assays showed a clear dose dependence (Figures 14A and 14B). Increased 8-oxo-G and O<sup>6</sup>-me-G levels were also detected by immuno-histochemistry in the aorta and heart of GTN-treated rats throughout the transversal tissue sections (Figures 14C and 14D).

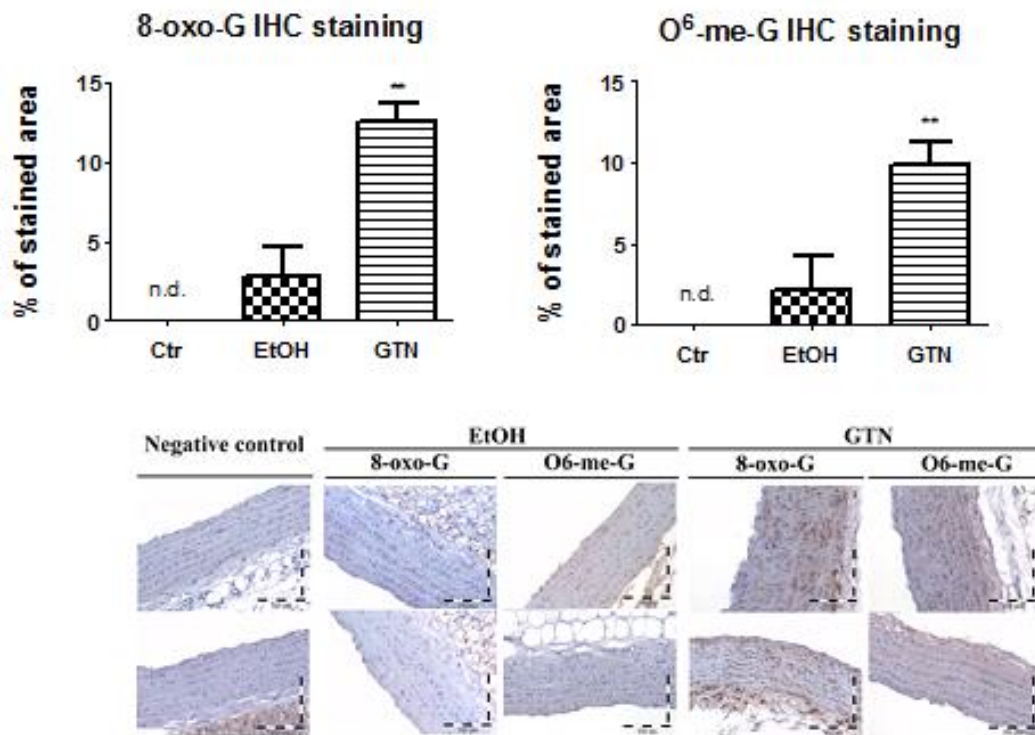
**A**



**B**



C



D

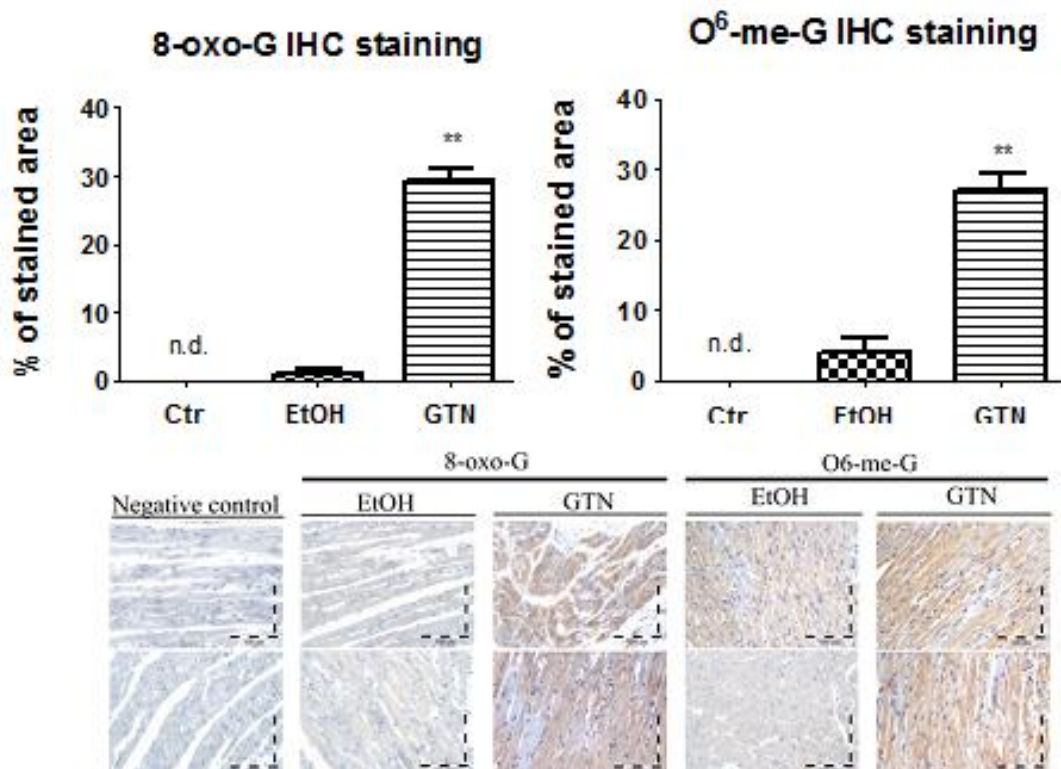


**Figure 14. Oxidative and alkylating DNA modifications in GTN-treated Wistar rats.**

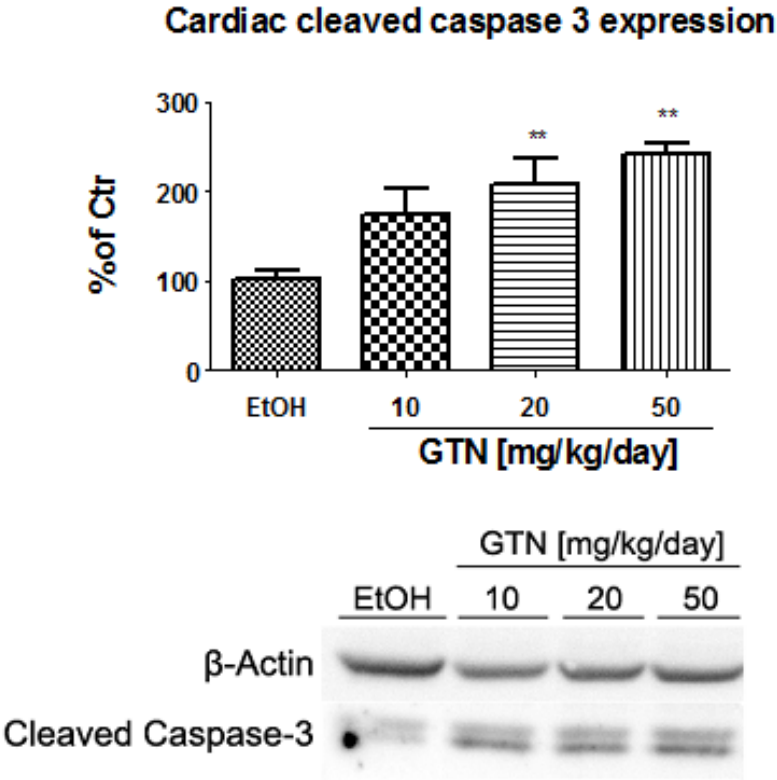
**A** Aortic and cardiac levels of 8-oxo-G after 3.5 days of GTN administration (10, 20 and 50 mg/kg/d) to Wistar rats. Representative dot blots are shown below the densitometric quantification. **B** Aortic and cardiac levels of O<sup>6</sup>-me-G in response to increasing GTN doses. Representative dot blots are shown below the densitometric quantification. **C** Aortic levels of 8-oxo-G and O<sup>6</sup>-me-G were measured by immuno-histochemistry in samples of solvent (EtOH) or GTN (50 mg/kg/d)-treated rats. **D** Cardiac levels of 8-oxo-G and O<sup>6</sup>-me-G were measured by immuno-histochemistry in samples of solvent (EtOH) or GTN (50 mg/kg/d)-treated rats. Representative images are shown below the densitometric quantification. The data are presented as mean value  $\pm$  SEM of **(A)** 5-18; **(B)** 5-18; **(C)** 6; **(D)** 6 experimental animals per group. \*\*  $p < 0.01$  vs EtOH as solvent control, \*\*\*  $p < 0.001$  vs EtOH solvent control.

#### **4.5 Chronic GTN treatment causes apoptosis.**

Several markers of apoptosis were elevated in tissues from nitrate tolerant rats. Caspase-3 is a pro-apoptotic protein. Cleavage of caspase-3 is an essential step in this specific apoptotic pathway and cleaved caspase-3 was increased significantly in the heart in a GTN dose-dependent manner (Figure 15A). One of the recently identified caspase-3 molecular targets is fractin and its increase in cardiac tissue showed GTN dose dependence (Figure 15B). Upon activation of apoptotic pathways, cleavage of the genomic DNA takes place, which either leads to low molecular weight DNA fragments or single strand breaks in the high molecular weight DNA fraction. The cell death detection assay (CDD) can be used to quantify the

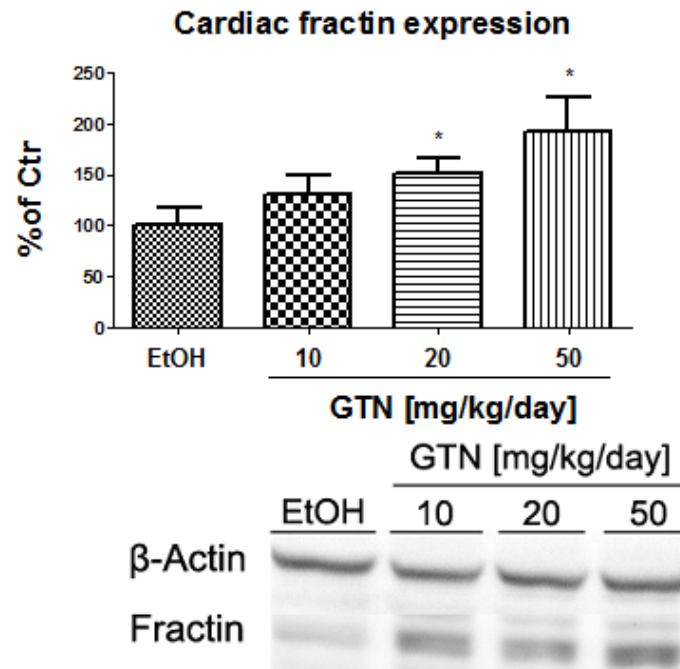
fragmentation of DNA by labeling the free 3'-OH termini with modified nucleotides through an enzymatic reaction (TUNEL). The CDD assay confirmed increased apoptosis in the aorta of GTN-treated rats (Figure 15C).

**A**





**B**



**C**

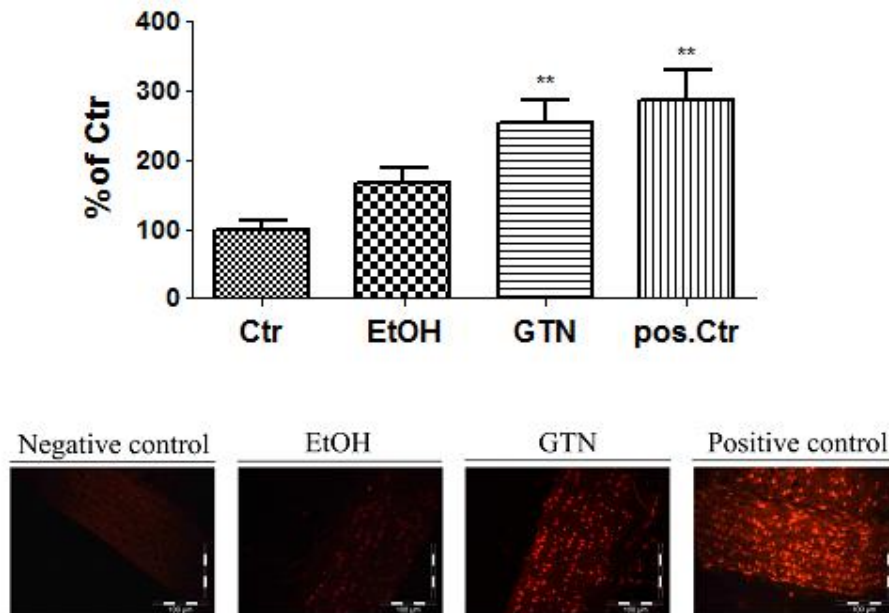


**Figure 15. Increased apoptosis in cardiac and aortic tissue from nitrate tolerant animals.**

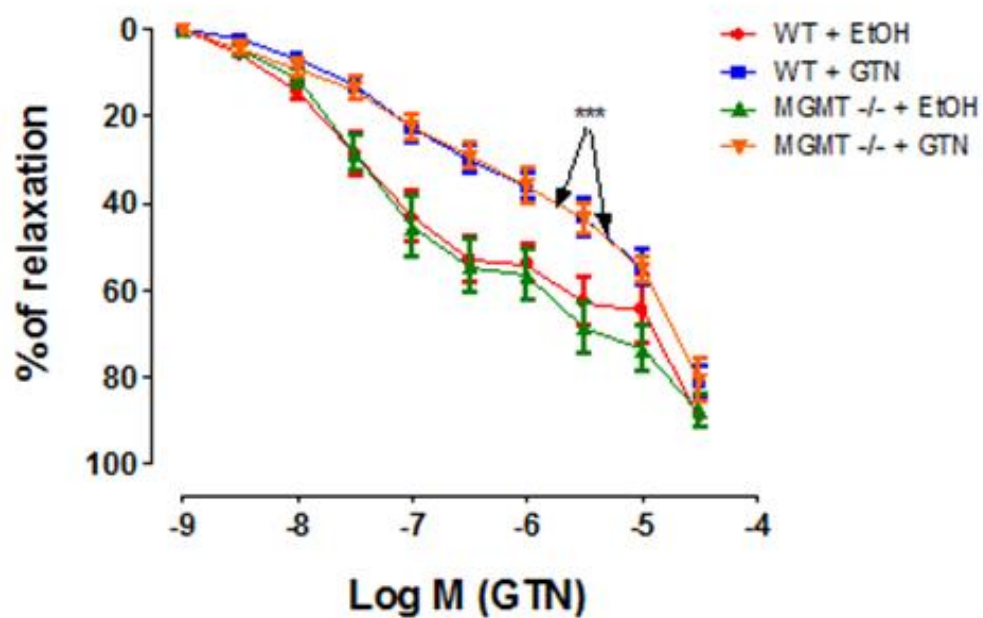
**A** Western blot analysis for cardiac protein expression levels of cleaved caspase-3 as read-out for apoptosis in response to increasing concentrations of GTN. Original Western blots are shown below the densitometric quantification. **B** Western blot results for the cardiac fractin levels in response to increasing concentrations of GTN. Representative blots are shown below the densitometric quantification. **C** Results of the *In situ* Cell Death Detection kit for quantification of apoptotic endpoints with the help of TUNEL hybridization. Measurement was performed in samples of solvent- or GTN (50 mg/kg/d)-treated rats. As a positive control treatment with DNase was used. Representative images are shown below the densitometric quantification. The densitometry data are presented as mean value  $\pm$  SEM of **(A)** 3-5, **(B)** 3-5; **(C)** 6 experimental animals per group. \*  $p < 0.05$  vs. EtOH treated solvent control, \*\*  $p < 0.01$  vs EtOH treated solvent control, \*\*\*  $p < 0.001$  vs EtOH treated solvent control.

#### **4.6 Nitrate tolerance parameters in MGMT<sup>-/-</sup> mice.**

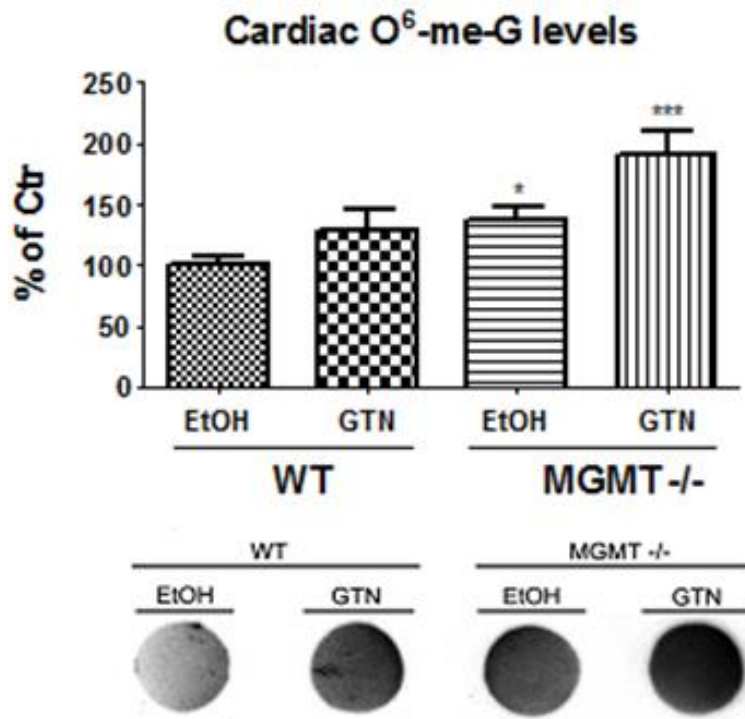
Assessment of the vascular function of isolated aortic ring segments by GTN concentration-relaxation-curves revealed a similar degree of nitrate tolerance in control and MGMT<sup>-/-</sup> mice upon treatment with GTN for 3.5 days but without any difference between the two groups (Figure 16A). Despite this lack of functional consequence of DNA repair deficiency at the level of vascular function, the levels of O<sup>6</sup>-me-G were increased in the untreated and GTN-treated MGMT<sup>-/-</sup> group (Figure 16B and 16C). Along with this side effect at the DNA damage level, markers of oxidative and nitrosative stress showed a more pronounced increase in GTN-treated MGMT<sup>-/-</sup> mice as compared to controls (Figure 16D and 16E). These findings imply

that the direct effect of prolonged GTN therapy on vascular function and the development of nitrate tolerance are not affected by GTN-induced DNA damage but the overall nitrate-dependent pathogenesis seems to be aggravated in DNA repair deficient mice, which potentially contributes to the long-term adverse effects of GTN therapy such as increased mortality (e.g. due to increased oxidative stress and cellular apoptosis).

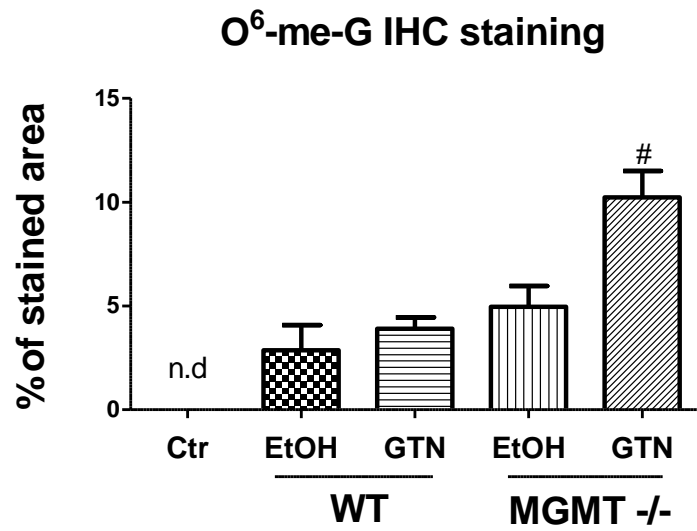
A

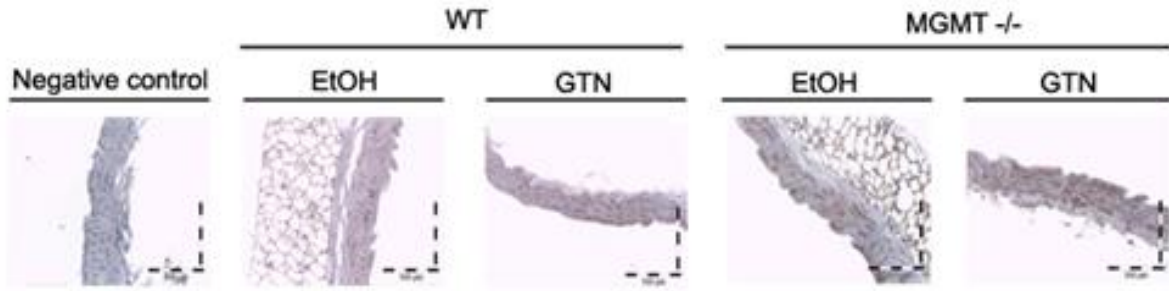


B

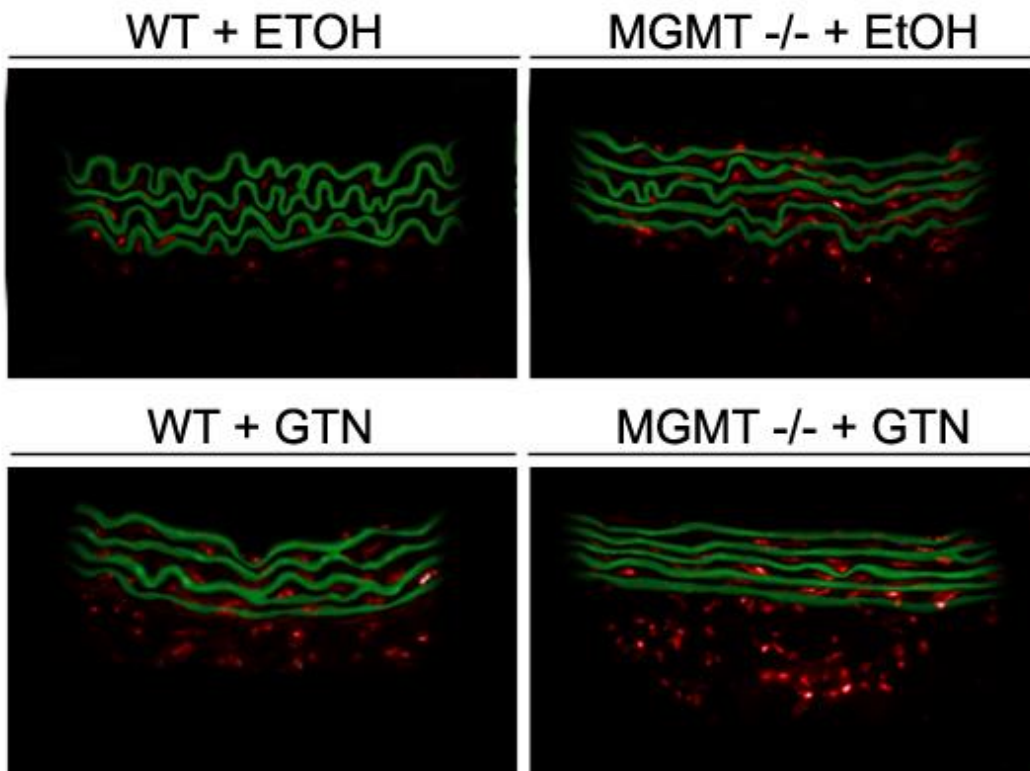
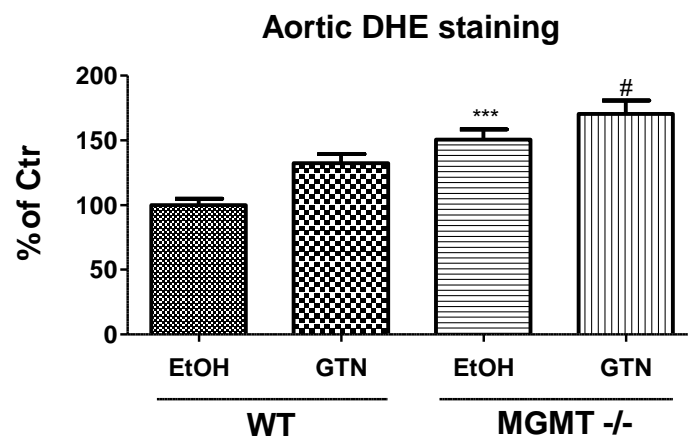


C





D



E

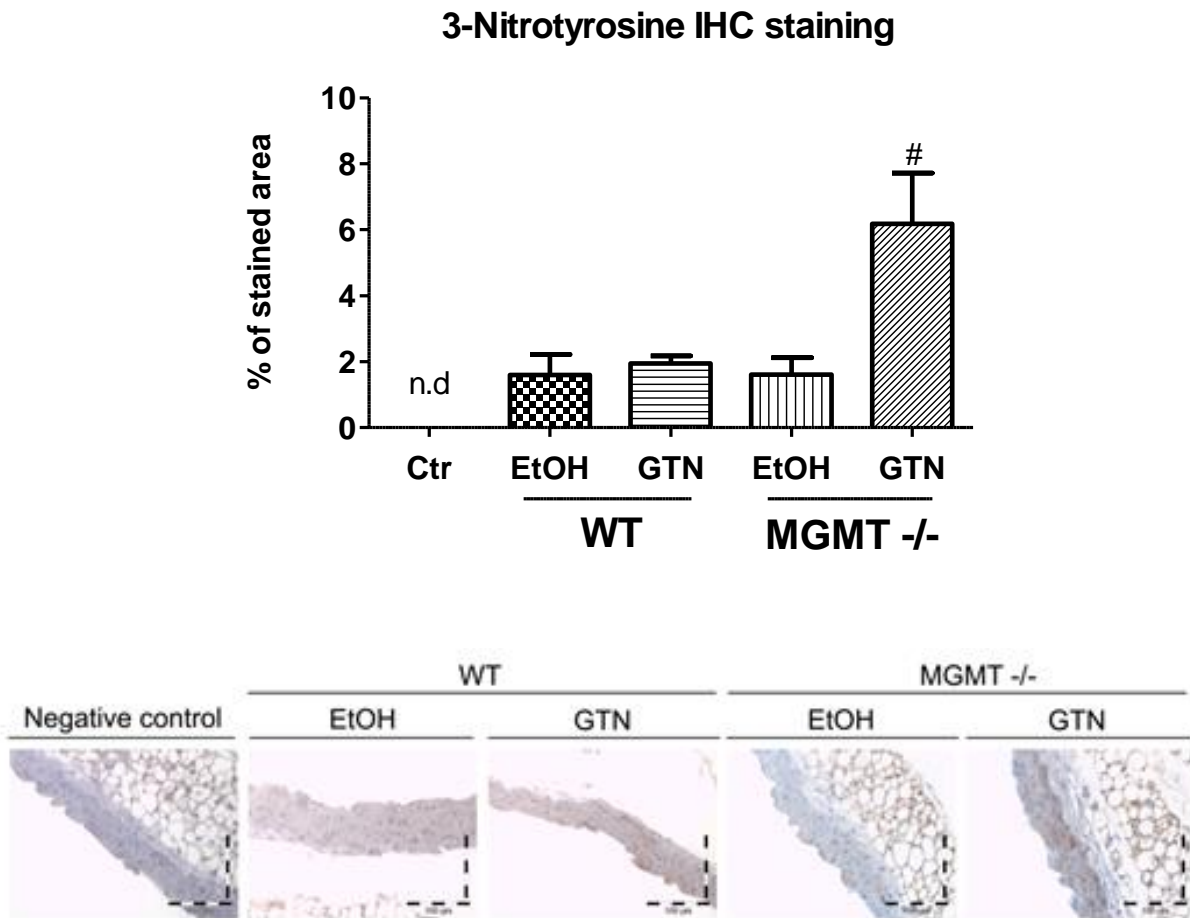


**Figure 16. Comparison of GTN (30 mg/kg/d) effects in MGMT<sup>-/-</sup> and C57BL/6 mice.**

**A** Isometric tension recordings of the endothelium-independent relaxation as a confirmation of nitrate tolerance development. **B** Immuno-dot blot analysis for cardiac levels of O<sup>6</sup>-me-G. Representative dot blot is shown below the densitometric quantification. **C** Immuno-histochemical evaluation of the O<sup>6</sup>-me-G levels in aorta. Representative images are shown below the densitometric quantification. **D** DHE-dependent oxidative fluorescence microtopography in cryo-preserved aortic segments as a read-out for vascular RONS formation. Representative images are shown below the densitometric quantification. Red

fluorescence indicates RONS formation, green fluorescence indicates autofluorescence of the basal laminae. **E** Immuno-histochemical quantification of 3NT-positive proteins, as a read-out for the presence of peroxynitrite. Representative images are shown below the densitometric quantification. The data are presented as mean value  $\pm$  SEM of **(A)** 10-11; **(B)** 10-11; **(C)** 6 experimental animals per group, **(D)** 6 experimental animals per group, **(E)** 6 experimental animals per group. \*  $p < 0.05$  vs. WT EtOH treated solvent control, \*\*  $p < 0.01$  vs WT EtOH treated solvent control, \*\*\*  $p < 0.001$  vs WT EtOH treated solvent control, #  $p < 0.05$  vs WT GTN.

## 5. Discussion

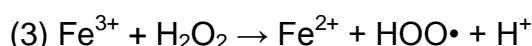
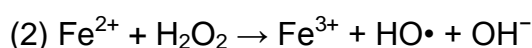
Within the scope of the present study I investigated the molecular mechanisms involved in the pathogenesis of nitrate tolerance, a serious side effect of organic nitrate, especially GTN, therapy. Until now, very little attention has been paid to the impact of DNA damage in nitrate tolerance research and its potential mutagenic effects.

Andreassi and co-workers have previously demonstrated that organic nitrates are causing somatic DNA damage [95], however, this data was quite limited and without mechanistic insights. There have been also several major limitations within this study that are worth to be mentioned. Since the results of these particular investigations strongly rely only on one parameter, micronucleus formation, other genetic factors that can contribute to their formation should be considered. For example, genetic polymorphisms have a strong influence on the DNA susceptibility to extrinsic and intrinsic damage. The investigation of human subjects in this study is of high relevance for further clinical conclusions but a great degree of variability is introduced by studying human subjects in general and patients in particular. The patient's cohort that has been studied by Andreassi and co-workers also requires further analysis. Since the majority of individuals studied suffer from cardiovascular complications for a prolonged period of time, they have been subjected to various genotoxic and DNA damaging manipulations (coronary angiography, cardiac scintigraphy) on multiple occasions. Additionally, DNA repair status of these patients was not taken into consideration.

Following the initial observation of Andreassi and co-workers, in the present work, I focused on nuclear processes, in particular DNA damaging effects in GTN-induced nitrate tolerance and could confirm potential mutagenic and apoptotic effects of GTN treatment in cultured cells and animals.



In the cell culture setting, using human endothelial EA.hy 926 cells, I determined increased DNA damage upon 48 h treatment with GTN. I confirmed the elevation of the classical oxidative DNA damage markers, 8-oxo-G and O<sup>6</sup>-me-G, and also showed an increase in DNA strand breaks. As a positive control for 8-oxo-G modification I used Fenton reaction treatment. Major components of the Fenton reaction are H<sub>2</sub>O<sub>2</sub> (1 mM) and FeSO<sub>4</sub> (100 μM). As it can be seen in reaction 2, iron (II) from the FeSO<sub>4</sub> salt is oxidized by hydrogen peroxide to iron (III), forming a hydroxyl radical and a hydroxide ion. Iron (III) formed in reaction 2 is then reduced back to iron (II) in the reaction 3 by another molecule of hydrogen peroxide, forming a hydroperoxyl radical and a proton. As a summary of these two reactions, two different oxygen-radical species are formed together with water (H<sup>+</sup> + OH<sup>-</sup>) as a byproduct [117].



The free radicals generated by this process are very reactive and engage in secondary reactions within a short period of time. Hydroxyl radical among them is a powerful, non-selective oxidant, which is able to attack nucleic acids and cause extensive oxidative damage. Typical modification introduced by HO• to DNA is 8-oxo-G [118].

N-nitroso-N-methylurea (MNU) in a concentration of 500 μM was used as a positive control for O<sup>6</sup>-me-G modification. MNU is a highly reactive mutagenic compound which exhibits its toxicity through the methylation of DNA. Typical positions for the MNU attack are strong nucleophilic centers, such as N7- and O6- positions on guanine [119].

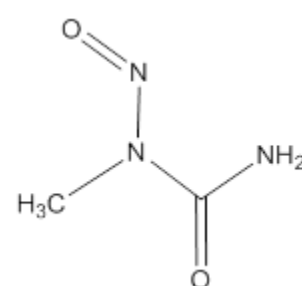


**Figure 17. MNU chemical structure**

In line with previous reports, DNA modifications were found upon challenges with nitric oxide. At least at higher concentrations, nitric oxide has DNA damaging potential, confers mutagenic effects and triggers apoptotic pathways [67]. Other nitric oxide releasing compounds (e.g. SIN-1) also possess DNA damaging properties as previously shown by significant induction of DNA strand breaks in isolated rat islets by application of the Comet assay [120]. The DNA damaging spectrum of redox active compounds in general and ·NO releasing compounds in particular is not limited to the direct effects on the nucleic acids, but may also affect the DNA repair machinery [121, 122], e.g. by inhibition of the MGMT enzyme, which is responsible for the removal of O<sup>6</sup>-me-G lesion [123]. It has been shown that diethylamine NONOate - DEA/NO at a concentration of 80 µM inhibited the activity of MGMT by 50%. The proposed explanation for the enzyme inhibition was the formation of a -S-NO protein adduct [123]. MGMT inhibition is not a unique case. Formamidopyrimidine-DNA glycosylase (Fpg enzyme) is another example for an enzyme of the DNA repair machinery that was inhibited by ·NO [124]. Fpg is a zinc finger-containing bi-functional glycosylase with an AP-lyase activity. It is responsible for the removal of imidazole ring-opened purines, including Fapy (2,6-diamino-4-hydroxy-5-N-methylformamidopyrimidine) and 8-oxo-G lesions [125]. It has been shown that ~110-120 µmol/L of ·NO released in a steady state manner from diethylamine NONOate (DEA/NO) effectively inhibited the activity of Fpg enzyme. Such ·NO concentrations are within the pathophysiological range and are expected in the cellular environment of neutrophils and stimulated macrophages [126]. Nitrite or diethylamine, the decomposition products of DEA/NO, did not inhibit Fpg activity, even not after prolonged incubation time. Furthermore, the inhibitory effect of ·NO was not reversible since incubation with reducing agents and/or Zn<sup>2+</sup> had no effect [124].

With the model of GTN-induced nitrate tolerance in rats I showed that the concept of nitrosative/oxidative stress-induced DNA damage also holds true for *in vivo* conditions and accordingly might have some impact in the clinical setting as well [95]. Nitrate tolerance was clearly correlated in a GTN dose-dependent fashion with increased cardiovascular nitro-oxidative stress and GTN treatment induced a nitrosative stress milieu, all of which is known to contribute to a higher burden of oxidative/nitrosative DNA damage and strand breaks. Increased formation of 8-oxo-G and O<sup>6</sup>-me-G modifications upon prolonged treatment with GTN was confirmed in aorta and heart of rats by two independent methodologies. These DNA lesions are highly mutagenic and their detection in rats treated with GTN at least warrants caution for the clinical long-term use of this drug. In human embryonic kidney cells (HEK 293T) the induction of 8-oxo-G lesions was correlated with highly mutagenic GC→AT transversions [127]. GC→AT transversions can lead to point mutations and abnormalities in the gene transcription process. Using the same cellular model, O<sup>6</sup>-me-G was found to be responsible for incorporation of uridine in the RNA, which leads to a point mutation with profound negative effects on the down-stream protein structure and function [128].

Besides the potential mutagenic effects, the present study has shown that GTN-induced nitrosative/oxidative stress and DNA damage leads to the activation of apoptotic pathways, DNA fragmentation and cell death. For the precise investigation of the cellular apoptotic processes I used a specific method – the Cell death detection kit. The peculiarity of this method lies in the enzymatic *in situ* labeling of the apoptosis induced DNA strand breaks. With the help of DNA polymerase and terminal deoxynucleotidyl transferase (TdT) fluorescence labeled nucleotides were incorporated into DNA strand breaks and later on evaluated by fluorescent

microscopy. The tailing reaction using TdT (TUNEL) has several advantages in comparison to other apoptotic detection methods:

- 1) The label intensity with TUNEL is much higher comparing to other methods, like ISNT.
- 2) The kinetics of nucleotide incorporation with TUNEL is very rapid.
- 3) TUNEL preferentially labels apoptosis in comparison to necrosis, thereby discriminating between these two cellular pathways and from primary DNA strand breaks induced by exogenous or endogenous sources.

The findings on increased apoptosis could translate to the higher mortality in the group of organic nitrate-treated patients as reported by two independent meta-analysis [98, 99]. Myocardial infarction patients showed a higher cardiovascular mortality in the organic nitrate treatment group, which could be related to pro-apoptotic effects of the organic nitrate. The recovery of cardiac tissue after myocardial infarction largely depends on the healing process in the infarcted area and apoptotic (as well as necrotic) cell death pathways play an important role for the prognosis [129]. In support of this hypothesis, nitrate tolerance aggravated post-ischemic myocardial apoptosis and impaired the functional recovery of the post-ischemic heart [130]. Pro-apoptotic effects of GTN were also reported for endothelial progenitor cells (EPC) from in vivo GTN-treated volunteers but also upon *ex vivo* exposure to the organic nitrate [131] and endothelial progenitor cells play an important role for recovery after cardiovascular events [132, 133].

Additionally, it came to our attention that GTN patches have been recently used as an adjuvant anti-cancer therapy in the treatment of late stages (III-IV) non-small cell lung cancer and rectal cancer [134-136]. Within initial investigations in the phases I-II clinical trials, it has been shown that topical administration of GTN in a dose of 25 mg for a duration of 5 days (most of the trials tested administration of the

GTN 2 days before the treatment with platinum-containing third generation agents, such as vinorelbine, cisplatin and additionally 5-fluorouracil; during the treatment and 2 days after it) yielded a substantial improvement in anti-cancer therapy responsiveness by 30% and improved time to disease progression on average by 142 days [134]. Though, when these studies were followed up in large-scale, multicenter, open-label, randomized phase III trial, these improvements by GTN treatment were not observed [136]. There was no significant difference between progression-free survival rates between two groups of patients and the frequency and severity of adverse effects was even higher in the GTN group, consisting of headache, hypotension, diarrhea and anorexia [136]. Such discrepancies can be potentially explained by several reasons: 1) patients selected for these trials were very non-homogeneous in age, sex, smoking habits and molecular sub-types of cancer; 2) in phase III trial a bigger number of patients was recruited, eventually providing a more complete picture of the effects of GTN therapy, as well as yielding higher statistical power to this investigation; 3) variation in medications selection – vinorelbine + cisplatin/GTN vs carboplatin + gemcitabine/GTN or carboplatin + paclitaxel/GTN. Furthermore, the obtained clinical data doesn't provide information on the mechanism of action of GTN therapy as an adjuvant anti-cancer drug. So far, there is a proposal based on the vasodilating properties of this drug, leading to increased blood flow in tumors and better targeting of the tumors by first line anti-neoplasia treatment [137]. It has been also suggested that by increasing the blood flow in tumors, GTN would improve tumor tissue oxygen tension and enhance therapy response in patients. Thus, alteration of the free radicals balance in tumors, could lead to DNA damage [138] followed either by apoptosis, as we also observed, or by necrosis. Though, it is important to note that no experiments have been done to elucidate the GTN DNA damaging profile in these studies. By all means, the data

presented in these recent publications goes hand in hand with the results presented in the present work.

O<sup>6</sup>-me-G repair-deficient MGMT<sup>-/-</sup> mice were used to investigate whether accumulation of O<sup>6</sup>-me-G DNA lesions in GTN-treated animals plays a role for the degree of nitrate tolerance or only represents another side effect of nitrate therapy without significant impact on the pathogenesis of the drug-induced complications. Literature data do not support a severe phenotype and only demonstrated moderate impact of MGMT deficiency on the life span of mice [139], but MGMT gene polymorphism has been shown to be associated with increased incidence of neck cancer [140] and other tumors. Nevertheless, our initial working hypothesis was that DNA damage plays a key role for the development and aggravation of nitrate tolerance. This hypothesis was proven negative since mice deficient in the MGMT gene did neither show more pronounced nitrate tolerance as compared to wild type mice (Fig. 17A) nor more pronounced endothelial dysfunction (not shown). However, the MGMT<sup>-/-</sup> mice were more susceptible to the GTN-induced nitro-oxidative stress, which is in our opinion a major trigger of the pathogenesis underlying nitrate tolerance and accounts for a part of the serious side effects of long-term organic nitrate therapy (e.g. increased mortality). In addition, O<sup>6</sup>-me-G only represents one out of many deleterious DNA modifications (e.g. 8-oxo-G and single strand breaks) and the sum of the DNA damage might contribute to nitrate tolerance possibly at the functional level. Therefore, single knockout of MGMT might not be enough to cause severe pathophysiological and genotoxic effects of GTN and might be efficiently compensated by other repair pathways for alkylated DNA.

## 6. Summary

Despite the lack of direct evidence from large clinical trials for mutagenic and genotoxic effects of GTN therapy, the present study shows the induction of pre-mutagenic lesions, such as 8-oxo-G and O<sup>6</sup>-me-G by GTN treatment as well as increased formation of DNA strand breaks. These results were obtained in an *in vitro* (EA.hy 926 – human endothelial cell line) and *in vivo* (Wistar rats and C57BL/6 mice) setting. However, GTN-induced DNA damage had no effect on the degree of nitrate tolerance but only on other pathological side effects such as oxidative stress, as confirmed by studies in MGMT knockout mice. Of clinical importance, this study establishes potent apoptotic properties of organic nitrates, which has been demonstrated by the levels of the novel apoptotic marker and caspase-3 substrate, fractin, as well as levels of cleaved caspase-3, the activated form of this pro-apoptotic enzyme. The protein analytical data have been confirmed by an independent assay for the apoptosis, Cell death detection assay (TUNEL). First, these GTN-mediated apoptotic effects may account for the previously reported anti-cancer effects of GTN therapy (probably based on induction of apoptosis in tumor cells). Second, these GTN-mediated apoptotic effects may account for the increased mortality rates observed in the group of organic nitrate-treated patients as reported by two independent meta-analysis (probably due to induction of apoptosis in highly beneficial endothelial progenitor cells as well as in cardiomyocytes during wound healing and cardiac remodeling). Summary of the current investigations can be seen in Figure 18.

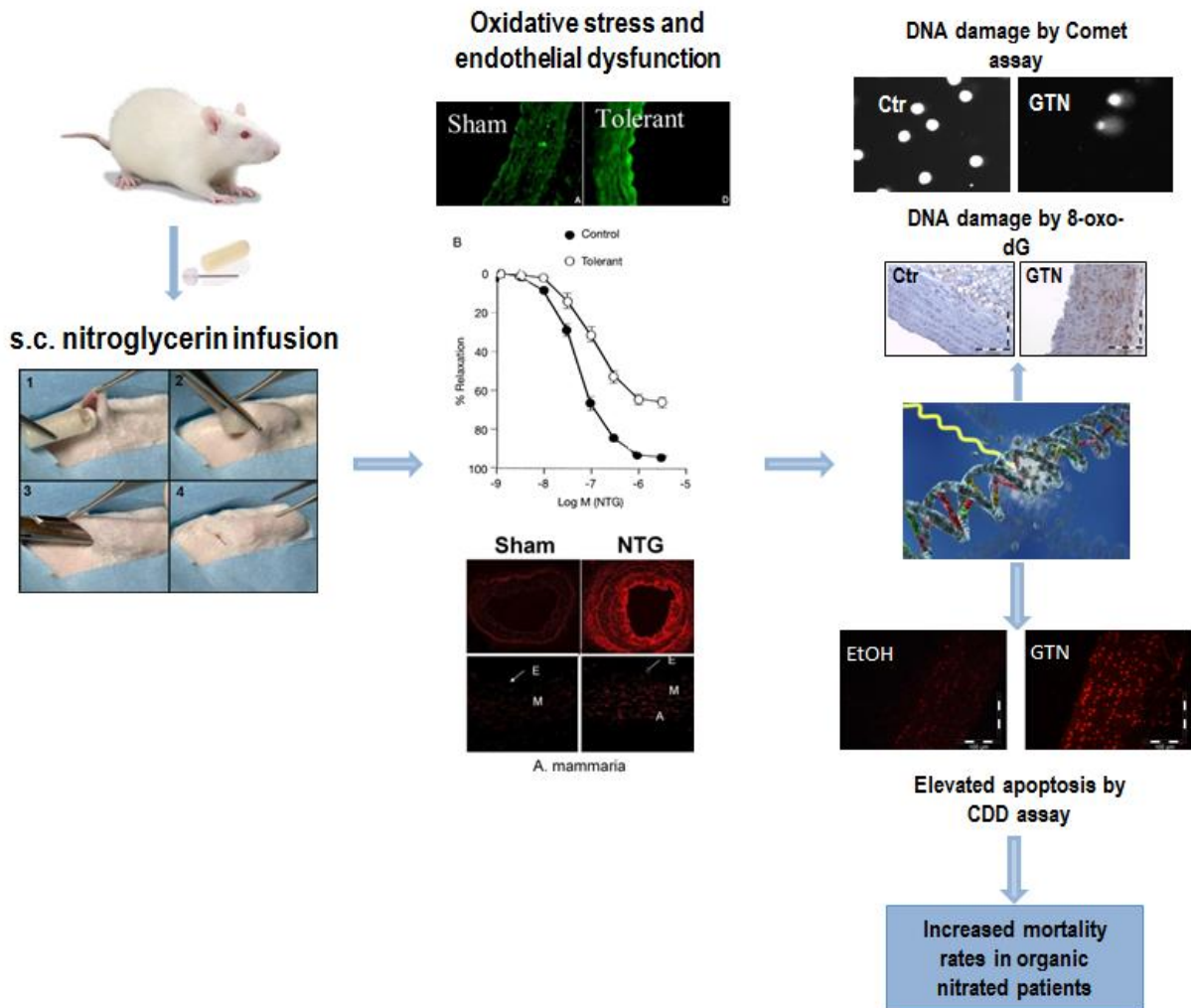


**Figure 18 Summary of the study protocol and outcome.**

Subcutaneous administration of GTN solution by osmotic mini-pumps causes the development of organic nitrate tolerance (impaired GTN-dependent relaxation by isometric tension recording) that is associated with increased oxidative stress (nitration of protein tyrosine residues, green fluorescence by 3NT immunostaining; vascular ROS formation, red fluorescence by DHE staining) and endothelial dysfunction. Additionally, nitrate tolerance causes DNA damage in the form of 8-oxo-G,  $O^6$ -me-G and DNA strand breaks (immunostaining for DNA lesions and Comet assay). Such changes to DNA activate apoptotic pathways (red fluorescence by CDD assay) that might be



the cause for increased mortality rates among patients receiving organic nitrate therapy. Rat/osmotic pump image courtesy: Harlan laboratories, [www.alzet.com](http://www.alzet.com), [www.cgsociety.org](http://www.cgsociety.org). Other parts of the Figure are partially adapted from [34, 141].

## References

- [1] Ferreira, J. C.; Mochly-Rosen, D. Nitroglycerin use in myocardial infarction patients. *Circulation journal : official journal of the Japanese Circulation Society* **76**:15-21; 2012.
- [2] Munzel, T.; Wenzel, P.; Daiber, A. Do we still need organic nitrates? *J Am Coll Cardiol* **49**:1296-1298; 2007.
- [3] Munzel, T.; Daiber, A.; Gori, T. Nitrate therapy: new aspects concerning molecular action and tolerance. *Circulation* **123**:2132-2144; 2011.
- [4] Chen, Z.; Foster, M. W.; Zhang, J.; Mao, L.; Rockman, H. A.; Kawamoto, T.; Kitagawa, K.; Nakayama, K. I.; Hess, D. T.; Stamler, J. S. An essential role for mitochondrial aldehyde dehydrogenase in nitroglycerin bioactivation. *Proceedings of the National Academy of Sciences of the United States of America* **102**:12159-12164; 2005.
- [5] Minamiyama, Y.; Takemura, S.; Yamasaki, K.; Hai, S.; Hirohashi, K.; Okada, S. Continuous treatment with organic nitrate affects hepatic cytochrome P450. *Redox report : communications in free radical research* **9**:360-364; 2004.
- [6] Chen, Z.; Zhang, J.; Stamler, J. S. Identification of the enzymatic mechanism of nitroglycerin bioactivation. *Proceedings of the National Academy of Sciences of the United States of America* **99**:8306-8311; 2002.
- [7] Minamiyama, Y.; Takemura, S.; Akiyama, T.; Imaoka, S.; Inoue, M.; Funae, Y.; Okada, S. Isoforms of cytochrome P450 on organic nitrate-derived nitric oxide release in human heart vessels. *FEBS letters* **452**:165-169; 1999.
- [8] Fung, H. L.; Chong, S.; Kowaluk, E.; Hough, K.; Kakemi, M. Mechanisms for the pharmacologic interaction of organic nitrates with thiols. Existence of an extracellular pathway for the reversal of nitrate vascular tolerance by N-

acetylcysteine. *The Journal of pharmacology and experimental therapeutics* **245**:524-530; 1988.

[9] Munzel, T.; Daiber, A.; Mulsch, A. Explaining the phenomenon of nitrate tolerance. *Circ Res* **97**:618-628; 2005.

[10] Daiber, A.; Munzel, T.; Gori, T. Organic nitrates and nitrate tolerance--state of the art and future developments. *Adv Pharmacol* **60**:177-227; 2010.

[11] Katsuki, S.; Arnold, W. P.; Murad, F. Effects of sodium nitroprusside, nitroglycerin, and sodium azide on levels of cyclic nucleotides and mechanical activity of various tissues. *J Cyclic Nucleotide Res* **3**:239-247; 1977.

[12] Daiber, A.; Wenzel, P.; Oelze, M.; Munzel, T. New insights into bioactivation of organic nitrates, nitrate tolerance and cross-tolerance. *Clin Res Cardiol* **97**:12-20; 2008.

[13] Schlossmann, J.; Ammendola, A.; Ashman, K.; Zong, X.; Huber, A.; Neubauer, G.; Wang, G. X.; Allescher, H. D.; Korth, M.; Wilm, M.; Hofmann, F.; Ruth, P. Regulation of intracellular calcium by a signalling complex of IRAG, IP3 receptor and cGMP kinase Ibeta. *Nature* **404**:197-201; 2000.

[14] Vaandrager, A. B.; Ehlert, E. M.; Jarchau, T.; Lohmann, S. M.; de Jonge, H. R. N-terminal myristoylation is required for membrane localization of cGMP-dependent protein kinase type II. *The Journal of biological chemistry* **271**:7025-7029; 1996.

[15] Jarchau, T.; Hausler, C.; Markert, T.; Pohler, D.; Vanderkerckhove, J.; De Jonge, H. R.; Lohmann, S. M.; Walter, U. Cloning, expression, and in situ localization of rat intestinal cGMP-dependent protein kinase II. *Proceedings of the National Academy of Sciences of the United States of America* **91**:9426-9430; 1994.

[16] Rangaswami, H.; Marathe, N.; Zhuang, S.; Chen, Y.; Yeh, J. C.; Frangos, J. A.; Boss, G. R.; Pilz, R. B. Type II cGMP-dependent protein kinase mediates

osteoblast mechanotransduction. *The Journal of biological chemistry* **284**:14796-14808; 2009.

[17] Gambaryan, S.; Wagner, C.; Smolenski, A.; Walter, U.; Poller, W.; Haase, W.; Kurtz, A.; Lohmann, S. M. Endogenous or overexpressed cGMP-dependent protein kinases inhibit cAMP-dependent renin release from rat isolated perfused kidney, microdissected glomeruli, and isolated juxtaglomerular cells. *Proceedings of the National Academy of Sciences of the United States of America* **95**:9003-9008; 1998.

[18] Forte, L. R.; London, R. M.; Krause, W. J.; Freeman, R. H. Mechanisms of guanylin action via cyclic GMP in the kidney. *Annual review of physiology* **62**:673-695; 2000.

[19] Sausbier, M.; Schubert, R.; Voigt, V.; Hirneiss, C.; Pfeifer, A.; Korth, M.; Kleppisch, T.; Ruth, P.; Hofmann, F. Mechanisms of NO/cGMP-dependent vasorelaxation. *Circ Res* **87**:825-830; 2000.

[20] Salvemini, D.; Currie, M. G.; Mollace, V. Nitric oxide-mediated cyclooxygenase activation. A key event in the antiplatelet effects of nitrovasodilators. *J Clin Invest* **97**:2562-2568; 1996.

[21] Needleman, P. Tolerance to the vascular effects of glyceryl trinitrate. *The Journal of pharmacology and experimental therapeutics* **171**:98-102; 1970.

[22] Parker, J. O.; Parker, J. D. Neurohormonal activation during nitrate therapy: a possible mechanism for tolerance. *The American journal of cardiology* **70**:93B-97B; 1992.

[23] Kosmicki, M.; Sadowski, Z.; Szwed, H.; Kowalik, I. What intervals in oral therapy of isosorbide dinitrate in various doses are sufficient to prevent nitrate tolerance? *Medical science monitor : international medical journal of experimental and clinical research* **6**:763-768; 2000.

- [24] Jahnchen, E. Plasma profile and haemodynamic tolerance to isosorbide-5-mononitrate in controlled-release form. *Br J Clin Pharmacol* **34 Suppl 1**:15S-17S; 1992.
- [25] Parker, J. D.; Parker, J. O. Nitrate therapy for stable angina pectoris. *The New England journal of medicine* **338**:520-531; 1998.
- [26] Elkayam, U.; Kulick, D.; McIntosh, N.; Roth, A.; Hsueh, W.; Rahimtoola, S. H. Incidence of early tolerance to hemodynamic effects of continuous infusion of nitroglycerin in patients with coronary artery disease and heart failure. *Circulation* **76**:577-584; 1987.
- [27] Munzel, T.; Daiber, A.; Gori, T. More answers to the still unresolved question of nitrate tolerance. *Eur Heart J* **34**:2666-2673; 2013.
- [28] Knorr, M.; Hausding, M.; Kroller-Schuhmacher, S.; Steven, S.; Oelze, M.; Heeren, T.; Scholz, A.; Gori, T.; Wenzel, P.; Schulz, E.; Daiber, A.; Munzel, T. Nitroglycerin-induced endothelial dysfunction and tolerance involve adverse phosphorylation and S-Glutathionylation of endothelial nitric oxide synthase: beneficial effects of therapy with the AT1 receptor blocker telmisartan. *Arterioscler Thromb Vasc Biol* **31**:2223-2231; 2011.
- [29] Munzel, T.; Heitzer, T.; Kurz, S.; Harrison, D. G.; Luhman, C.; Pape, L.; Olschewski, M.; Just, H. Dissociation of coronary vascular tolerance and neurohormonal adjustments during long-term nitroglycerin therapy in patients with stable coronary artery disease. *Journal of the American College of Cardiology* **27**:297-303; 1996.
- [30] Parker, J. D.; Farrell, B.; Fenton, T.; Cohanin, M.; Parker, J. O. Counter-regulatory responses to continuous and intermittent therapy with nitroglycerin. *Circulation* **84**:2336-2345; 1991.

- [31] Packer, M.; Lee, W. H.; Kessler, P. D.; Gottlieb, S. S.; Medina, N.; Yushak, M. Prevention and reversal of nitrate tolerance in patients with congestive heart failure. *The New England journal of medicine* **317**:799-804; 1987.
- [32] Munzel, T.; Giaid, A.; Kurz, S.; Stewart, D. J.; Harrison, D. G. Evidence for a role of endothelin 1 and protein kinase C in nitroglycerin tolerance. *Proceedings of the National Academy of Sciences of the United States of America* **92**:5244-5248; 1995.
- [33] Schulz, E.; Tsilimingas, N.; Rinze, R.; Reiter, B.; Wendt, M.; Oelze, M.; Woelken-Weckmuller, S.; Walter, U.; Reichenspurner, H.; Meinertz, T.; Munzel, T. Functional and biochemical analysis of endothelial (dys)function and NO/cGMP signaling in human blood vessels with and without nitroglycerin pretreatment. *Circulation* **105**:1170-1175; 2002.
- [34] Daiber, A.; Munzel, T. Organic Nitrate Therapy, Nitrate Tolerance, and Nitrate-Induced Endothelial Dysfunction: Emphasis on Redox Biology and Oxidative Stress. *Antioxidants & redox signaling*; 2015.
- [35] Jabs, A.; Oelze, M.; Mikhed, Y.; Stamm, P.; Kroller-Schon, S.; Welschof, P.; Jansen, T.; Hausding, M.; Kopp, M.; Steven, S.; Schulz, E.; Stasch, J. P.; Munzel, T.; Daiber, A. Effect of soluble guanylyl cyclase activator and stimulator therapy on nitroglycerin-induced nitrate tolerance in rats. *Vascul Pharmacol* **71**:181-191; 2015.
- [36] Needleman, P.; Hunter, F. E., Jr. Effects of organic nitrates on mitochondrial respiration and swelling: possible correlations with the mechanism of pharmacologic action. *Molecular pharmacology* **2**:134-143; 1966.
- [37] Lehninger, A. L. Water uptake and extrusion by mitochondria in relation to oxidative phosphorylation. *Physiological reviews* **42**:467-517; 1962.

- [38] Needleman, P.; Jakschik, B.; Johnson, E. M., Jr. Sulfhydryl requirement for relaxation of vascular smooth muscle. *The Journal of pharmacology and experimental therapeutics* **187**:324-331; 1973.
- [39] Fung, H. L.; Chung, S. J.; Chong, S.; Hough, K.; Kakami, M.; Kowaluk, E. Cellular mechanisms of nitrate action. *Zeitschrift fur Kardiologie* **78 Suppl 2**:14-17; discussion 64-17; 1989.
- [40] Boesgaard, S.; Aldershvile, J.; Poulsen, H. E. Preventive administration of intravenous N-acetylcysteine and development of tolerance to isosorbide dinitrate in patients with angina pectoris. *Circulation* **85**:143-149; 1992.
- [41] Molina, C. R.; Andresen, J. W.; Rapoport, R. M.; Waldman, S.; Murad, F. Effect of in vivo nitroglycerin therapy on endothelium-dependent and independent vascular relaxation and cyclic GMP accumulation in rat aorta. *J Cardiovasc Pharmacol* **10**:371-378; 1987.
- [42] Sayed, N.; Baskaran, P.; Ma, X.; van den Akker, F.; Beuve, A. Desensitization of soluble guanylyl cyclase, the NO receptor, by S-nitrosylation. *Proc Natl Acad Sci U S A* **104**:12312-12317; 2007.
- [43] Sayed, N.; Kim, D. D.; Fioramonti, X.; Iwahashi, T.; Duran, W. N.; Beuve, A. Nitroglycerin-induced S-nitrosylation and desensitization of soluble guanylyl cyclase contribute to nitrate tolerance. *Circ Res* **103**:606-614; 2008.
- [44] Axelsson, K. L.; Karlsson, J. O. Nitroglycerin tolerance in vitro: effect on cGMP turnover in vascular smooth muscle. *Acta pharmacologica et toxicologica* **55**:203-210; 1984.
- [45] Ahlner, J.; Andersson, R. G.; Axelsson, K. L.; Bunnfors, I.; Wallentin, L. Effects of dipyridamole on the glyceryl-trinitrate-induced inhibition of coronary artery muscle tone and platelet aggregation in relation to cyclic nucleotide metabolism. *Acta pharmacologica et toxicologica* **57**:88-95; 1985.

- [46] Kim, D.; Rybalkin, S. D.; Pi, X.; Wang, Y.; Zhang, C.; Munzel, T.; Beavo, J. A.; Berk, B. C.; Yan, C. Upregulation of phosphodiesterase 1A1 expression is associated with the development of nitrate tolerance. *Circulation* **104**:2338-2343; 2001.
- [47] Daiber, A.; Oelze, M.; Coldewey, M.; Bachschmid, M.; Wenzel, P.; Sydow, K.; Wendt, M.; Kleschyov, A. L.; Stalleicken, D.; Ullrich, V.; Mulsch, A.; Munzel, T. Oxidative stress and mitochondrial aldehyde dehydrogenase activity: a comparison of pentaerythritol tetranitrate with other organic nitrates. *Mol Pharmacol* **66**:1372-1382; 2004.
- [48] Munzel, T.; Sayegh, H.; Freeman, B. A.; Tarpey, M. M.; Harrison, D. G. Evidence for enhanced vascular superoxide anion production in nitrate tolerance. A novel mechanism underlying tolerance and cross-tolerance. *J Clin Invest* **95**:187-194; 1995.
- [49] Hink, U.; Oelze, M.; Kolb, P.; Bachschmid, M.; Zou, M. H.; Daiber, A.; Mollnau, H.; August, M.; Baldus, S.; Tsilimingas, N.; Walter, U.; Ullrich, V.; Munzel, T. Role for peroxynitrite in the inhibition of prostacyclin synthase in nitrate tolerance. *J Am Coll Cardiol* **42**:1826-1834; 2003.
- [50] Sage, P. R.; de la Lande, I. S.; Stafford, I.; Bennett, C. L.; Phillipov, G.; Stubberfield, J.; Horowitz, J. D. Nitroglycerin tolerance in human vessels: evidence for impaired nitroglycerin bioconversion. *Circulation* **102**:2810-2815; 2000.
- [51] Jurt, U.; Gori, T.; Ravandi, A.; Babaei, S.; Zeman, P.; Parker, J. D. Differential effects of pentaerythritol tetranitrate and nitroglycerin on the development of tolerance and evidence of lipid peroxidation: a human in vivo study. *J Am Coll Cardiol* **38**:854-859; 2001.
- [52] Daiber, A.; Oelze, M.; Sulyok, S.; Coldewey, M.; Schulz, E.; Treiber, N.; Hink, U.; Mulsch, A.; Scharffetter-Kochanek, K.; Munzel, T. Heterozygous Deficiency of Manganese Superoxide Dismutase in Mice (Mn-SOD<sup>+/-</sup>): A Novel Approach to



Assess the Role of Oxidative Stress for the Development of Nitrate Tolerance. *Mol Pharmacol* **68**:579-588; 2005.

[53] Esplugues, J. V.; Rocha, M.; Nunez, C.; Bosca, I.; Ibiza, S.; Herance, J. R.; Ortega, A.; Serrador, J. M.; D'Ocon, P.; Victor, V. M. Complex I dysfunction and tolerance to nitroglycerin: an approach based on mitochondrial-targeted antioxidants. *Circ Res* **99**:1067-1075; 2006.

[54] Wenzel, P.; Mollnau, H.; Oelze, M.; Schulz, E.; Wickramanayake, J. M.; Muller, J.; Schuhmacher, S.; Hortmann, M.; Baldus, S.; Gori, T.; Brandes, R. P.; Munzel, T.; Daiber, A. First evidence for a crosstalk between mitochondrial and NADPH oxidase-derived reactive oxygen species in nitroglycerin-triggered vascular dysfunction. *Antioxidants & redox signaling* **10**:1435-1447; 2008.

[55] Munzel, T.; Li, H.; Mollnau, H.; Hink, U.; Matheis, E.; Hartmann, M.; Oelze, M.; Skatchkov, M.; Warnholtz, A.; Duncker, L.; Meinertz, T.; Forstermann, U. Effects of long-term nitroglycerin treatment on endothelial nitric oxide synthase (NOS III) gene expression, NOS III-mediated superoxide production, and vascular NO bioavailability. *Circulation research* **86**:E7-E12; 2000.

[56] Daiber, A. Redox signaling (cross-talk) from and to mitochondria involves mitochondrial pores and reactive oxygen species. *Biochimica et biophysica acta* **1797**:897-906; 2010.

[57] Wenzel, P.; Hink, U.; Oelze, M.; Schuppan, S.; Schaeuble, K.; Schildknecht, S.; Ho, K. K.; Weiner, H.; Bachschmid, M.; Munzel, T.; Daiber, A. Role of reduced lipoic acid in the redox regulation of mitochondrial aldehyde dehydrogenase (ALDH-2) activity. Implications for mitochondrial oxidative stress and nitrate tolerance. *The Journal of biological chemistry* **282**:792-799; 2007.

[58] Oelze, M.; Knorr, M.; Schell, R.; Kamuf, J.; Pautz, A.; Art, J.; Wenzel, P.; Munzel, T.; Kleinert, H.; Daiber, A. Regulation of human mitochondrial aldehyde

dehydrogenase (ALDH-2) activity by electrophiles in vitro. *J Biol Chem* **286**:8893-8900; 2011.

[59] Schulz, E.; Jansen, T.; Wenzel, P.; Daiber, A.; Munzel, T. Nitric oxide, tetrahydrobiopterin, oxidative stress, and endothelial dysfunction in hypertension. *Antioxidants & redox signaling* **10**:1115-1126; 2008.

[60] Thomas, G. R.; DiFabio, J. M.; Gori, T.; Parker, J. D. Once daily therapy with isosorbide-5-mononitrate causes endothelial dysfunction in humans: evidence of a free-radical-mediated mechanism. *Journal of the American College of Cardiology* **49**:1289-1295; 2007.

[61] Abrams, J. The role of nitrates in coronary heart disease. *Arch Intern Med* **155**:357-364; 1995.

[62] Chen, C. A.; Wang, T. Y.; Varadharaj, S.; Reyes, L. A.; Hemann, C.; Talukder, M. A.; Chen, Y. R.; Druhan, L. J.; Zweier, J. L. S-glutathionylation uncouples eNOS and regulates its cellular and vascular function. *Nature* **468**:1115-1118; 2010.

[63] Daiber, A.; Munzel, T. Organic nitrate therapy, nitrate tolerance and nitrate induced endothelial dysfunction - emphasis on redox biology and oxidative stress. *Antioxidants & redox signaling*; 2015.

[64] Azevedo, E. R.; Schofield, A. M.; Kelly, S.; Parker, J. D. Nitroglycerin withdrawal increases endothelium-dependent vasomotor response to acetylcholine. *Journal of the American College of Cardiology* **37**:505-509; 2001.

[65] Munzel, T.; Daiber, A.; Ullrich, V.; Mulsch, A. Vascular consequences of endothelial nitric oxide synthase uncoupling for the activity and expression of the soluble guanylyl cyclase and the cGMP-dependent protein kinase. *Arteriosclerosis, thrombosis, and vascular biology* **25**:1551-1557; 2005.

[66] Gori, T.; Burstein, J. M.; Ahmed, S.; Miner, S. E.; Al-Hesayen, A.; Kelly, S.; Parker, J. D. Folic acid prevents nitroglycerin-induced nitric oxide synthase

dysfunction and nitrate tolerance: a human in vivo study. *Circulation* **104**:1119-1123; 2001.

[67] Felley-Bosco, E. Role of nitric oxide in genotoxicity: implication for carcinogenesis. *Cancer Metastasis Rev* **17**:25-37; 1998.

[68] Wink, D. A.; Kasprzak, K. S.; Maragos, C. M.; Elespuru, R. K.; Misra, M.; Dunams, T. M.; Cebula, T. A.; Koch, W. H.; Andrews, A. W.; Allen, J. S.; et al. DNA deaminating ability and genotoxicity of nitric oxide and its progenitors. *Science* **254**:1001-1003; 1991.

[69] Liu, R. H.; Hotchkiss, J. H. Potential genotoxicity of chronically elevated nitric oxide: a review. *Mutat Res* **339**:73-89; 1995.

[70] Marnett, L. J.; Burcham, P. C. Endogenous DNA adducts: potential and paradox. *Chem Res Toxicol* **6**:771-785; 1993.

[71] Kissner, R.; Nauser, T.; Bugnon, P.; Lye, P. G.; Koppenol, W. H. Formation and properties of peroxyxynitrite as studied by laser flash photolysis, high-pressure stopped-flow technique, and pulse radiolysis. *Chem Res Toxicol* **10**:1285-1292; 1997.

[72] Beckman, J. S.; Koppenol, W. H. Nitric oxide, superoxide, and peroxyxynitrite: the good, the bad, and ugly. *Am J Physiol* **271**:C1424-1437; 1996.

[73] Inoue, S.; Kawanishi, S. Oxidative DNA damage induced by simultaneous generation of nitric oxide and superoxide. *FEBS Lett* **371**:86-88; 1995.

[74] Zingarelli, B.; O'Connor, M.; Wong, H.; Salzman, A. L.; Szabo, C. Peroxyxynitrite-mediated DNA strand breakage activates poly-adenosine diphosphate ribosyl synthetase and causes cellular energy depletion in macrophages stimulated with bacterial lipopolysaccharide. *J Immunol* **156**:350-358; 1996.

- [75] Juedes, M. J.; Wogan, G. N. Peroxynitrite-induced mutation spectra of pSP189 following replication in bacteria and in human cells. *Mutat Res* **349**:51-61; 1996.
- [76] Yermilov, V.; Rubio, J.; Becchi, M.; Friesen, M. D.; Pignatelli, B.; Ohshima, H. Formation of 8-nitroguanine by the reaction of guanine with peroxynitrite in vitro. *Carcinogenesis* **16**:2045-2050; 1995.
- [77] Ames, B. N.; Gold, L. S. Endogenous mutagens and the causes of aging and cancer. *Mutat Res* **250**:3-16; 1991.
- [78] Nguyen, T.; Brunson, D.; Crespi, C. L.; Penman, B. W.; Wishnok, J. S.; Tannenbaum, S. R. DNA damage and mutation in human cells exposed to nitric oxide in vitro. *Proc Natl Acad Sci U S A* **89**:3030-3034; 1992.
- [79] Kim, Y. J.; Wilson, D. M., 3rd. Overview of base excision repair biochemistry. *Curr Mol Pharmacol* **5**:3-13; 2012.
- [80] Lee, D. H.; Liu, Y.; Lee, H. W.; Xia, B.; Brice, A. R.; Park, S. H.; Balduf, H.; Dominy, B. N.; Cao, W. A structural determinant in the uracil DNA glycosylase superfamily for the removal of uracil from adenine/uracil base pairs. *Nucleic Acids Res* **43**:1081-1089; 2015.
- [81] Ba, X.; Aguilera-Aguirre, L.; Sur, S.; Boldogh, I. 8-Oxoguanine DNA glycosylase-1-driven DNA base excision repair: role in asthma pathogenesis. *Curr Opin Allergy Clin Immunol* **15**:89-97; 2015.
- [82] Tarry-Adkins, J. L.; Martin-Gronert, M. S.; Fernandez-Twinn, D. S.; Hargreaves, I.; Alfaradhi, M. Z.; Land, J. M.; Aiken, C. E.; Ozanne, S. E. Poor maternal nutrition followed by accelerated postnatal growth leads to alterations in DNA damage and repair, oxidative and nitrosative stress, and oxidative defense capacity in rat heart. *FASEB J* **27**:379-390; 2013.

- [83] Hegde, M. L.; Hegde, P. M.; Bellot, L. J.; Mandal, S. M.; Hazra, T. K.; Li, G. M.; Boldogh, I.; Tomkinson, A. E.; Mitra, S. Prereplicative repair of oxidized bases in the human genome is mediated by NEIL1 DNA glycosylase together with replication proteins. *Proc Natl Acad Sci U S A* **110**:E3090-3099; 2013.
- [84] Park, J. S.; Kim, H. L.; Kim, Y. J.; Weon, J. I.; Sung, M. K.; Chung, H. W.; Seo, Y. R. Human AP endonuclease 1: a potential marker for the prediction of environmental carcinogenesis risk. *Oxid Med Cell Longev* **2014**:730301; 2014.
- [85] Dizdaroglu, M. Oxidatively induced DNA damage: mechanisms, repair and disease. *Cancer Lett* **327**:26-47; 2012.
- [86] Brennerman, B. M.; Illuzzi, J. L.; Wilson, D. M., 3rd. Base excision repair capacity in informing healthspan. *Carcinogenesis* **35**:2643-2652; 2014.
- [87] Radicella, J. P.; Dherin, C.; Desmaze, C.; Fox, M. S.; Boiteux, S. Cloning and characterization of hOGG1, a human homolog of the OGG1 gene of *Saccharomyces cerevisiae*. *Proc Natl Acad Sci U S A* **94**:8010-8015; 1997.
- [88] Dianov, G.; Bischoff, C.; Piotrowski, J.; Bohr, V. A. Repair pathways for processing of 8-oxoguanine in DNA by mammalian cell extracts. *J Biol Chem* **273**:33811-33816; 1998.
- [89] Jena, N. R. DNA damage by reactive species: Mechanisms, mutation and repair. *J Biosci* **37**:503-517; 2012.
- [90] Koag, M. C.; Lee, S. Metal-dependent conformational activation explains highly promutagenic replication across O6-methylguanine by human DNA polymerase beta. *J Am Chem Soc* **136**:5709-5721; 2014.
- [91] Cabrini, G.; Fabbri, E.; Lo Nigro, C.; Dececchi, M. C.; Gambari, R. Regulation of expression of O6-methylguanine-DNA methyltransferase and the treatment of glioblastoma (Review). *Int J Oncol* **47**:417-428; 2015.

- [92] Belanich, M.; Randall, T.; Pastor, M. A.; Kibitel, J. T.; Alas, L. G.; Dolan, M. E.; Schold, S. C., Jr.; Gander, M.; Lejeune, F. J.; Li, B. F.; White, A. B.; Wasserman, P.; Citron, M. L.; Yarosh, D. B. Intracellular Localization and intercellular heterogeneity of the human DNA repair protein O(6)-methylguanine-DNA methyltransferase. *Cancer Chemother Pharmacol* **37**:547-555; 1996.
- [93] Daniels, D. S.; Tainer, J. A. Conserved structural motifs governing the stoichiometric repair of alkylated DNA by O(6)-alkylguanine-DNA alkyltransferase. *Mutation research* **460**:151-163; 2000.
- [94] Adams, J.; Apple, F. Cardiology patient page. New blood tests for detecting heart disease. *Circulation* **109**:E12-14; 2004.
- [95] Andreassi, M. G.; Picano, E.; Del Ry, S.; Botto, N.; Colombo, M. G.; Giannessi, D.; Lubrano, V.; Vassalle, C.; Biagini, A. Chronic long-term nitrate therapy: possible cytogenetic effect in humans? *Mutagenesis* **16**:517-521; 2001.
- [96] Andreassi, M. G.; Botto, N.; Simi, S.; Casella, M.; Manfredi, S.; Lucarelli, M.; Venneri, L.; Biagini, A.; Picano, E. Diabetes and chronic nitrate therapy as co-determinants of somatic DNA damage in patients with coronary artery disease. *J Mol Med (Berl)* **83**:279-286; 2005.
- [97] Kiziltepe, T.; Hideshima, T.; Ishitsuka, K.; Ocio, E. M.; Raje, N.; Catley, L.; Li, C. Q.; Trudel, L. J.; Yasui, H.; Vallet, S.; Kutok, J. L.; Chauhan, D.; Mitsiades, C. S.; Saavedra, J. E.; Wogan, G. N.; Keefer, L. K.; Shami, P. J.; Anderson, K. C. JS-K, a GST-activated nitric oxide generator, induces DNA double-strand breaks, activates DNA damage response pathways, and induces apoptosis in vitro and in vivo in human multiple myeloma cells. *Blood* **110**:709-718; 2007.
- [98] Nakamura, Y.; Moss, A. J.; Brown, M. W.; Kinoshita, M.; Kawai, C. Long-term nitrate use may be deleterious in ischemic heart disease: A study using the

databases from two large-scale postinfarction studies. Multicenter Myocardial Ischemia Research Group. *American heart journal* **138**:577-585; 1999.

[99] Kanamasa, K.; Hayashi, T.; Kimura, A.; Ikeda, A.; Ishikawa, K. Long-term, continuous treatment with both oral and transdermal nitrates increases cardiac events in healed myocardial infarction patients. *Angiology* **53**:399-408; 2002.

[100] Glassner, B. J.; Weeda, G.; Allan, J. M.; Broekhof, J. L.; Carls, N. H.; Donker, I.; Engelward, B. P.; Hampson, R. J.; Hersmus, R.; Hickman, M. J.; Roth, R. B.; Warren, H. B.; Wu, M. M.; Hoeijmakers, J. H.; Samson, L. D. DNA repair methyltransferase (Mgmt) knockout mice are sensitive to the lethal effects of chemotherapeutic alkylating agents. *Mutagenesis* **14**:339-347; 1999.

[101] Schuhmacher, S.; Schulz, E.; Oelze, M.; Konig, A.; Roegler, C.; Lange, K.; Sydow, L.; Kawamoto, T.; Wenzel, P.; Munzel, T.; Lehmann, J.; Daiber, A. A new class of organic nitrates: investigations on bioactivation, tolerance and cross-tolerance phenomena. *Br J Pharmacol* **158**:510-520; 2009.

[102] Vandier, C.; Le Guennec, J. Y.; Bedfer, G. What are the signaling pathways used by norepinephrine to contract the artery? A demonstration using guinea pig aortic ring segments. *Adv Physiol Educ* **26**:195-203; 2002.

[103] Kroller-Schon, S.; Steven, S.; Kossmann, S.; Scholz, A.; Daub, S.; Oelze, M.; Xia, N.; Hausding, M.; Mikhed, Y.; Zinssius, E.; Mader, M.; Stamm, P.; Treiber, N.; Scharffetter-Kochanek, K.; Li, H.; Schulz, E.; Wenzel, P.; Munzel, T.; Daiber, A. Molecular mechanisms of the crosstalk between mitochondria and NADPH oxidase through reactive oxygen species-studies in white blood cells and in animal models. *Antioxid Redox Signal* **20**:247-266; 2014.

[104] Daiber, A.; August, M.; Baldus, S.; Wendt, M.; Oelze, M.; Sydow, K.; Kleschyov, A. L.; Munzel, T. Measurement of NAD(P)H oxidase-derived superoxide with the luminol analogue L-012. *Free Radic Biol Med* **36**:101-111; 2004.

- [105] Oelze, M.; Daiber, A.; Brandes, R. P.; Hortmann, M.; Wenzel, P.; Hink, U.; Schulz, E.; Mollnau, H.; von Sandersleben, A.; Kleschyov, A. L.; Mulsch, A.; Li, H.; Forstermann, U.; Munzel, T. Nebivolol inhibits superoxide formation by NADPH oxidase and endothelial dysfunction in angiotensin II-treated rats. *Hypertension* **48**:677-684; 2006.
- [106] Oelze, M.; Kroller-Schon, S.; Steven, S.; Lubos, E.; Doppler, C.; Hausding, M.; Tobias, S.; Brochhausen, C.; Li, H.; Torzewski, M.; Wenzel, P.; Bachschmid, M.; Lackner, K. J.; Schulz, E.; Munzel, T.; Daiber, A. Glutathione peroxidase-1 deficiency potentiates dysregulatory modifications of endothelial nitric oxide synthase and vascular dysfunction in aging. *Hypertension* **63**:390-396; 2014.
- [107] Daiber, A.; Oelze, M.; August, M.; Wendt, M.; Sydow, K.; Wieboldt, H.; Kleschyov, A. L.; Munzel, T. Detection of superoxide and peroxynitrite in model systems and mitochondria by the luminol analogue L-012. *Free Radic Res* **38**:259-269; 2004.
- [108] Guzzi, R.; Bartucci, R. Electron spin resonance of spin-labeled lipid assemblies and proteins. *Archives of biochemistry and biophysics* **580**:102-111; 2015.
- [109] Dikalov, S.; Griendling, K. K.; Harrison, D. G. Measurement of reactive oxygen species in cardiovascular studies. *Hypertension* **49**:717-727; 2007.
- [110] Bradford, M. M. A rapid and sensitive method for the quantitation of microgram quantities of protein utilizing the principle of protein-dye binding. *Analytical biochemistry* **72**:248-254; 1976.
- [111] Edgell, C. J.; McDonald, C. C.; Graham, J. B. Permanent cell line expressing human factor VIII-related antigen established by hybridization. *Proc Natl Acad Sci U S A* **80**:3734-3737; 1983.



- [112] Fahrner, J.; Huelsenbeck, J.; Jaurich, H.; Dorsam, B.; Frisan, T.; Eich, M.; Roos, W. P.; Kaina, B.; Fritz, G. Cytolethal distending toxin (CDT) is a radiomimetic agent and induces persistent levels of DNA double-strand breaks in human fibroblasts. *DNA repair* **18**:31-43; 2014.
- [113] Dorsam, B.; Wu, C. F.; Efferth, T.; Kaina, B.; Fahrner, J. The eucalyptus oil ingredient 1,8-cineol induces oxidative DNA damage. *Archives of toxicology* **89**:797-805; 2015.
- [114] Nehls, P.; Adamkiewicz, J.; Rajewsky, M. F. Immuno-slot-blot: a highly sensitive immunoassay for the quantitation of carcinogen-modified nucleosides in DNA. *Journal of cancer research and clinical oncology* **108**:23-29; 1984.
- [115] Schuhmacher, S.; Foretz, M.; Knorr, M.; Jansen, T.; Hortmann, M.; Wenzel, P.; Oelze, M.; Kleschyov, A. L.; Daiber, A.; Keaney, J. F., Jr.; Wegener, G.; Lackner, K.; Munzel, T.; Viollet, B.; Schulz, E. alpha1AMP-activated protein kinase preserves endothelial function during chronic angiotensin II treatment by limiting Nox2 upregulation. *Arterioscler Thromb Vasc Biol* **31**:560-566; 2011.
- [116] Steven, S.; Hausding, M.; Kroller-Schon, S.; Mader, M.; Mikhed, Y.; Stamm, P.; Zinssius, E.; Pfeffer, A.; Welschof, P.; Agdauletova, S.; Sudowe, S.; Li, H.; Oelze, M.; Schulz, E.; Klein, T.; Munzel, T.; Daiber, A. Gliptin and GLP-1 analog treatment improves survival and vascular inflammation/dysfunction in animals with lipopolysaccharide-induced endotoxemia. *Basic Res Cardiol* **110**:6; 2015.
- [117] Winterbourn, C. C. The biological chemistry of hydrogen peroxide. *Methods in enzymology* **528**:3-25; 2013.
- [118] Chevion, M. A site-specific mechanism for free radical induced biological damage: the essential role of redox-active transition metals. *Free radical biology & medicine* **5**:27-37; 1988.

- [119] Tsubura, A.; Lai, Y. C.; Miki, H.; Sasaki, T.; Uehara, N.; Yuri, T.; Yoshizawa, K. Review: Animal models of N-Methyl-N-nitrosourea-induced mammary cancer and retinal degeneration with special emphasis on therapeutic trials. *In vivo* **25**:11-22; 2011.
- [120] Green, I. C.; Cunningham, J. M.; Delaney, C. A.; Elphick, M. R.; Mabley, J. G.; Green, M. H. Effects of cytokines and nitric oxide donors on insulin secretion, cyclic GMP and DNA damage: relation to nitric oxide production. *Biochemical Society transactions* **22**:30-37; 1994.
- [121] Mikhed, Y.; Daiber, A.; Steven, S. Mitochondrial Oxidative Stress, Mitochondrial DNA Damage and Their Role in Age-Related Vascular Dysfunction. *International journal of molecular sciences* **16**:15918-15953; 2015.
- [122] Mikhed, Y.; Gorchach, A.; Knaus, U. G.; Daiber, A. Redox regulation of genome stability by effects on gene expression, epigenetic pathways and DNA damage/repair. *Redox biology* **5**:275-289; 2015.
- [123] Laval, F.; Wink, D. A. Inhibition by nitric oxide of the repair protein, O6-methylguanine-DNA-methyltransferase. *Carcinogenesis* **15**:443-447; 1994.
- [124] Wink, D. A.; Laval, J. The Fpg protein, a DNA repair enzyme, is inhibited by the biomediator nitric oxide in vitro and in vivo. *Carcinogenesis* **15**:2125-2129; 1994.
- [125] Prakash, A.; Doublet, S.; Wallace, S. S. The Fpg/Nei family of DNA glycosylases: substrates, structures, and search for damage. *Progress in molecular biology and translational science* **110**:71-91; 2012.
- [126] Hickok, J. R.; Vasudevan, D.; Jablonski, K.; Thomas, D. D. Oxygen dependence of nitric oxide-mediated signaling. *Redox biology* **1**:203-209; 2013.
- [127] Suzuki, T.; Harashima, H.; Kamiya, H. Effects of base excision repair proteins on mutagenesis by 8-oxo-7,8-dihydroguanine (8-hydroxyguanine) paired with cytosine and adenine. *DNA repair* **9**:542-550; 2010.

- [128] Burns, J. A.; Dreij, K.; Cartularo, L.; Scicchitano, D. A. O6-methylguanine induces altered proteins at the level of transcription in human cells. *Nucleic acids research* **38**:8178-8187; 2010.
- [129] Rassaf, T.; Weber, C.; Bernhagen, J. Macrophage migration inhibitory factor in myocardial ischaemia/reperfusion injury. *Cardiovasc Res* **102**:321-328; 2014.
- [130] Fan, Q.; Gao, F.; Zhang, L.; Christopher, T. A.; Lopez, B. L.; Ma, X. L. Nitrate tolerance aggravates postischemic myocardial apoptosis and impairs cardiac functional recovery after ischemia. *Apoptosis : an international journal on programmed cell death* **10**:1235-1242; 2005.
- [131] DiFabio, J. M.; Thomas, G. R.; Zucco, L.; Kuliszewski, M. A.; Bennett, B. M.; Kutryk, M. J.; Parker, J. D. Nitroglycerin attenuates human endothelial progenitor cell differentiation, function, and survival. *J Pharmacol Exp Ther* **318**:117-123; 2006.
- [132] Britten, M. B.; Abolmaali, N. D.; Assmus, B.; Lehmann, R.; Honold, J.; Schmitt, J.; Vogl, T. J.; Martin, H.; Schachinger, V.; Dimmeler, S.; Zeiher, A. M. Infarct remodeling after intracoronary progenitor cell treatment in patients with acute myocardial infarction (TOPCARE-AMI): mechanistic insights from serial contrast-enhanced magnetic resonance imaging. *Circulation* **108**:2212-2218; 2003.
- [133] Werner, C.; Bohm, M.; Friedrich, E. B. Progenitor cell therapy and myocardial infarction: the importance of microvascular function. *Nat Clin Pract Cardiovasc Med* **5**:78-79; 2008.
- [134] Yasuda, H.; Yamaya, M.; Nakayama, K.; Sasaki, T.; Ebihara, S.; Kanda, A.; Asada, M.; Inoue, D.; Suzuki, T.; Okazaki, T.; Takahashi, H.; Yoshida, M.; Kaneta, T.; Ishizawa, K.; Yamanda, S.; Tomita, N.; Yamasaki, M.; Kikuchi, A.; Kubo, H.; Sasaki, H. Randomized phase II trial comparing nitroglycerin plus vinorelbine and cisplatin with vinorelbine and cisplatin alone in previously untreated stage IIIB/IV non-small-

cell lung cancer. *Journal of clinical oncology : official journal of the American Society of Clinical Oncology* **24**:688-694; 2006.

[135] Illum, H.; Wang, D. H.; Dowell, J. E.; Hittson, W. J.; Torrissi, J. R.; Meyer, J.; Huerta, S. Phase I dose escalation trial of nitroglycerin in addition to 5-fluorouracil and radiation therapy for neoadjuvant treatment of operable rectal cancer. *Surgery* **158**:460-465; 2015.

[136] Davidson, A.; Veillard, A. S.; Tognela, A.; Chan, M. M.; Hughes, B. G.; Boyer, M.; Briscoe, K.; Begbie, S.; Abdi, E.; Crombie, C.; Long, J.; Boyce, A.; Lewis, C. R.; Varma, S.; Broad, A.; Muljadi, N.; Chinchin, S.; Espinoza, D.; Coskinas, X.; Pavlakakis, N.; Millward, M.; Stockler, M. R.; Australasian Lung cancer Trials, G.; Australasian Lung cancer Trials Group, A. A phase III randomized trial of adding topical nitroglycerin to first-line chemotherapy for advanced nonsmall-cell lung cancer: the Australasian lung cancer trials group NITRO trial. *Annals of oncology : official journal of the European Society for Medical Oncology / ESMO*; 2015.

[137] Reinmuth, N.; Meyer, A.; Hartwigsen, D.; Schaeper, C.; Huebner, G.; Skock-Lober, R.; Bier, A.; Gerecke, U.; Held, C. P.; Reck, M. Randomized, double-blind phase II study to compare nitroglycerin plus oral vinorelbine plus cisplatin with oral vinorelbine plus cisplatin alone in patients with stage IIIB/IV non-small cell lung cancer (NSCLC). *Lung cancer* **83**:363-368; 2014.

[138] Arrieta, O.; Blake, M.; de la Mata-Moya, M. D.; Corona, F.; Turcott, J.; Orta, D.; Alexander-Alatorre, J.; Gallardo-Rincon, D. Phase II study. Concurrent chemotherapy and radiotherapy with nitroglycerin in locally advanced non-small cell lung cancer. *Radiotherapy and oncology : journal of the European Society for Therapeutic Radiology and Oncology* **111**:311-315; 2014.

- [139] Meira, L. B.; Calvo, J. A.; Shah, D.; Klapacz, J.; Moroski-Erkul, C. A.; Bronson, R. T.; Samson, L. D. Repair of endogenous DNA base lesions modulate lifespan in mice. *DNA repair* **21**:78-86; 2014.
- [140] Zhang, Z.; Wang, L.; Wei, S.; Liu, Z.; Wang, L. E.; Sturgis, E. M.; Wei, Q. Polymorphisms of the DNA repair gene MGMT and risk and progression of head and neck cancer. *DNA Repair (Amst)* **9**:558-566; 2010.
- [141] A. Daiber, T. M. *Oxidativer Stress, Redoxregulation und NO-Bioverfügbarkeit—experimentelle und klinische Aspekte* 2006.

## **Acknowledgments**

I am indebted to my advisor, who was an incredible mentor throughout these 3 years. I'm sure that every student who had the immense luck to have this mentor will agree with me that the amount of time, efforts and passion that professor is willing to share with his students is just incredible. I always felt that whenever I have any question regarding my project, lab routine or even day-to-day life in Germany I could always drop by his office and he was happy to help me. Thank you for giving me this feeling!

I would like to extend my gratitude to the committee members who helped me to mature as a scientist, gave a new perspective for my research and sometimes brought me back down to earth with the extensive goals that I have previously thought of achieving during my PhD time.

I would also like to thank all members of my mentor's team. I think I will never forget how on one occasion, when I was trying without success to get the DNA immuno-dot blot to work for 4 months, my colleague saw my exasperation and said: "Ok, now calm down and tell me step-by-step what are you doing in that crazy method of yours". My colleague sat there with me for 1 hour and listened to every tiny detail of my method and afterwards gave me so many valuable comments that my method later on yielded good results. On top of that, my colleague was always my closest friend in the lab. Thank you once again for everything you ever did for me! I will never forget your kindness.

I'm also very thankful to my mother for constantly giving me a kick to move forward and for her constant openness to listen about all the challenges that I think are extremely important at that particular moment of time.

These acknowledgements will not be complete unless I would mention my friends and close ones that supported me through this PhD journey – my friends and family.

Thank you so much for being there in my life!

## **Curriculum Vitae**

**Name:** Yuliya Mikhed

**Date of birth:** 02.11.1988

**Place of birth:** Lviv, Ukraine

**Nationality:** Ukrainian

**Parents:** Svitlana Mikhed and Alexander Mikhed

**Familial status:** Single

**Education:**

- 1) **School:** Lviv general secondary specialized school #45 of the I-III stage with advanced studies of English, 1995-2004.
- 2) **Bachelor's program:** National University "Lviv Polytechnik", Lviv, Ukraine. Specialty – Pharmacy, 2004-2008. Graduated with honors. GPA: 97% out of 100%
- 3) **Master's program:** University of Illinois at Chicago, Chicago, IL, USA. Specialty – Medicinal chemistry, 2009-2012. GPA: 3.0. Recipient of Fulbright scholarship for 3 years.
- 4) **PhD program:** Johannes Gutenberg University, Mainz, Germany. Specialty – Biology. 2012-2015. Recipient of the stipend from the International PhD Program on the "Dynamics of Gene Regulation, Epigenetics and DNA Damage Response" from the Institute of Molecular Biology gGmbH, (Mainz, Germany) funded by the Boehringer Ingelheim Foundation. PhD advisor: Prof. Dr. Andreas Daiber.

## **List of publications**



## **Original research articles:**

### *Submitted, under review*

- 1) Nitroglycerin induces DNA damage and vascular cell death in the setting of nitrate tolerance. **Y. Mikhed**, J. Fahrner, M. Oelze, S. Kröller-Schön, S. Steven, P. Welschof, E. Zinßius, P. Stamm, F. Kashani, S. Roohani, B. Epe, B. Kaina, T. Münzel, A. Daiber. Proc Natl Acad Sci USA, **under review**.
- 2) Formation of 2-nitrophenol from salicylaldehyde as a suitable test for low peroxynitrite fluxes. **Y. Mikhed**, K. Bruns, S. Schildknecht, M. Jörg, M. Dib, M. Oelze, K. J. Lackner, T. Münzel, V. Ullrich, A. Daiber. Redox Biology, **under review**.

### *Published*

- 3) Effect of soluble guanylyl cyclase activator and stimulator therapy on nitroglycerin-induced nitrate tolerance in rats. Jabs A, Oelze M, **Mikhed Y**, Stamm P, Kröller-Schön S, Welschof P, Jansen T, Hausding M, Kopp M, Steven S, Schulz E, Stasch JP, Münzel T, Daiber A. Vascul Pharmacol. 2015 Aug;71:181-91. doi: 10.1016/j.vph.2015.03.007. Epub 2015 Apr 11.
- 4) Gliptin and GLP-1 analog treatment improves survival and vascular inflammation/dysfunction in animals with lipopolysaccharide-induced endotoxemia. Steven S, Hausding M, Kröller-Schön S, Mader M, **Mikhed Y**, Stamm P, Zinßius E, Pfeffer A, Welschof P, Agdauletova S, Sudowe S, Li H, Oelze M, Schulz E, Klein T, Münzel T, Daiber A. Basic Res Cardiol. 2015 Mar;110(2):6. doi: 10.1007/s00395-015-0465-x. Epub 2015 Jan 20.
- 5) The sodium-glucose co-transporter 2 inhibitor empagliflozin improves diabetes-induced vascular dysfunction in the streptozotocin diabetes rat model by interfering with oxidative stress and glucotoxicity. Oelze M, Kröller-Schön

S, Welschof P, Jansen T, Hausding M, Mikhed Y, Stamm P, Mader M, Zinßius E, Agdauletova S, Gottschlich A, Steven S, Schulz E, Bottari SP, Mayoux E, Münzel T, Daiber A. PLoS One. 2014 Nov 17;9(11):e112394. doi: 10.1371/journal.pone.0112394. eCollection 2014.

- 6) Inflammatory monocytes determine endothelial nitric-oxide synthase uncoupling and nitro-oxidative stress induced by angiotensin II. Kossmann S, Hu H, Steven S, Schönfelder T, Fraccarollo D, Mikhed Y, Brähler M, Knorr M, Brandt M, Karbach SH, Becker C, Oelze M, Bauersachs J, Widder J, Münzel T, Daiber A, Wenzel P. J Biol Chem. 2014 Oct 3;289(40):27540-50. doi: 10.1074/jbc.M114.604231. Epub 2014 Aug 20.
- 7) CD40L contributes to angiotensin II-induced pro-thrombotic state, vascular inflammation, oxidative stress and endothelial dysfunction. Hausding M, Jurk K, Daub S, Kröller-Schön S, Stein J, Schwenk M, Oelze M, Mikhed Y, Kerahrodi JG, Kossmann S, Jansen T, Schulz E, Wenzel P, Reske-Kunz AB, Becker C, Münzel T, Grabbe S, Daiber A. Basic Res Cardiol. 2013 Nov;108(6):386. doi: 10.1007/s00395-013-0386-5. Epub 2013 Sep 24.
- 8) Molecular mechanisms of the crosstalk between mitochondria and NADPH oxidase through reactive oxygen species-studies in white blood cells and in animal models. Kröller-Schön S, Steven S, Kossmann S, Scholz A, Daub S, Oelze M, Xia N, Hausding M, Mikhed Y, Zinssius E, Mader M, Stamm P, Treiber N, Scharffetter-Kochanek K, Li H, Schulz E, Wenzel P, Münzel T, Daiber A. Antioxid Redox Signal. 2014 Jan 10;20(2):247-66. doi: 10.1089/ars.2012.4953. Epub 2013 Aug 17.
- 9) **Before PhD:** Nitric oxide suppresses tumor cell migration through N-Myc downstream-regulated gene-1 (NDRG1) expression: role of chelatable iron.

Hickok JR, Sahni S, **Mikhed Y**, Bonini MG, Thomas DD. J Biol Chem. 2011 Dec 2;286(48):41413-24. doi: 10.1074/jbc.M111.287052. Epub 2011 Oct 5.

### **Reviews:**

- 1) Mitochondrial Oxidative Stress, Mitochondrial DNA Damage and Their Role in Age-Related Vascular Dysfunction. **Mikhed Y**, Daiber A, Steven S. Int J Mol Sci. 2015 Jul 13;16(7):15918-53. doi: 10.3390/ijms160715918. Review.
- 2) Redox regulation of genome stability by effects on gene expression, epigenetic pathways and DNA damage/repair. **Mikhed Y**, Görlach A, Knaus UG, Daiber A. Redox Biol. 2015 Jun 3;5:275-289. doi: 10.1016/j.redox.2015.05.008. [Epub ahead of print] Review.

### **Oral presentations and posters:**

#### **Oral presentation:**

- 1) DNA damage in the pathogenesis of nitrate tolerance. **Yuliya Mikhed** and Andreas Daiber. PhD symposium, Mainz, Germany, 2014.
- 2) Use of electron paramagnetic resonance spectroscopy in murine aging models as a detection tool for measuring NO bioavailability. **Yuliya Mikhed**, Matthias Oelze, Swenja Kröller-Schön, Edith Lubos, Michael Hausding, Huige Li, Michael Torzewski, Philip Wenzel, Markus Bachschmid, Karl J. Lackner, Thomas Münzel, and Andreas Daiber. Biochemical basis of healthy ageing. SFRR-Europe/IUBMB Advanced School, Spetses, Greece, September 22-28, 2014.

## Poster presentations:

### *As a presenter*

- 1) The role of DNA damage in the pathogenesis of nitrate tolerance. **Yuliya Mikhed**, Matthias Oelze, Swenja Kröller-Schön, Elena Zinßius, Michael Mader, Paul Stamm, Philipp Welschhof, Thomas Münzel, Andreas Daiber. IMB conference 2015, Mainz, Germany, 2015
- 2) DNA damage as an oxidative stress parameter in the pathogenesis of nitrate tolerance. **Yuliya Mikhed**, Matthias Oelze, Swenja Kröller-Schön, Elena Zinßius, Michael Mader, Paul Stamm, Philipp Welschhof, Thomas Münzel, Andreas Daiber. The 81th Annual Meeting of the German Society of Cardiology (DGK), Mannheim, Germany, 2015
- 3) The role of DNA damage in the pathogenesis of nitrate tolerance. **Yuliya Mikhed**, Matthias Oelze, Swenja Kröller-Schön, Elena Zinßius, Michael Mader, Paul Stamm, Philipp Horst, Amanda Pfeffer, Thomas Münzel, Andreas Daiber. Experimental Biology Meeting 2015, Boston, MA, USA, 2015.
- 4) Use of electron paramagnetic resonance spectroscopy in murine aging models as a detection tool for measuring NO bioavailability. **Yuliya Mikhed**, Matthias Oelze, Swenja Kröller-Schön, Edith Lubos, Michael Hausding, Huige Li, Michael Torzewski, Philip Wenzel, Markus Bachschmid, Karl J. Lackner, Thomas Münzel, and Andreas Daiber. Biochemical basis of healthy ageing. SFRR-Europe/IUBMB Advanced School, Spetses, Greece, 2014.
- 5) The role of DNA damage in the pathogenesis of nitrate tolerance. **Yuliya Mikhed**, Matthias Oelze, Swenja Kröller-Schön, Elena Zinßius, Michael Mader, Paul

Stamm, Philipp Horst, Amanda Pfeffer, Thomas Münzel , Andreas Daiber.  
SFRBM 20<sup>th</sup> Annual Meeting, San Antonio, TX, USA, 2013.

- 6) Unique Features of the Low Molecular Weight Probe Salicylaldehyde in the Detection of Nanomolar Peroxynitrite Fluxes. **Mikhed, Y** ; Bruns, K; Jorg, M; Kerahrodi, JG; Gottschlich, A; Oelze, M; Schildknecht, S; Ullrich, V; Daiber, A. SFRBM 19<sup>th</sup> Annual Meeting, San Diego, CA, USA, 2012.
- 7) **Before PhD:** Oxygen Regulates Nitric Oxide-Mediated Signaling by Determining the Rate of NO Synthesis and Metabolism. **Mikhed, Y**; Hickok, JR; Thomas, DD. SFRBM 18<sup>th</sup> Annual Meeting, Atlanta, GA, USA, 2011.

*As a co-author*

- 1) Empagliflozin decreases inflammation and AGE/RAGE markers in the aortic vessel wall of a streptozotocin type 1 diabetic model. Steven, S; Oelze, M; Kroller-Schon, S; Welschhof, P; **Mikhed, Y**; Agdauletova, S; Schulz, E; Mayoux, E; Munzel, T; Daiber, A. DIABETOLOGIA Volume: 57 Pages: S331-S331 Supplement: 1 Meeting Abstract: 819, 2014
- 2) Comparison of DPP-4 inhibition versus GLP-1 analogue supplementation on survival and vascular complications in experimental sepsis. Stamm, P; Hausding, M; Kroller-Schon, S; Mader, M; Agdauletova, S; **Mikhed, Y**; Pfeffer, A; Welschhof, P; Steven, S; Oelze, M; Schulz, E; Klein, T; Munzel, T; Daiber, A. 0FASEB JOURNAL Volume: 28 Issue: 1 Supplement: S Meeting Abstract: 145.2, 2014.
- 3) **Before PhD:** Nitric Oxide Suppresses Tumor Cell Migration Through N-Myc Downstream Regulated Gene-1 (NDRG1) Expression: the Role of Chelatable Iron. Hickok, JR; Sahni, S; **Mikhed, Y**; Thomas, DD. SFRBM 18<sup>th</sup> Annual Meeting, Atlanta, GA, USA, 2011.

